Study on Buckling-Restrained Steel Bar Dampers for Spine Frame Systems

（心棒架構における座屈拘束丸鋼ダンパーに関する研究）

2021 年 3 月

Mateus Segura Jhon Alexander

ACKNOWLEDGEMENTS

First and foremost, I would like to express my deepest gratitude to my supervisor Professor Hiroshi Tagawa for his guidance, patience, kindness and unconditional support. I have admiration for his commitment, work ethic, calmness, wisdom and passion, which have been a great life example to me. He made it possible for me to continue through my studies. I will always be grateful for the years he took care of me in Japan. I also have enormous gratitude toward assistant professor Dr. Xingchen Chen. Her cheerfulness, kindness, passion, positivity and patience made it very pleasant and encouraging during these years. My deepest gratitude to Professors Takaaki Ookubo, Naohiro Nakamura, and Hiroyuki Miura, who took time out of their busy schedule to revise my work, listen my presentation and provide positive feedback.

My immense gratitude to the Japanese Government, who supported my studies, and provided me with a unique opportunity to experience this marvelous country, and to realize how amazing, peaceful, hard-working and committed a nation's people can be.

Many thanks to my fellow labmates, who always were kind and willing to cooperate to one another. Special thanks for the friendship of my bro Mr. Unur who took care of me during these years and was my PhD. battling partner, and also to Mr. Chou who always showed kindness and support. Working all together was a great inspiration and wish to all of them a brilliant future.

Last but not least, I would not be anything without my family. To my wife my deepest appreciation for her patience, positivism, hard work and support during my studies, as it was not an easy time for her; Always grateful to my mother for devoting her life to me; To my extraordinary sister whose unconditional support is everything to me and the reason of my achievements; To my dad and my Indonesian mother who always, no matter what, believe in me; To the joy and best experience of my life, my charming girls Alysha and Ameesha, whose smile and happiness give me strength, purpose and bliss beyond description.

ABSTRACT

This study aims to reveal the applicability of "buckling-restrained steel bar dampers" as energy dissipaters for spine frame systems through experimental tests.

Chapter 1 presents a brief literature review on buckling-restrained braced dampers and spine frame systems. The dissertation objectives and outline are presented.

In Chapter 2, the application of round steel bars as cores for buckling-restrained braces (BRBs) is presented as a preliminary study of the proposed damper. The BRBs were composed of round steel bars buckling-restrained by double round tubes, and differed mainly on the number of "contraction allowance zones" (the portions of the core bar which are not buckling restrained). This study aimed to reveal the applicability of the BRB by performing loading tests on two test specimens. Overall, the experimental test revealed satisfactory performance for both specimens as both presented stable hysteretic performance.

In Chapter 3, the BRB concept of preliminary research (Chapter 2) was implemented as energy dissipater for a spine frame system. In this study, the proposed "buckling-restrained steel bar damper" is composed of a round steel bar, buckling-restrained by a round steel tube. A key feature of the damper is the use of "supporters" (thin-plate elements attached to the spine column) which are able to partially restrain the round tube, thus reducing the damper's buckling length. To assess the functionality and energy dissipation performance of the proposed damper, cyclic loading tests were conducted on 10 damper specimens. The damper specimens mainly differed in their buckling length, the type of connection to the spine frame base, the number of contraction allowances zones, and damper length. Test results revealed that dampers with two contraction allowance zones, at least one supporter at the center, and fixed connections at their base exhibit the most satisfactory performance. Overall, functionality of the spine, the supporters and end-connections were satisfactory as visually confirmed after the test.

In Chapter 4, the proposed buckling-restrained steel bar damper was implemented into a sample real scale building with spine frame systems to assess the practicality of its application. The implementation of the damper was notably influenced by the required damper length to satisfy the strain demand, and by the required number of dampers to satisfy the strength demand. Up to six supporters were necessary to partially restrain the damper. The supporters required welding to avoid difficulty of installation and obstacle at the spine column web. Welding was also necessary for the end connections. It was concluded that for a building with dimensions and strength demand as in the design example, it is necessary that the proposed damper be set up and attached to the spine column at the assembly factory, where welding of the supporters and connections shall be performed.

In Chapter 5, conclusions of the research are presented.

TABLE OF CONTENTS

1. INTRODUCTION

1.1 Background and previous research

The research proposed in this dissertation is related to Buckling-restrained braces and to spine frame systems. Thus, background on these topics is presented in the following sections.

1.1.1 Dampers as buckling-restrained braces

Since the development of the first buckling-restrained braces (BRBs) in the 1970s [1.1–1.2], BRBs have proven to be very effective seismic-energy dissipation systems, contributing remarkably to the field of building structure stability.

Buckling-restrained braces (Fig. 1.1) are seismic energy dissipation devices used to reduce damage in main structural components. They are composed of a yielding steel core which is longitudinally confined within a restraining mechanism (an axially decoupled element which restrains the yielding core against buckling). BRBs can be used as an alternative to conventional steel braces [1.3]. While conventional braces are also used to stabilize structures against lateral loads, they exhibit notable poor behavior when submitted to compression, which results in buckling and significant strength deterioration (Fig. 1.2 (a)). In contrast, BRBs are able to perform superiorly as the buckling restrainer enhances the core stiffness (Fig. 1.2 (b)), enabling it to achieve the same strength in both tension and compression, and to notably enhance the energy absorption capacity and hysteretic behavior (Fig. 1.2 (c)).

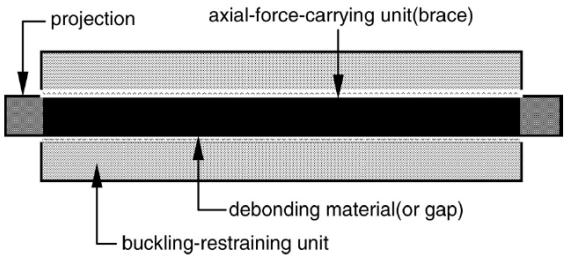

Figure 1.1 Composition of a typical BRB [1.3]

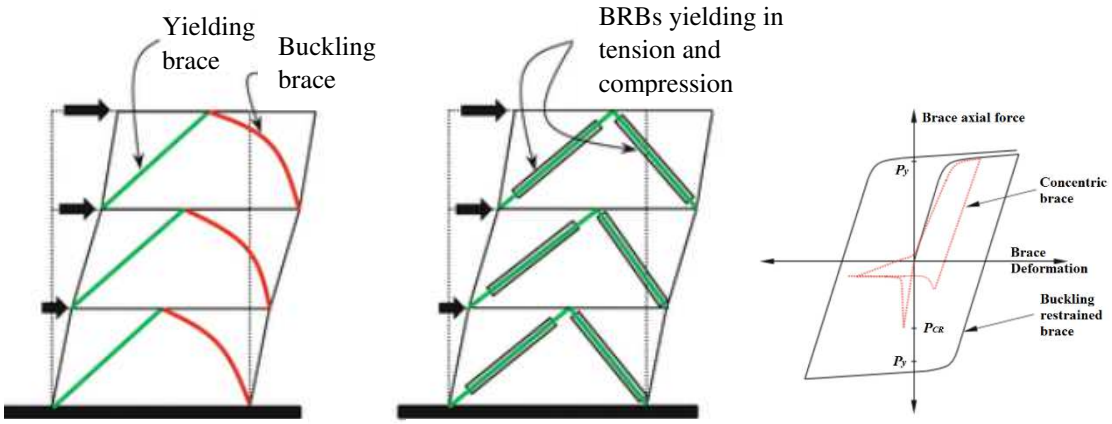

a) Conventional braced frame b) Buckling-restrained braced frame c) Hysteresis

Figure 1.2 Comparative behavior between conventional braces and BRBs [1.1]

Investigations on BRBs with a wide range of mechanical and geometrical characteristics have been conducted [1.3 – 1.6]. Several examples of BRB cross-section configurations are displayed in Fig 1.3. The most popular configuration of BRB uses single rectangular plates or crucifix shaped plates as cores, restrained by a mortar-filled hollow sections [1.3, 1.5–1.9] (Fig. 1.3 (a), (c) and Fig 1.4). Steel tubes (Fig. 1.3 (f)), and H-sections (Figs. 1.3 (b), (e) and (i)) are also applicable as cores. BRB cores can also be buckling-restrained by steel tubes or steel assemblies without mortar filling (Figs. 1.3 (e) - (i)).

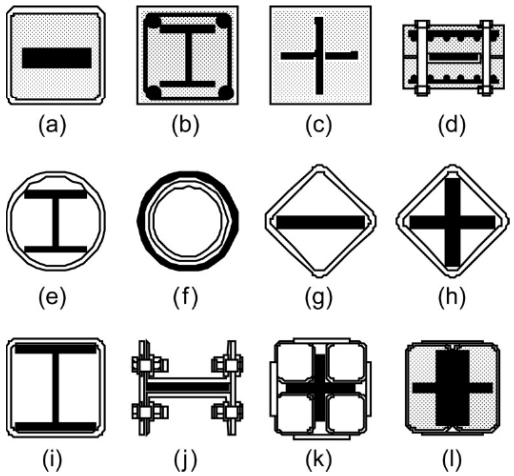

Figure 1.3 Cross-Sections of BRBs [1.3]

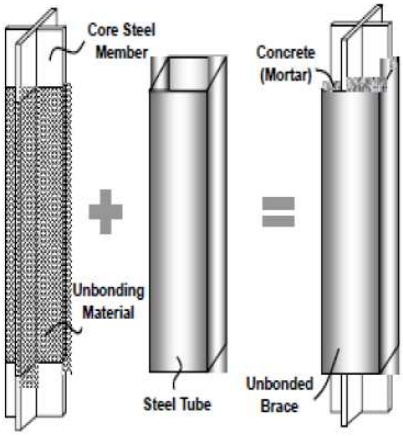

Figure 1.4 scheme of a mortar-filled BRB [1.1]

1.1.2 Application of round steel bars to buckling-restrained braces

Innovative researches using round steel bars as dampers have been conducted. Aghara [1.10] proposed metallic dampers using assemblies of common hot-rolled square hollow sections, C-channels and plates, which dissipates energy through replaceable steel bars (Fig.1.5). The bars are installed transversally to the axial load direction, and dissipates energy through a combination of flexural and tensile resistance of the steel bar.

Researches of BRBs using round steel bars as cores have also gained popularity. Tagawa et al. [1.11] implemented buckling-restrained round steel bars as dampers for bolted beam-to-column connections (Fig.1.6). The bar has screw-ends for fixation and uses a rectangular steel solid as the buckling restraining member. The damper has a simple assembly attained through bolting, and seismic energy is expected to be dissipated through the axial yield deformation of the round steel bar.

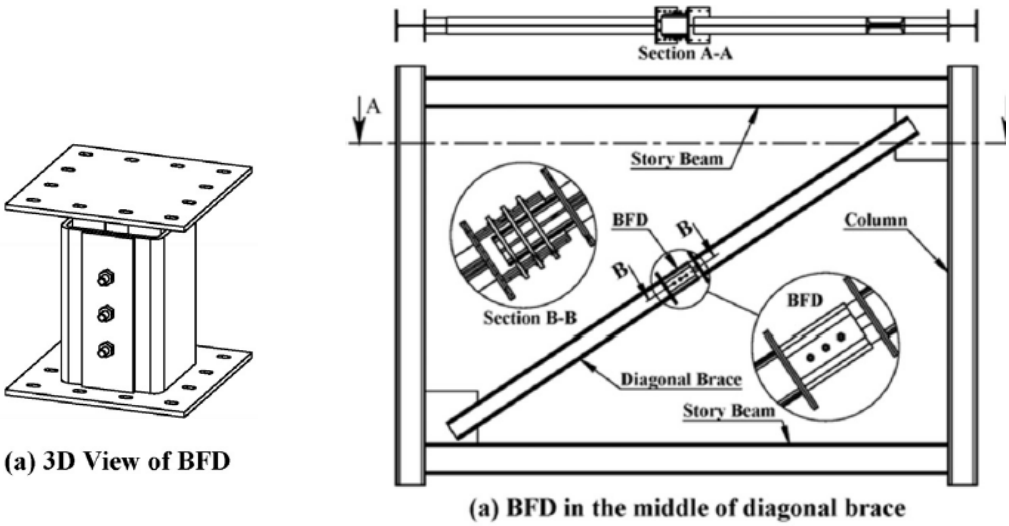

Figure 1.5 damper using replaceable round steel bars [1.10]

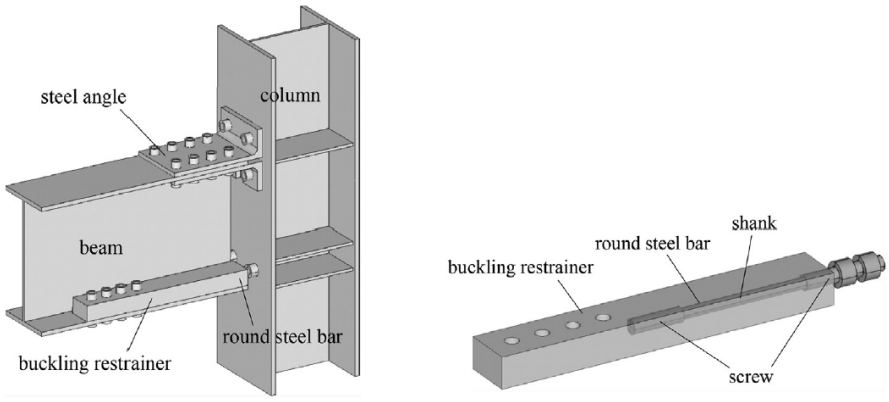

(a) Overall view (b) Damper detail

Figure 1.6 Buckling-restrained steel bars dampers at beam-to-column connection [1.11]

Sarti et al. [1.12] used small capacity BRBs as featured in Fig. 1.7 (a) to provide damping at beam-column joints, wall-foundation joints, and post-tensioned rocking systems. The BRBs were made of milled-down steel bar confined within a steel tube in-filled with grout or epoxy (and obtained good results in structural performance). Wang et al. [1.13] proposed an all-steel BRB using a "bamboo-shaped core" buckling-restrained by a steel tube (Fig. 1.7 (b)), to avoid difficulties in grouting and to enhance hysteretic performance of small BRBs. The core was composed of bar segments and a series of elastic slubs which enhanced the buckling performance of the core. Furthermore, enhancements of the interaction between the core bar and the buckling-restrainer have been studied, such as: longitudinally milled-down core bars buckling-restrained by round steel tubes [1.14] in Fig. 1.7(c)., and triangular shaped core bars manufactured via wire-electrode cutting [1.15] in Fig. 1.7(d).

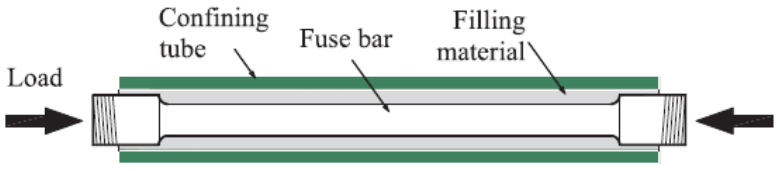

(a) Fuse-type dissipater [1.12]

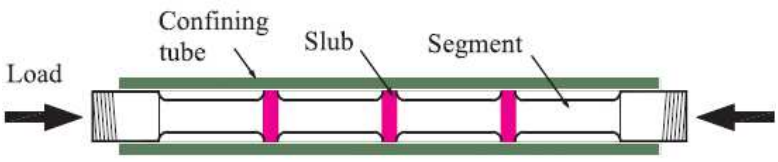

(b) Bamboo-shaped energy dissipater [1.13]

Figure 1.7 Configuration of different steel core bar dissipaters

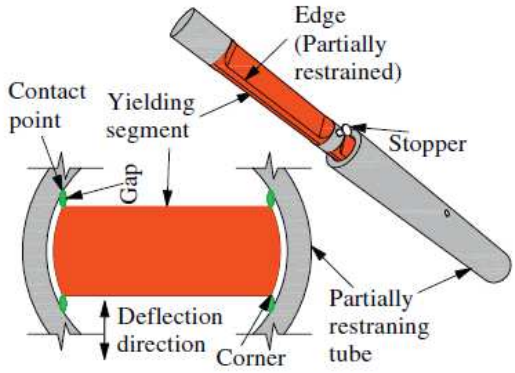

(c) Longitudinally milled-down core bars buckling-restrained by round steel tubes [1.14]

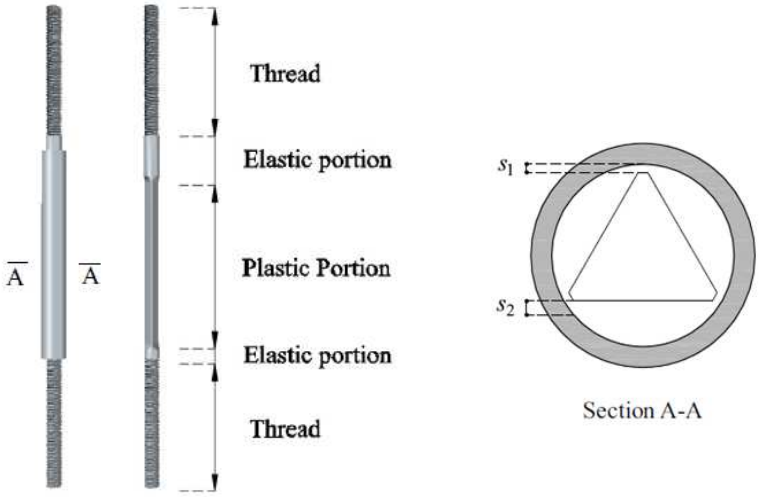

(d) Triangular shaped core bars [1.15]

Figure 1.7 Configuration of different steel core bar dissipaters (cont.)

In the prior research to this paper, Fujii-Tagawa [1.16 – 1.17] pioneered the use of round steel bars as core by proposing a BRB equipped with round steel bar cores, and restrained by double round steel tubes separated by spacers (Fig. 1.8). In that study, full-scale loading tests were conducted on test specimens having different characteristics, such as restrainer's size, number of contraction allowance zones, spacer type, and fixation method of the outer restrainer. Test results revealed the applicability and limitations of the round-steel-core-bar-based BRB, the influence of using different fixing methods for the steel tube restrainers, and the influence of unrestrained zones of the core bar. A finite element analysis of their study [1.18] produced results regarding the buckling and failure behaviors of the core bar and inner tube, respectively.

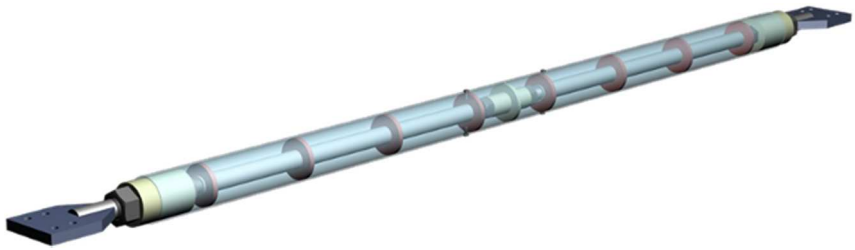

Figure 1.8 BRB model researched by Fujii-Tagawa [1.17]

Despite the efficiency of BRBs as energy dissipaters, structures equipped with BRBs have displayed damage concentration and residual drift, particularly at weak stories, when the structures undergo large seismic intensity.

1.1.3 Spine frame systems

Spine-frame systems have become more noticeable in the last decade for both new building design and retrofitting [1.19]. Spine-frames limit the residual drift of structures to negligible magnitudes through rocking of the spine (a rigid frame or wall), and they can be equipped with dampers for seismic energy dissipation. Additionally, spine frames can achieve self-centering through either restoring gravity forces or through using post-tensioned (PT) elements.

Spine frames have been applied to real structures successfully. For instance, Wada et al. [1.20] the concept of pivoting spine in the seismic retrofitting of concrete building in Japan as portrayed in Fig 1.9. Janhunen et al. [1.21] also used a similar spine concept in the seismic retrofitting of a steel building in the USA, in which a concrete wall acts as the core of the rocking to redistribute the lateral forces and displacements without adding significant strength.

Researches on spine frames and on the use of a variety of energy dissipaters for the spines have also gained popularity. Seismic performance of a non-ductile reinforced concrete frame (retrofitted with rocking infill walls) was investigated by Günay et al. [1.22], proving the spine efficacy in reducing soft-story failure risks. Eatherton et al. [1.23] studied an uplifting rocking frame system with PT strands that provided self-centering resistance, and was equipped with steel butterfly shaped fuses and BRBs as replaceable energy dissipation members (Fig. 1.10). Pampanin et al. [1.24] investigated rocking wall systems that used post-tensioned tendons for re-centering and dissipated energy through viscous fluid dampers and/or tension compression-yielding steel dampers installed at the base of the wall (Figs. 1.11 and 1.12). In this system, the yielding steel dampers consisted of mild steel bars confined within epoxy and a steel tube (resembling BRB systems). Tremblay et al. [1.25] proposed a

braced steel frame with viscous dampers vertically equipped between the column bases and the foundations as shown in Fig. 1.13.

(a) 3D-View

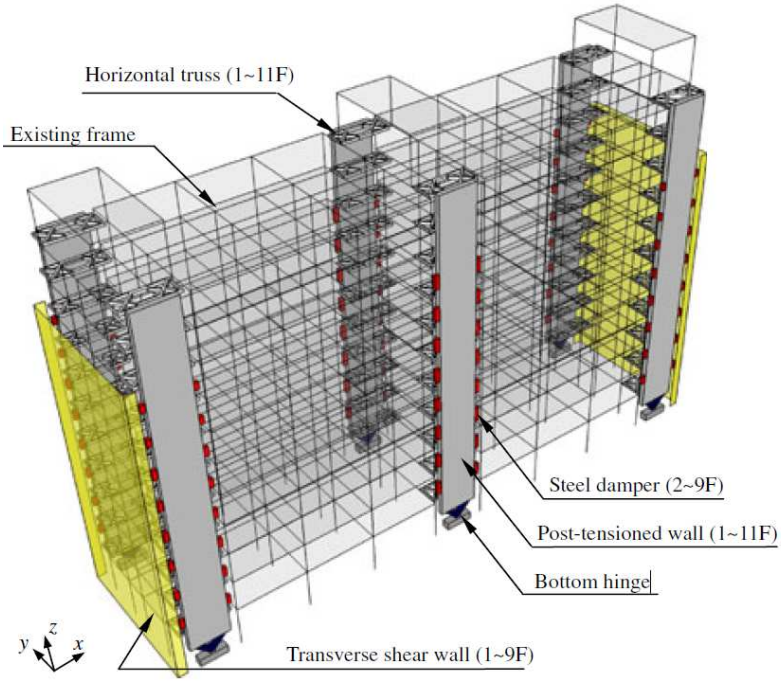

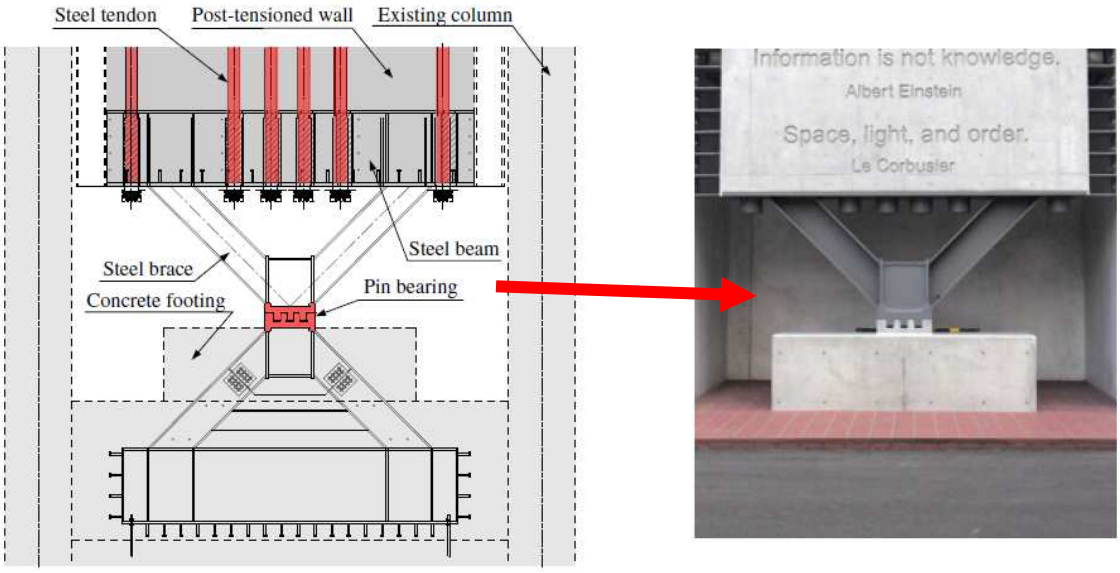

(b) Details at the bottom of the rocking wall

Figure 1.9 Retrofit plan of G3 building using post-tensioned walls with shear dampers [1.20]

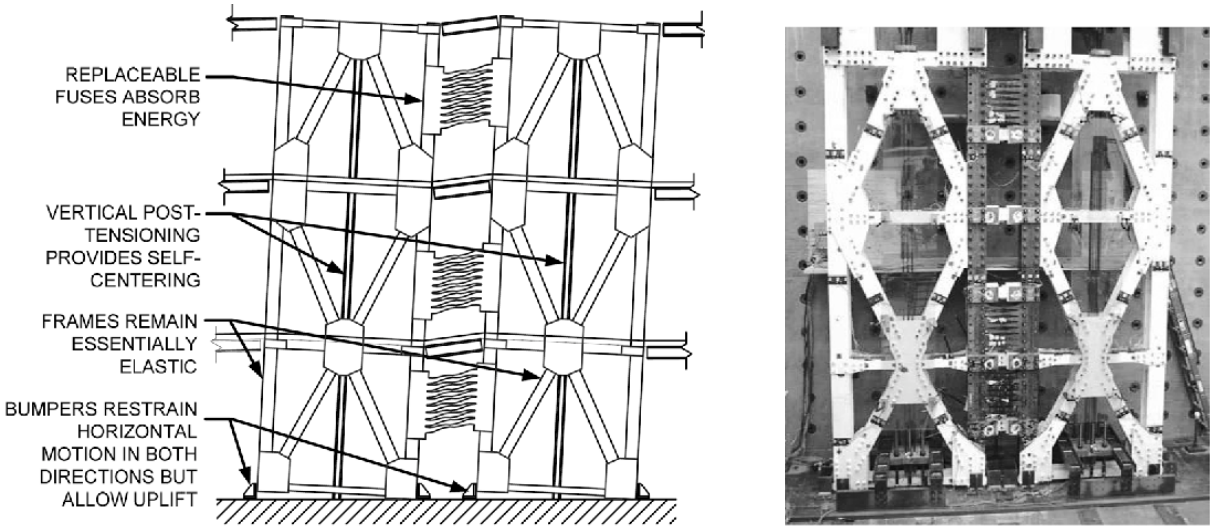

(a) Schematic illustration (b) large-scale test specimen

Figure 1.10 Uplifting rocking frame system with PT strands and steel butterfly shaped fuses [1.23]

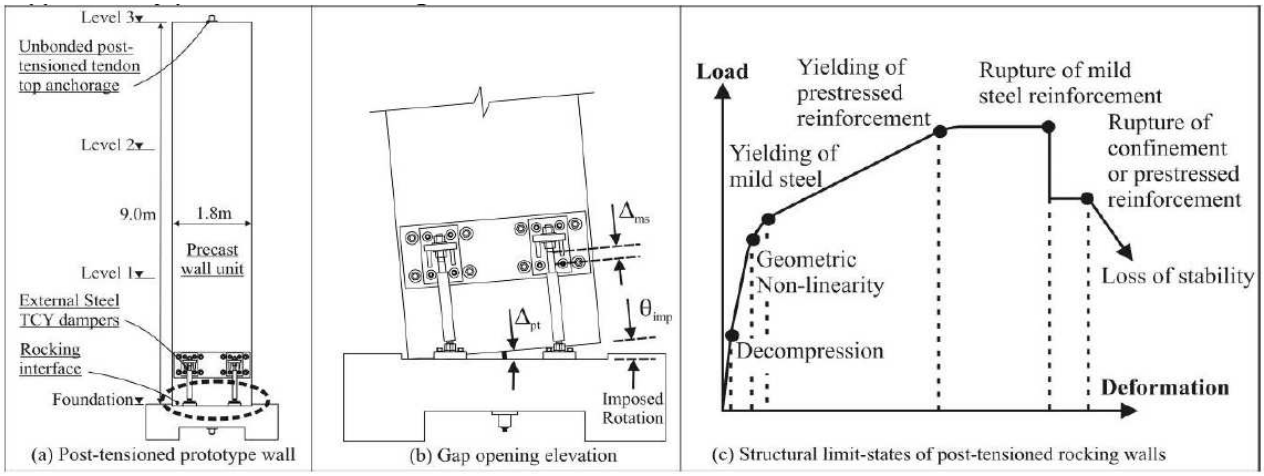

Figure 1.11 Post-tensioned precast rocking wall system with externally mounted mild steel dampers [1.24]

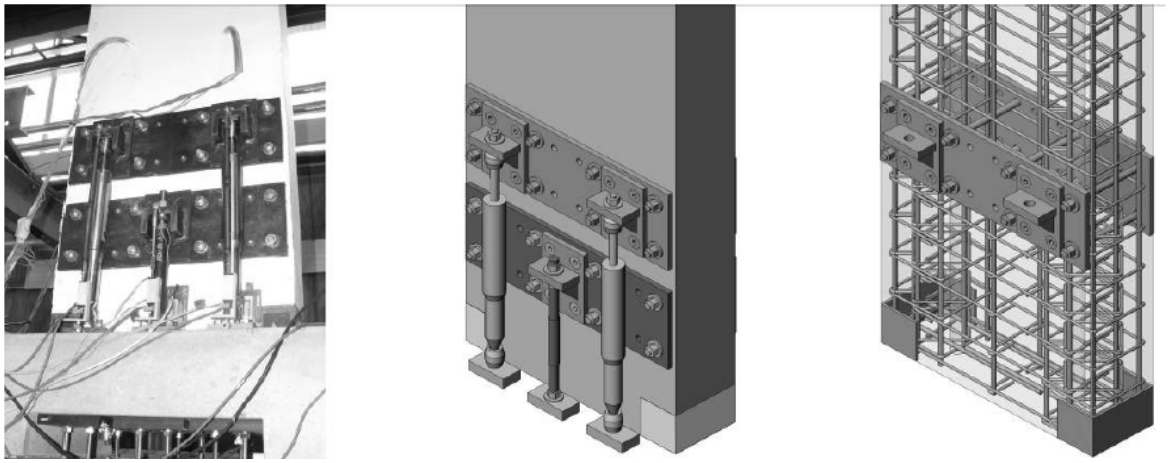

(a) As-built post-tensioned wall (b) Connection detail (c) Reinforcement, confinement and steel bracket details

Figure 1.12 Post-tensioned, precast wall unit [1.24]

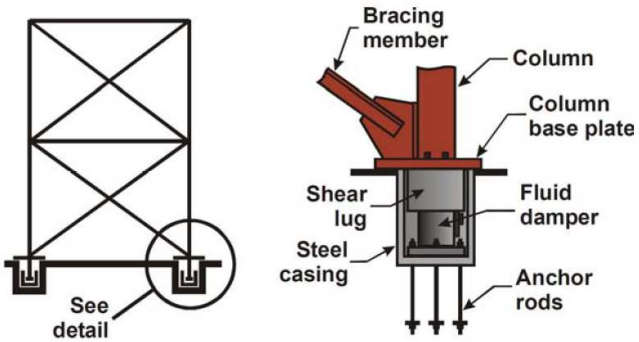

Figure 1.13 A viscously damped controlled seismic rocking braced steel frame system [1.25]

1.1.4 Application of BRCs to spine frame systems

A pin-supported self-centering rocking core system with buckling-restrained columns (SCRC-BRC), portrayed in Fig. 1.14, was investigated by Blebo [1.26] to prevent soft-story failure and reduce residual drift under earthquake loading. The Buckling-Restrained Columns (BRCs) were incorporated at the base of the self-centering rocking system to increase the energy dissipation capacity and to reduce peak drift response to ground motions of the system.

In the previous research, Takeuchi et al. [1.19] proposed a non-uplifting spine frame system (Fig. 1.15) that uses mortar-infilled buckling-restrained columns (BRCs) for seismic energy dissipation and is re-centered via elastic frames. The spine was pin-connected to the main structure and to the

base, allowing it to absorb lateral loads through BRCs located at the lower sides of the spine, which were also pin-connected to the spine and to the base.

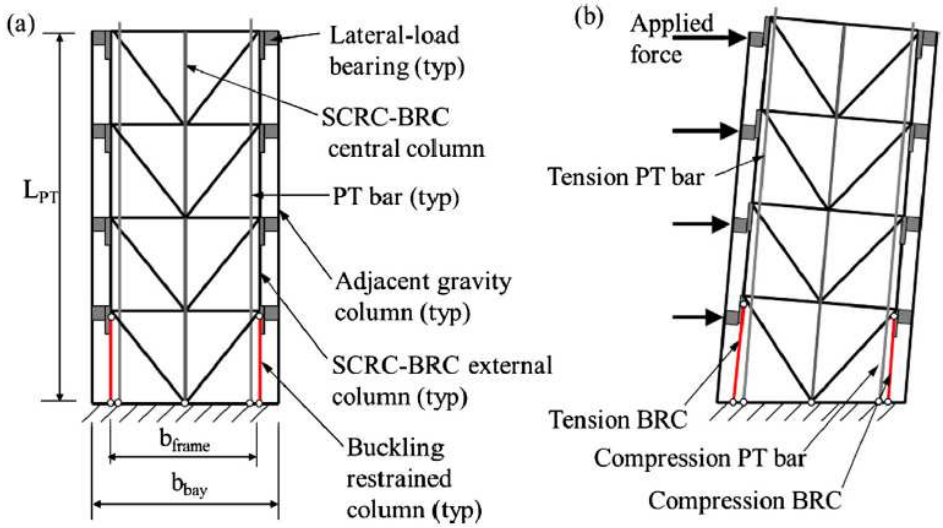

Figure 1.14 Concept of SCRC-BRC: (a) configuration; (b) Rotation about the base of the central column [1.26]

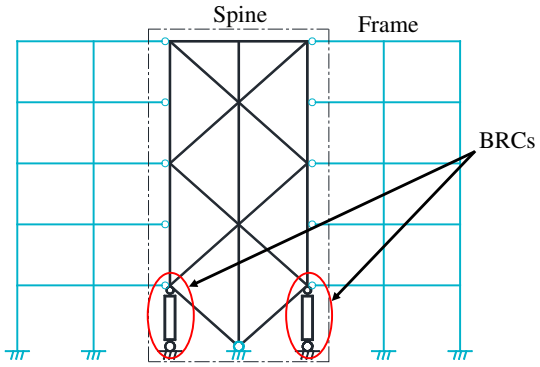

Figure 1.15. Spine frame system with BRCs [1.19]

1.2 Objectives of the dissertation

The main aim of this dissertation is to reveal the applicability of "buckling-restrained steel bar dampers", similar to the previous research by Tagawa et al. [1.16–1.18], as energy dissipation devices for spine frame systems, by performing cycling loading tests. The proposed dampers, portrayed in Fig. 1.16, are composed of round steel bar cores restrained by round steel tubes. Instead of installing BRCs such as in the spine system proposed by Takeuchi et al. [1.19] (Fig. 1.15), the columns of the

spine side are extended to the base (Fig. 16(a)) to enable the proposed dampers to be attached (Fig. 16(b)) to these columns using thin-plate elements called “supporters” which partially restrain the round tubes.

The damper is able to absorb earthquake forces transmitted through the building lateral movement and through the spine frame. When the spine sways, the core bars at both sides of the spine dissipate these seismic forces axially by undergoing tension in one damper, which results in elongation of the bar, and by undergoing compression on the damper at the opposite side, which results in buckling of the core bar. One particular feature of the damper is that during compression, its core is aided to resist compressive forces not only by the buckling restrainer, but also by the supporters which are attached to the spine frame column.

The main benefit of the proposed damper is that its buckling length can be reduced by using supporters attached to the column web, thereby also reducing the section of the buckling restrainer. Additionally, the usage of the round steel core bar with roll-threaded screws and non-reduced shank section is another specific feature of the proposed damper, which will be described in Section 3.4.1.2.

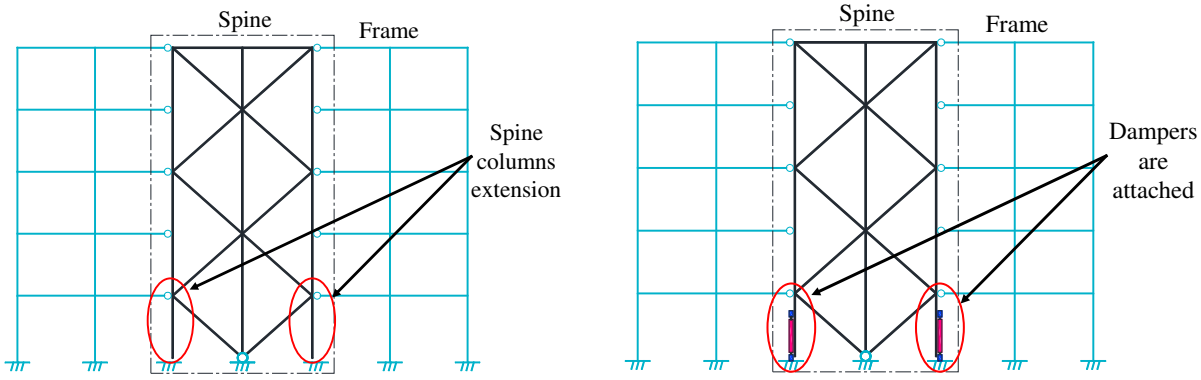

(a) Spine frame before attachment of dampers (b) Attachment of dampers

Figure 1.16. Proposed “buckling-restrained steel bar dampers” for spine frame

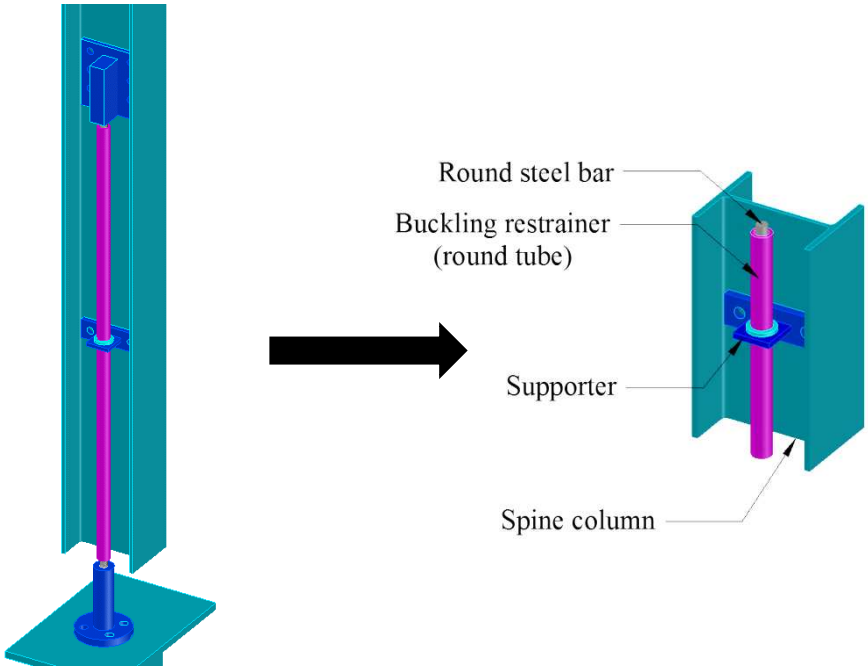

(c) Attachment to spine frame (d) Main components

Figure 1.16. Proposed buckling-restrained steel bar dampers (cont.)

The main objectives of this study are summarized as follows:

- To reveal the applicability of buckling-restrained round steel bars as dampers, as proposed in the preliminary research of Chapter 2, by performing loading tests.
- To implement the proposed damper from the preliminary research as an attachment to a spine frame system (instead of using a BRC).
- To reveal the applicability of the proposed buckling-restrained steel bar damper as energy dissipater for spine frame systems through scale loading tests of specimens with different configurations.
- To implement the proposed damper into a spine frame system of a real size building prototype sample in order to assess the practicality of its application.

1.3 Dissertation outline

This dissertation aim to reveal the applicability of “buckling-restrained steel bar dampers” as energy dissipaters for spine frame systems through experimental tests. The general content of this study is summarized as follows:

- Chapter 1 presents the background on buckling-restrained braces and spine frame systems, the dissertation objectives and the outline the dissertation.

- Chapter 2 presents a preliminary study in which experimental tests were performed to reveal the applicability of round steel bars as cores of buckling-restrained braces.
- Chapter 3 presents the main study of this dissertation, in which experimental tests on scaled specimens were performed to reveal the applicability of the proposed buckling-restrained steel bar damper as energy dissipater for spine frame systems.
- In Chapter 4, the buckling-restrained steel bar damper was implemented into a spine frame system of a real size building prototype sample to assess the practicality of its application.
- In Chapter 5, conclusions of this study are presented.

References

[1.1] Nayana S, Asha VP. Buckling Restrained Braces (BRB) – A review. International Research Journal of Engineering and Technology (IRJET) 2017 March; Vol 04, Issue 03.

[1.2] Takeda T, Takemoto Y, Furuya Y. An experimental study on moment frame with steel braces Part 3. Summaries of technical papers of Annual Meeting Architectural Institute of Japan 1972; Vol. 47: 1389-1390. (In Japanese).

[1.3] Qiang X. State of art of buckling-restrained braces in Asia. Journal of Constructional Steel Research 2005; Vol. 61:727-748.

[1.4] Takeuchi T, Iwada A. Buckling restrained braces and applications. The Japan Society of Seismic Isolation. Tokyo; 2017, p. 2-9, 18, 53, 115.

[1.5] Iwata M, Murai M: Buckling-restrained brace using steel mortar planks; performance evaluation as a hysteretic damper. Earthquake Engineering and Structural Dynamics 2006; Vol. 35:l807-1826.

[1.6] Byakuno Y, Koetaka Y, Inoue K, Morooka S. Design and experimental verification on the performance of the buckling-restrained knee brace. Steel Construction Engineering 2005; Vol.12 No.45:233-241.

[1.7] Nippon Steel Sumikin Engineering: Unbonded brace. http://www.unbondedbrace.com/ 2018 July.

[1.8] Star Seismic: Star Seismic, http://www.corebrace.com/ 2018 July.

[1.9] Ozcelik R, Dikiciasik Y, Erdil EF. The development of the buckling restrained braces with new end restrains. Journal of Constructional Steel Research 2017; Vol. 138:208-220.

[1.10] Aghara R, Tahirb M. A passive metallic damper with replaceable steel bar components for earthquake protection of structures. Engineering Structures 2018, Vol. 159: 185-197.

[1.11] Tagawa H, Nagoya Y, Chen X. Bolted beam-to-column connection with buckling-restrained round steel bar dampers. Journal of Constructional Steel Research 2020; Vol. 169:106036.

[1.12] Sarti F, Palermo A, Pampanin S. Fuse-Type External Replaceable Dissipaters: Experimental Program and Numerical Modeling. J Struct Eng (United States) 2016;142(12):Article 04016134.

[1.13] Wang CL, Liu Y, Zhou L. Experimental and numerical studies on hysteretic behavior of all-steel bamboo-shaped energy dissipaters. Eng Struct 2018;165(November 2017):38-49.

[1.14] Liu Y, Wang CL, Wu J. Development of a new partially restrained energy dissipater: Experimental and numerical analyses. J Constr Steel Res 2018;147:367-379.

[1.15] Yang S, Guan D, Jia LJ, Guo Z, Ge H. Local bulging analysis of a restraint tube in a new buckling-restrained brace. J Constr Steel Res 2019;161:98-113.

[1.16] Fujii S, Tagawa H. Experimental study on buckling-restrained braces using round steel bar cores and double steel tubes. Journal of Structural and Construction Engineering, Architectural Institute of Japan 2010; Vol. 75 No. 650:879-885.

[1.17] Fujii S. Tagawa H. Cyclic loading tests on buckling-restrained braces using round steel bar cores and double steel tubes. Joint Conf. Proc. 7th International Conference on Urban Earthquake Engineering (7CUEE) & 5th International Conference on Earthquake Engineering (5ICEE), Tokyo, Japan 2010:1133-6.

[1.18] Fujii S, Tagawa H. Finite element analysis of buckling-restrained braces using round steel bar cores and double steel tubes. Proceedings of Constructional Steel. Japan Society of Steel Construction, Tokyo, Japan 2010;18:377-382 (in Japanese).

[1.19] Takeuchi T, Chen X, Matsui R. Seismic performance of controlled spine frames with energy-dissipating members. Journal of Constructional Steel Research 2015;114:51-65.

[1.20] Qu Z, Wada A, Motoyui S, Sakata H, Kishiki S. Pin-supported walls for enhancing the seismic performance of building structures. Earthq. Eng. Struct. Dyn 2012;41:2075–2091.

[1.21] Janhunen B, Tipping S, Wolfe J, Mar T. Seismic retrofit of a 1960s steel moment frame high rise using a pivoting spine. Proceedings of the Structural Engineers Association of California 82nd Annual Convention, San Diego, USA 2013.

[1.22] Günay S, Korolyk M, Mar D, Mosalam K, Rodgers J. Infill walls as a spine to enhance the seismic performance of non-ductile reinforced concrete frames, ATC and SEI Conference on Improving the Seismic Performance of Existing Buildings and Other Structures 2009:1093–1104.

[1.23] Ma X, Deierlein G, Eatherton M, et al. Large-scale shaking table test of steel braced frame with controlled rocking and energy dissipating fuses. 9th US National and 10th Canadian Conference on Earthquake Engineering 2010, Including Papers from the 4th International Tsunami Symposium 2010;3:1914-1923.

[1.24] Marriott DJ, Pampanin S, Palermo A, Bull D. Shake-table testing of hybrid post-tensioned precast wall systems with alternative dissipating solutions. 2008 New Zeal Soc Earthq Eng 2008;(39):90-103.

[1.25] Tremblay R, Poirier LP, Bouaanani N, Leclerc M, Rene V, Fronteddu L, Rivest S. Innovative viscously damped rocking braced steel frames. Proceedings of the 14th World Conference on Earthquake Engineering, Beijing, China, 2008:Paper No. 05-01-0527.

[1.26] Blebo F, Roke D. Seismic-resistant self-centering rocking core system. Eng Struct 2015;101:193-204.

2. BUCKLING-RESTRAINED BRACES USING ROUND STEEL BAR CORES

2.1. Introduction

Buckling-restrained braces feature a variety of configurations as mentioned in Chapter 1. In this Chapter, as the preliminary research, a BRB which is composed of round steel bar cores restrained by inner round steel tubes and an outer steel square tube (Fig. 2.1) is proposed. One advantage of using round steel bar cores instead of steel plates and tubes is that the bar-ends can be connected to the structural members using screw-joints. In comparison to other type of BRB cores, the use of core bars with screw ends can simplify the assembly process. The steel core bars, which have roll-threaded screws at their ends, have sufficient plastic deformation capacity.

This study is based on the research conducted by Fujii and Tagawa (Fig. 2.2) [2.1-2.2] mentioned in Section 1.1.2, and aims to evaluate some improvements on the constructive details of the BRB. In contrast to that of the previous study, the BRB proposed in this research adopts a square outer tube section (Fig. 2.1(b)), which represents a dimensional advantage because of its larger inertia compared to that of a round tube section of the same dimension proportion. In the previous research BRB, the forces from the spacers act on the outer tube through the spacer surface. Thus, for the present research, careful attention should be paid upon the contact points between the spacers and the outer tube, as indicated by the highlighted red rectangles. Another improvement is a simplification of the brace-end connection through the use of a solid member, as presented in Fig. 2.3 (a). By contrast, the previous connection was composed of some built-up members [2.1-2.2].

Firstly, a study on two cyclic loading tests conducted to reveal the applicability and restraining performance of the proposed BRB is presented. The two loading test specimens mainly differ on the number of “contraction allowances” of the core bar, which are small spans of the core bar that are not restrained by the inner tube. They are used to allow a more uniform plastic deformation of the core when compressive forces occur, and represent a key parameter of performance comparison in this study. Secondly, a possible theoretical design method for designing the proposed BRB in a simplified and optimal way is presented.

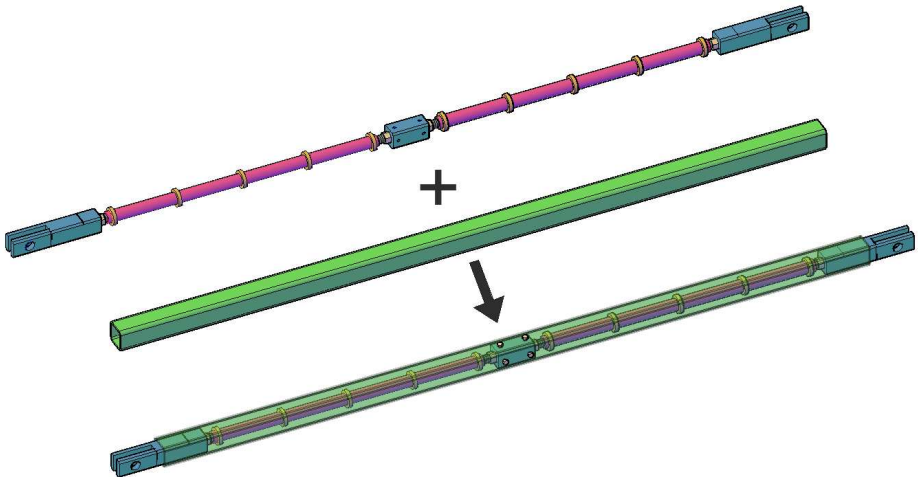

(a) 3D-view

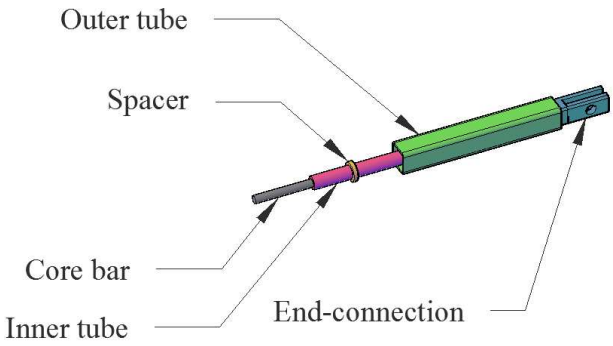

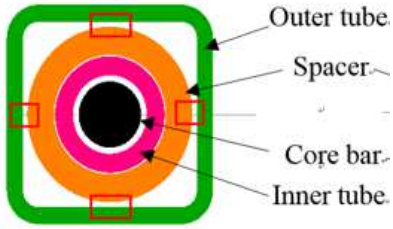

(b) 3D cut view of main components (c) Cross-section

Figure 2.1 BRB of present research

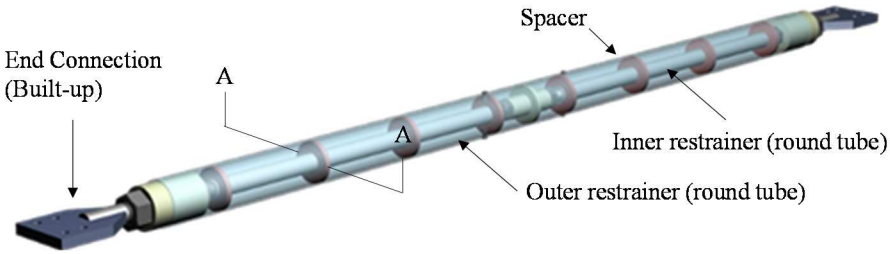

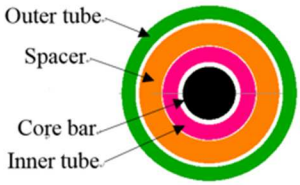

(a) (b)

Figure 2.2 BRB of previous research [2.1-2.2]: (a) 3D-view, (b) Cross-section

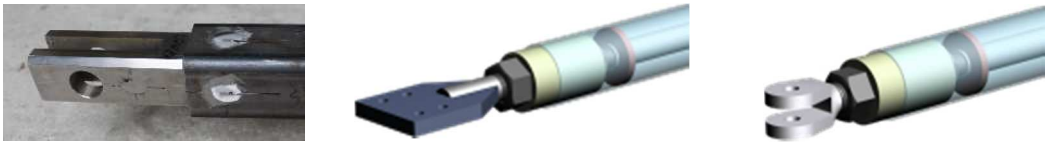

(a) (b) (c)

Figure 2.3 Comparison of brace ends: (a) Present connection, (b) Previous connection with bolts, (c) Previous connection with pin

2.2. Brace proposal

The proposed BRB and its general cross-section components are illustrated in Fig. 2.4. The main axial members are solid round steel bars (referred as "core bars") placed inside round steel tubes, which are the first buckling restrainers. Round-shaped thin plates called spacers are welded to the inner tube (Fig. 2.4(b)) to provide continuity of force transmission to the second restrainer, which is a square steel tube. By using spacers instead of filled mortar, the total weight of the BRB can be reduced dramatically.

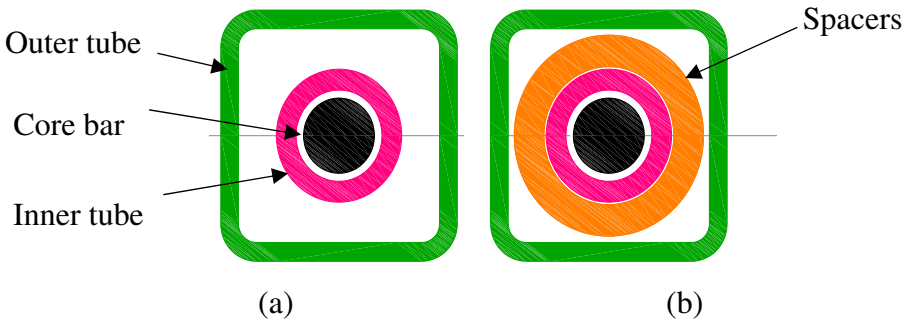

Figure 2.4 Proposed BRB: (a) General cross section, (b) Section including spacers

2.3. BRB Components

The complete assembled views of the proposed BRBs T-1 and T-2 are displayed in Fig. 2.5. They are both longitudinally and axially symmetric. Except for a few details, both specimens are practically identical. To illustrate more clearly the general configuration of the brace, the build-up process is depicted in Fig. 2.6. Both braces T-1 and T-2 adopt this assembly process, except that brace T-1 omits step 2 (insertion of springs).

As for the details of the connection, the core bars are connected at the midspan of the brace using a left-screw end to the "central coupler," which is a solid steel section whose main functions are not only to join and provide continuity to the core bars, but also to support and hold the outer tube in order to maintain the clearance between the spacers and the second restrainer. Similarly, the core bars are connected using a right screw end to the end couplers, which allow the brace to connect to the frame.

A couple of springs are inserted to increase the number of "contraction allowance zones" for brace T-2. Brace T-1 has two contraction allowance zones located near the end couplers, whereas brace T-2 has four zones located near the central coupler and the end couplers, as shown in the red circled areas of Figs. 2.5(a) and 2.5(b).

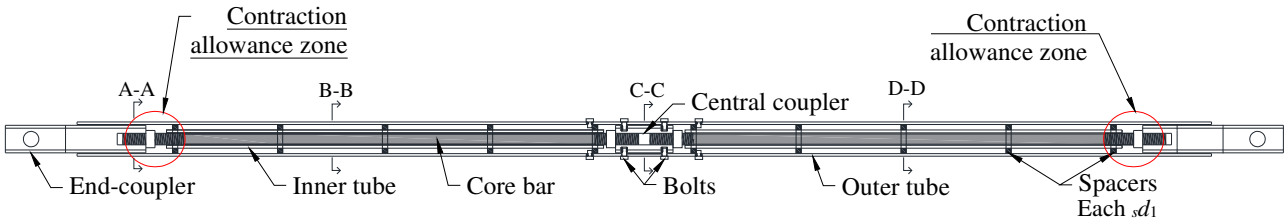

(a) T-1

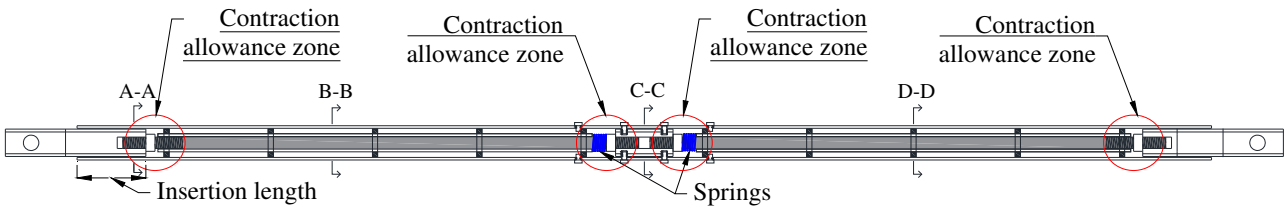

(b) T-2

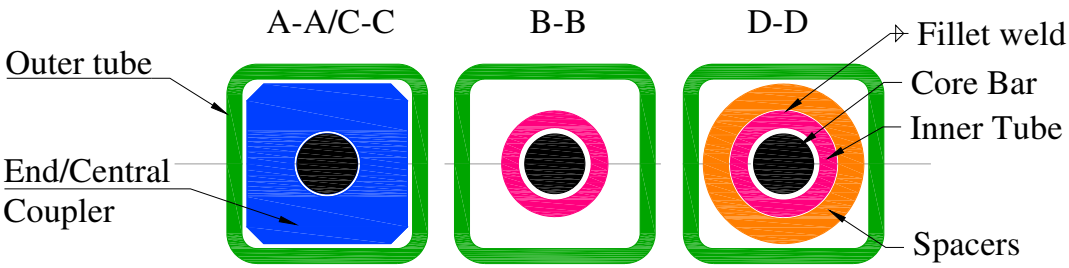

(b) Cross sections

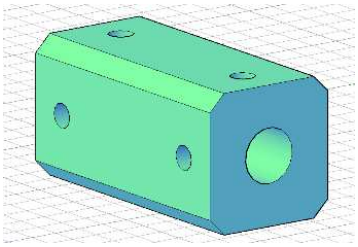

(d) Central coupler

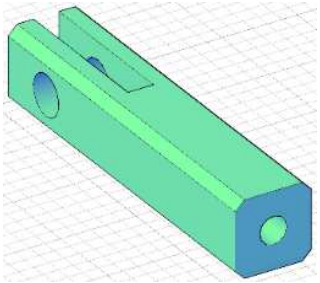

(e) End coupler

Figure 2.5 Assembled views of the proposed BRBs and their cross sections

Screw bolts are used to connect the outer tube to the central coupler at the center of the brace. Similarly, complementary screw bolts are used to limit free movement of the inner tubes in order to maintain the core bar's unrestrained spans that are within the contraction allowance zones (see also Fig. 2.12).

To avoid decoupling between the end couplers and the outer tube, to prevent out-of-plane instability, and to ensure transmission of bending moment forces between these components, a minimal distance of the end coupler needs to be inserted into the outer tube (Fig. 2.5(b)). Based on reference [2.3], this distance or insertion length L_{in} should be at least twice the coupler's width s, as defined in Eq. (2.1).

$$L_{in}/s \geq 2 \tag{2.1}$$

Clearances among the core bar and restrainers are used to isolate axial forces from the core bar to the restrainers. Fig. 2.7 portrays a graphic definition of these clearances by showing their key locations, where c_1 is the clearance between the bar screw and the inner tube, c_2 is the clearance between the core bar and the inner tube, c_3 is the clearance between the spacers and the outer tube, and c_4 is the clearance between the couplers and the outer tube.

Finally, the proposed brace is set up diagonally and pin-connected to a frame.

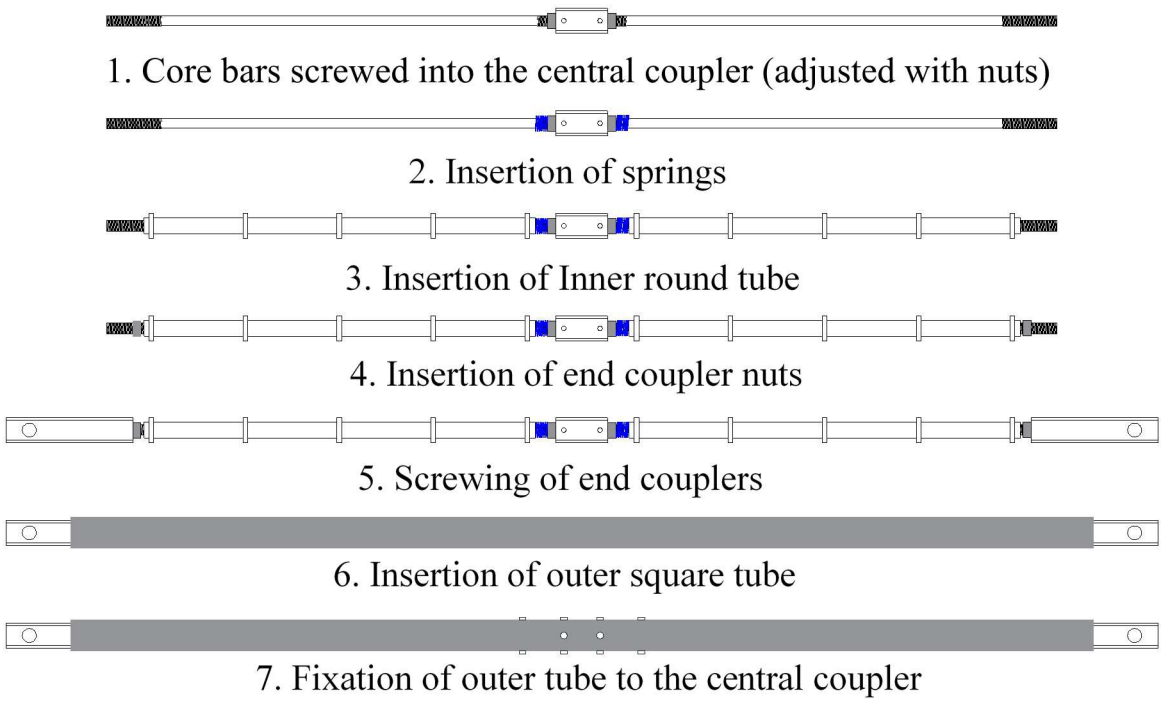

Figure 2.6 Built-up process of the proposed BRB

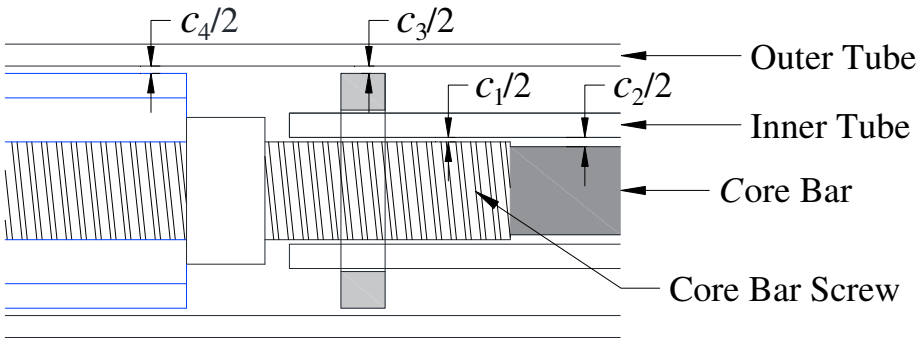

Figure 2.7 Clearances graphic definition

2.4. BRB design theory

2.4.1 Inner tube design

The components of the proposed brace are selected based on the design theory discussed in this section [2.4-2.6]. The inner tube's function is to directly restrain the core bar buckling when the bar undergoes compressive forces. Its buckling strength ${}_{I}N_{E}$ can be determined based on Eq. (2.2),

$$ {}_{I}N_{E} = \frac{\pi^2 E_{I} I}{{}_{s}d_1^{\,2}}, \tag{2.2} $$

where subscript $_I$ refers to the inner tube, E is the Young modulus of the steel material, ${}_{I}I$ is the moment of inertia of the inner tube, and ${}_{s}d_1$ is the separation between the spacers.

The inner tube shall restrain the buckling of the core bar based on Eq. (2.3),

$$ {}_{I}M_{y} > \frac{\xi N_{y} c_2}{1-\left(\xi N_{y} / {}_{I}N_{E}\right)}, \tag{2.3} $$

where ${}_{I}M_{y}$ is the inner tube flexural strength, N_y is the core bar yield strength, and ξ is an amplification factor which considers overstrength and strain hardening of the core bar. ξ = 1.5 is adopted in this study [2.4, 2.6].

To satisfy Eq. (2.3), the safety factor ${}_{I}SF$, as defined by Eq. (2.4), is considered.

$$_{I}SF = \frac{\left(_{I}M_{y}\right)}{\left(\frac{\xi N_{y} c_{2}}{1-\left(\xi N_{y} / {}_{I}N_{E}\right)}\right)} \geq 1.0 \tag{2.4}$$

2.4.2 Outer tube design

The outer tube works as an additional restrainer for both the inner tube and mainly the core bar. Its buckling strength $_{o}N_{E}$ can be determined based on Eq. (2.5),

$$_{O}N_{E} = \frac{\pi^{2} E_{O} I}{l_{k}^{2}}, \tag{2.5}$$

where subscript $_{O}$ refers to the outer tube, oI is the moment of inertia of the outer tube, and l_k is the total length of the brace (pin to pin).

The outer tube shall restrain the buckling of the inner tube and the core based on Eq. (2.6),

$$_{O}M_{y} > \frac{\left(\xi N_{y}\right)\left(c_{2}+c_{3}\right)}{1-\left(\left(\xi N_{y}\right) \Big/ {}_{O}N_{E}\right)} \quad , \tag{2.6}$$

where $_{o}M_{y}$ is the outer tube flexural strength.

To satisfy Eq. (2.6), the safety factor $_{o}SF$, as defined by Eq. (2.7), is considered.

$$_{O}SF = \frac{\left(_{O}M_{y}\right)}{\left(\frac{\xi N_{y}\left(c_{2}+c_{3}\right)}{1-\left(\xi N_{y} / {}_{O}N_{E}\right)}\right)} \geq 1.0 \tag{2.7}$$

2.5. Cyclic loading tests

2.5.1 Dimensional and mechanical characteristics of the test specimens

The main components of the proposed BRB were selected based on the design theory that was previously explained. Fig. 2.8 portrays the individual components of the test specimens to be used in this study. For the loading test, a total of two specimens were tested, which were built (Figs. 2.9 and

2.10) according to the explanation in the previous section. Their geometric details can be seen in Fig. 2.11. An inner round steel tube section with dimensions 31.8 × 5 (diameter D × thickness $_{it}$) and an outer square steel tube section with dimensions 60 × 4.5 (width B × thickness $_{ot}$) were used for both tests. The core bars have M20-roll-threaded screws at both ends and also have a non-threaded part 18.2 mm in diameter. Manufacturing via thread rolling strengthens the thread profile because of the hardening process of rolling, and thus the plastic deformation occurs only at the non-threaded part of the core bar, which is directly restrained by the inner tube. ABR product specification is issued for the anchor bolts and ensures sufficient plastic deformation capacity. Material properties of the main components of the test specimens are listed in Table 1. Both the central and end couplers were made of high-strength steel to ensure their elastic behavior during the loading test.

Among several details, the end couplers were inserted 120 mm (L_{in}) into the outer tube. Because the maximal expected elongation of the core is 40 mm, the ratio in Eq. (2.1) is expected to not be less than 1.5 during test conditions (for the maximal tension load case).

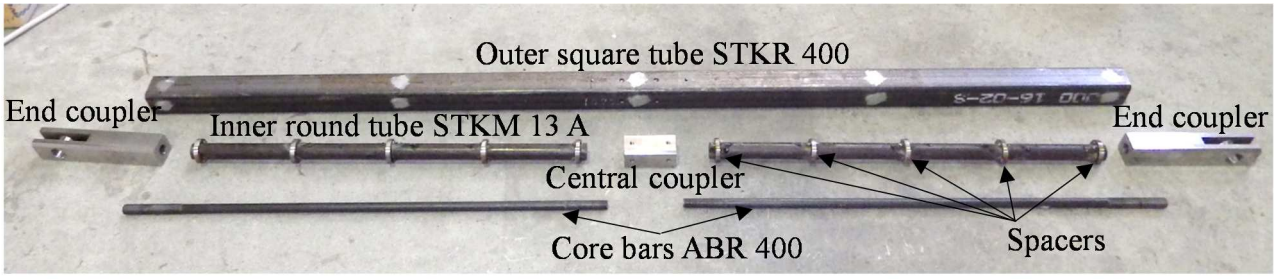

Figure 2.8. Component parts of the proposed BRB

Figure 2.9. Built-up specimen T-1: Core bars, central and end couplers, and inner tubes (prior to incorporating the outer tube)

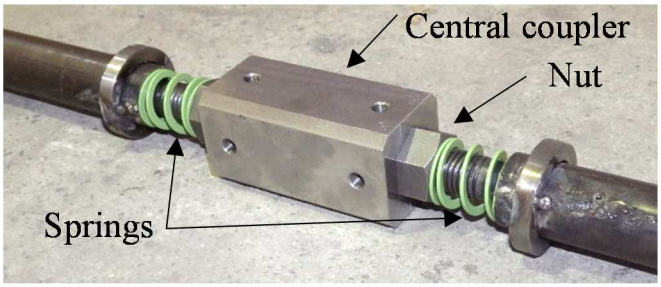

Figure 2.10 Central coupler detail of specimen T-2

Specimen T-1 has two contraction allowance zones with a length of 20 mm each for a total of 40 mm, whereas specimen T-2 has four zones: two by the end coupler, 5 mm each, and two by the central coupler, 25 mm each, for a total of 60 mm. Clearances (Fig. 2.7) are given as $c_1 = 1.8$, $c_2 = 3.6$ mm, and $c_3 = c_4 = 3$ mm. Detailed views of the central coupler zones for both specimens can be seen in Fig. 2.12.

Loading capacity characteristics of the inner and outer tubes are shown in Table 2. Prior to the test, it was decided that an overdesigned outer tube section would be used in order to focus on the deformation effects of the core bar and the inner tube. Therefore, the outer tube's safety factor is seen to have a high value.

Table 1

Material properties of the main components of the specimens

Item	Yield stress (N/mm^2)	Ultimate strength (N/mm^2)	Elongation (%)
Round steel bar	331	461	31
Round steel tube	312	492	50
Square steel tube	438	478	26

Table 2

Loading capacity characteristics of the inner and outer tubes

Item	Inner tube	Outer tube
N_E (kN)	2,389	209
M_y (kN·mm)	767	6,877
SF	1.5	2.8

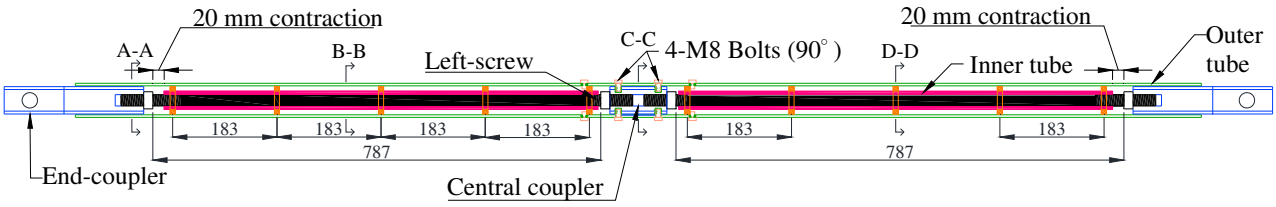

(a) T-1

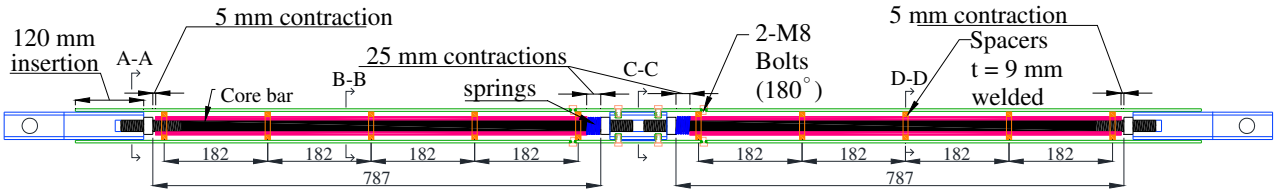

(b) T-2

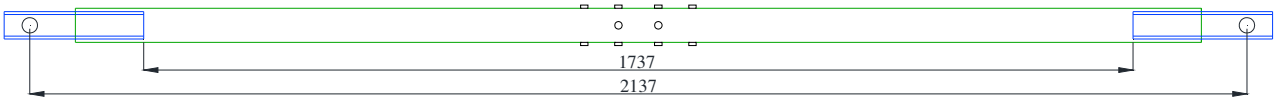

(c) Length of the brace

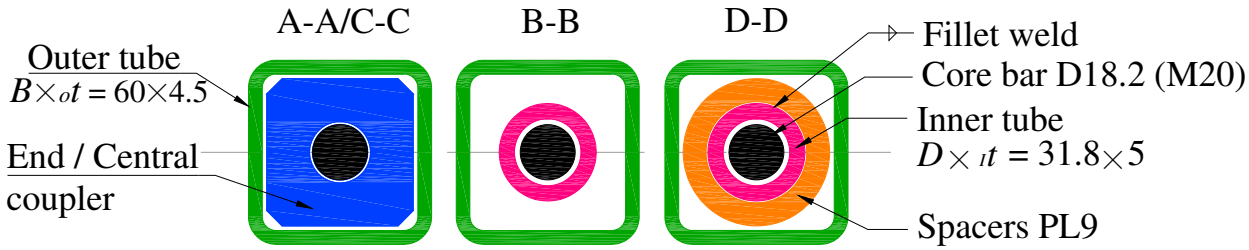

(d) Cross sections

Figure 2.11 Detail of dimensions

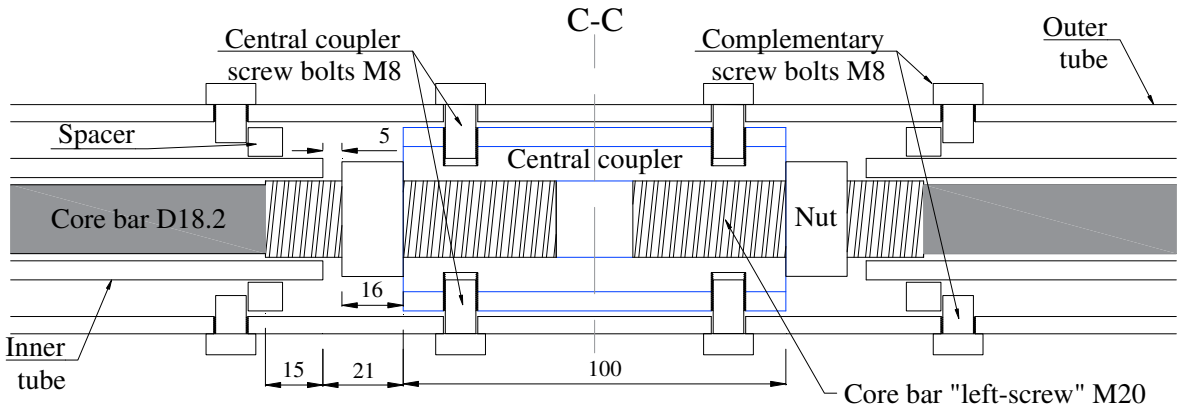

(a) Specimen T-1

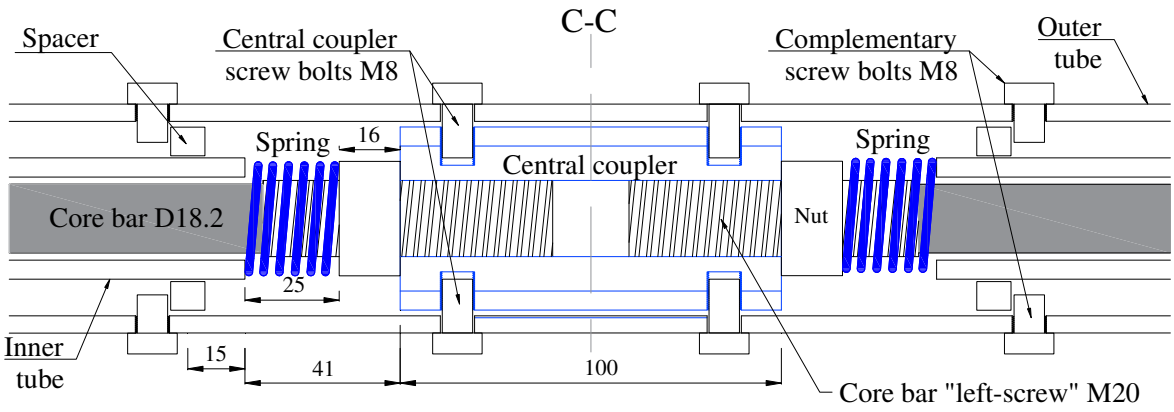

(b) Specimen T-2

Figure 2.12 Central coupler zone details

2.5.2 Test setup and loading program

Test specimens were placed diagonally and pin-connected to the loading testing frame as shown in Fig. 2.13. One displacement sensor was installed at the frame top-left to measure horizontal displacement δ, and two were installed parallel to the brace to measure axial brace deformation. Twenty strain gauges were strategically located along the brace surface to record the outer tube axial force and bending moment. Lateral cyclic loads P and $-P$ were applied in the horizontal direction by a load jack, which is located at the top right-hand side of the frame.

The axial force N and axial deformation u at the brace are obtained from Eqs. (2.8) and (2.9),

$$N = \frac{P}{\cos\theta}, \tag{2.8}$$

$$u = \delta\cos\theta, \tag{2.9}$$

where θ= 35° is the angle of the brace with respect to the horizontal.

The expected elongation of the core bar, 38.3 mm, was calculated based on the maximal expected story drift angle (R) during the test, where $R = 0.03$ rad, and on the frame dimensions. This elongation length was used as the minimum for the total free unrestrained span of the core bars for the contraction allowance zones of both specimens.

Finally, the loading program can be seen in Fig. 2.14, which compares the number of cycles against the story drift angle R (= δ/1568). The specimens were subjected to a total of 10 cycles, with two cycles at each amplitude. R was gradually increased from 0.5% up to 2.5% [2.4, 2.7-2.8].

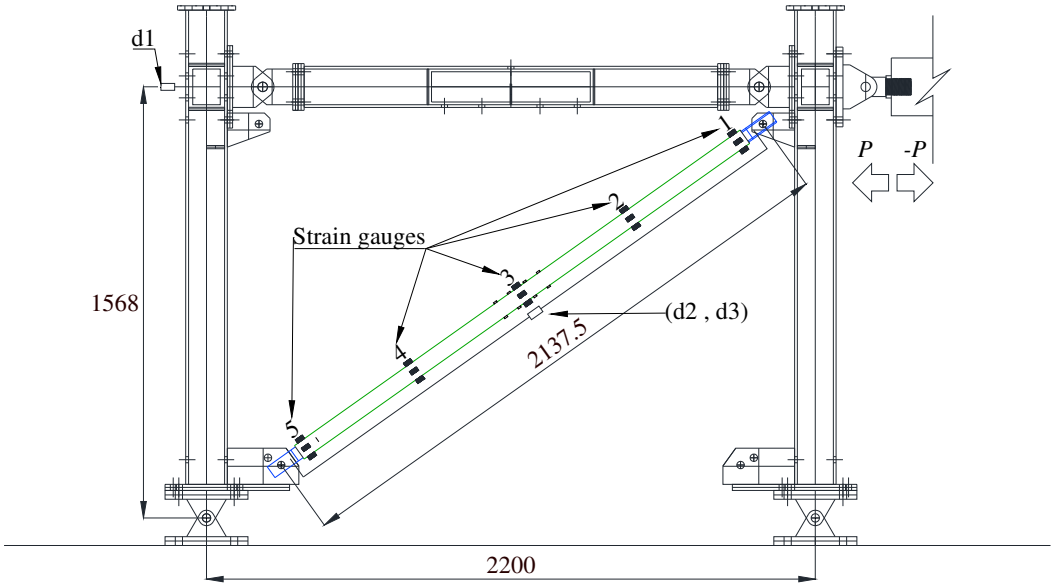

Figure 2.13. Frame dimensions and equipment of measuring devices

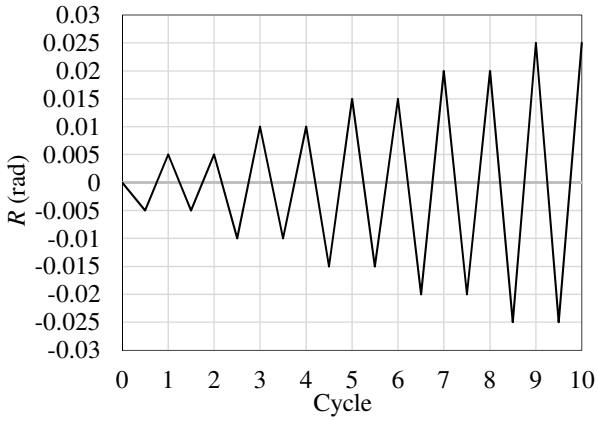

Figure 2.14 Loading program

2.6. Test results

2.6.1 Energy dissipation characteristics

Fig. 2.15 portrays test results showing the relation between brace axial deformation u and its axial force N. It can be seen for both specimens that the hysteretic loops are overall in good shape and stable, which in other words represents a good energy dissipation capacity for both specimens.

It can be observed from their performance that maximal tensile forces were practically the same for both specimens (102.5 kN for specimen T-1, 104.1 kN for specimen T-2). By contrast, specimen T-1 showed a considerably large compressive force (−151.8 kN) for R = 0.025 rad compared to that demonstrated by T-2 for the same R and cycle (−128.9 kN). The large compressive force of specimen T-1 was probably caused by concentration of deformations at the core bar's contraction allowance zones. The increasing friction between the core bar and the inner tube may had led to buckling at the contraction allowance zones, resulting in increase of compressive force on the inner tubes (Fig. 2.16). This overstrength effect on the restrainer may have led to local bulging of the outer tube or even global buckling of the brace.

As a result of the experiment on specimen T-1, steel springs were considered for specimen T-2 to increase the number of contraction allowance zones and therefore improve the core bar yielding deformation and the specimen performance. As seen in Fig. 2.15, a reduction in compressive forces for specimen T-2 reveals the efficacy of increasing the number of contraction zones via spring insertion, as this leads to a more uniform plastic deformation along the wider range of the core bars.

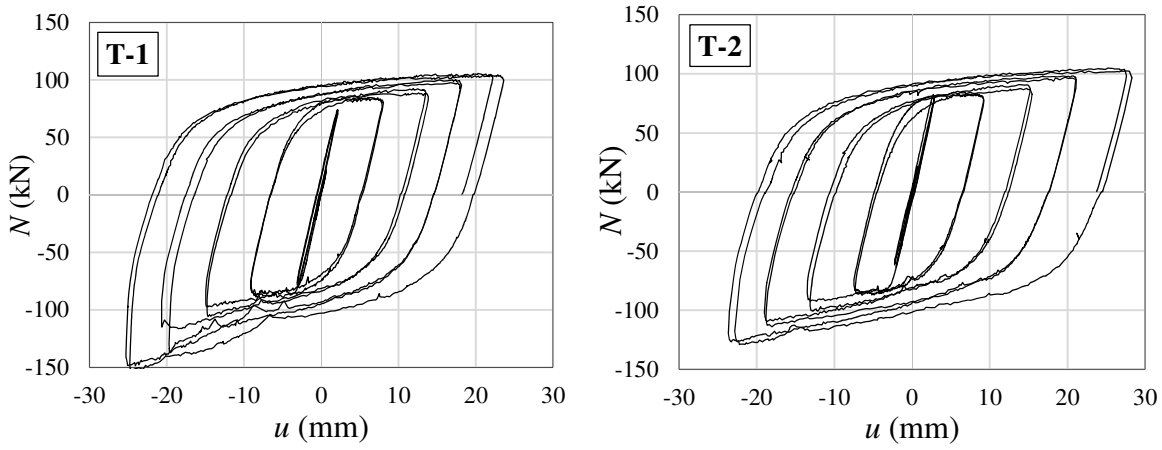

(a) Specimen T-1 (b) Specimen T-2

Figure 2.15 Brace axial force and deformation relations

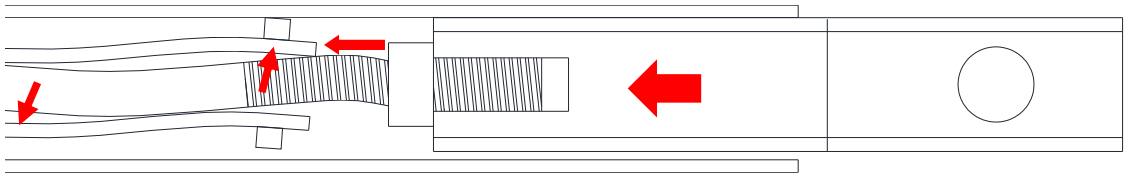

Figure 2.16 Core bar action on the inner tube (T-1)

2.6.2 Compression-to-tension ratio

Fig. 2.17 presents the variation of the compression-to-tension ratio [2.4, 2.8] β, which is defined as the ratio between the maximal compressive force and the maximal tensile force for each cycle. Within an amplitude of R = 0.01 rad, the ratios take values near unity for both specimens. However, it can be observed that the ratio β increases more rapidly for T-1 than for T-2, a result which also exhibits the efficacy of increasing the number of core contractions via utilization of springs. In Japan, the BCJ specification permits a ratio $\beta \leq 1.2$ [2.4, 2.8]. Based on these specifications, specimen T-2 overall satisfies the criterion, while specimen T-1 satisfies the criterion for story drift angle $R \leq 0.015$ rad, where no overstrength effect takes place.

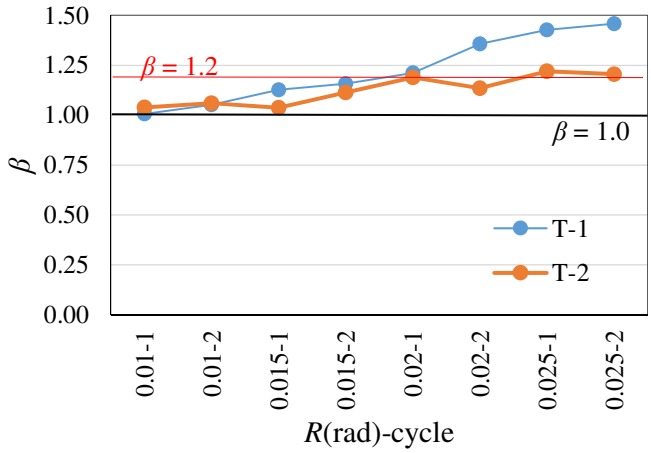

Figure 2.17 Compression-to-tension ratio

2.6.3 Variation of end coupler insertion during cyclic loads

Similar values of axial deformation were expected in both the upper and lower core bars (taking the central coupler as reference). However, it was observed that for the first specimen (T-1), the displacement of the outer tube relative to both the upper end -couplers was not symmetrical. Apparently, both core bars elongated and shrank differently, an effect which became more evident in the largest R cycles. This effect was therefore measured for specimen T-2 by recording its outer tube

axial displacement toward the end couplers, which is caused by shrinkage of the core bars during compression cycles, and displacement away from them, which is caused by the elongation of the core bars during tension cycles, at both upper and lower brace-ends for each cycle. These displacements reflect the shrinkage and elongation, respectively, of the core bars.

Fig. 2.18 portrays the measured shrinkage of the upper and lower core bars for each compressive loading cycle and story drift angle *R*. It can be clearly seen that shrinkage at the lower core bar increased sharply (Fig. 2.19 (a)) and was much larger compared to the shrinkage at the upper part of the brace (Fig. 2.19 (b)). In other words, the lower core bar exhibited larger buckling compared to the upper core bar.

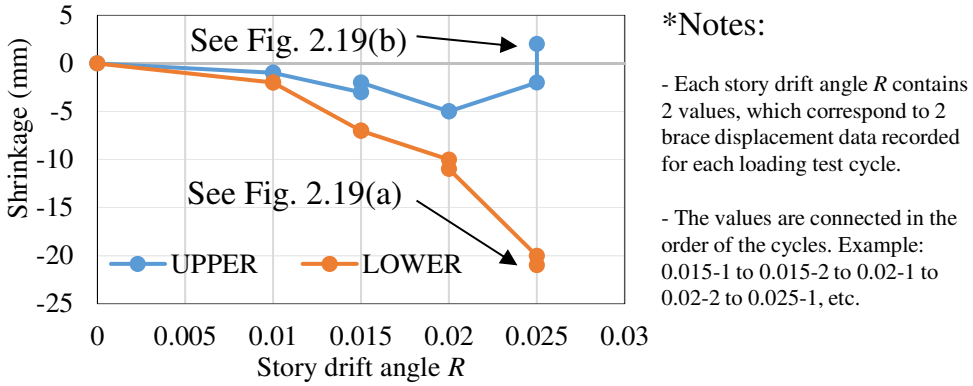

Figure 2.18 Shrinkage of the upper and lower core bars caused by compression (T-2)

(a) Lower end (b) Upper end

Figure 2.19 Effect of different shrinkage of the core bars observed at outer tube ends (T-2, *R* = 0.025)

Fig. 2.20 portrays the measured elongation of the upper and lower core bars for each tensile loading cycle and story drift angle *R*. It can be clearly seen that elongation at the upper core bar increased

sharply (Fig. 2.21 (b)) and was much larger compared to the elongation at the lower part of the brace (Fig. 2.21 (a)). In other words, yielding of the core bar was more severe at the upper part.

Overall, both core bar ends behaved differently during the cyclic loads. While the upper core bar showed a larger displacement compared to that of the lower core bar when subjected to tensile forces, the lower core bar presented a larger shrinkage during compressive forces compared to that of the upper one. This was true for both specimens. Although the reasons for this uneven deformation of the upper and lower core bars are not quite clear, it could have been induced by the weight effect of the outer tube supported by the central coupler. The weight acts on the lower core bar as compressive force and on the upper one as tensile force. This effect was very likely amplified during the final cycles, as displayed in Figs. 2.18 and 2.20.

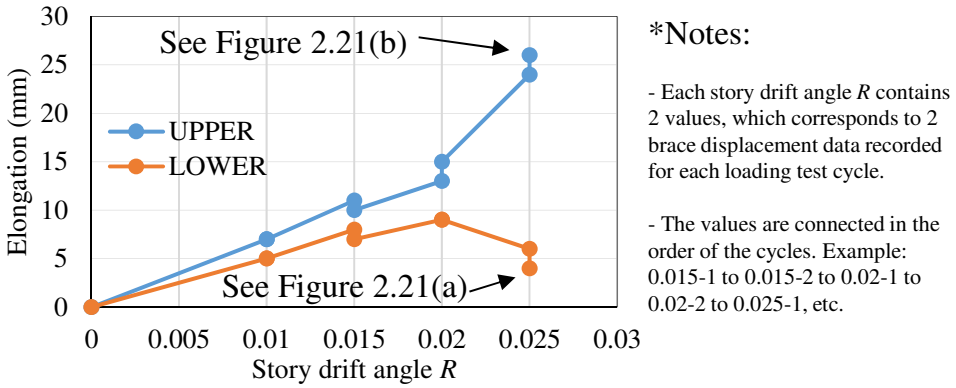

Figure 2.20 Elongation of the upper and lower core bars caused by tension (T-2)

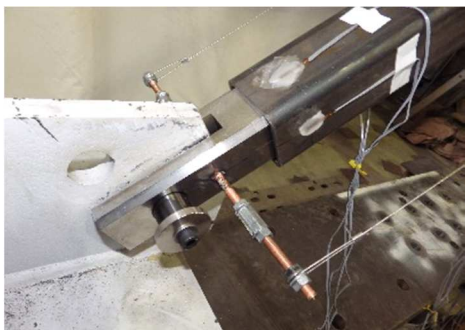

(a) Lower end coupler

(b) Upper end coupler

Figure 2.21 Effect of different elongation of the core bars observed at outer tube ends (T-2, R = 0.025)

2.6.4 Deformation of the proposed BRB elements after the loading test

Neither the outer tube nor the inner tube presented any noticeable deformation. Figs. 2.22 and 2.23 portray the outer tube axial force and bending moment measured by the strain gauges at different locations (Fig. 2.13). It can be clearly seen that axial forces are considerably below the yield strength of the outer tube, which is ${}_oN_y$ = 414.7 kN. Similarly, in-plane bending moments induced by buckling of the inner components of the brace are rather small, approximately one-fifth of the outer tube flexural strength, which is ${}_oM_y$ = 6.9 KN m.

The most outstanding buckling of the core appeared in the zones of contractions allowances for both specimens (Figs. 2.24 and 2.25). By contrast, the core bars presented slight buckling deformation along their lengths, being more noticeable for the lower part of the brace for both specimens (Fig. 2.24). Similar experimental results were found in [2.9].

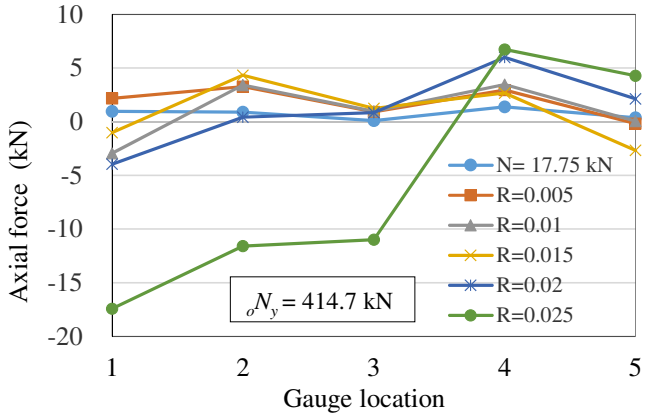

Figure 2.22 Outer tube axial force measured at different strain gauge locations

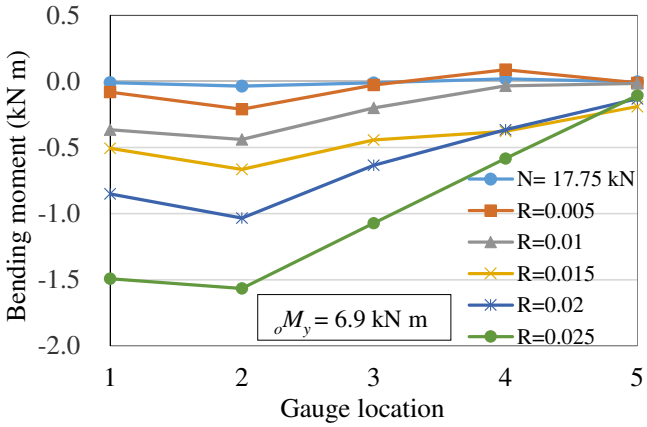

Figure 2.23 Outer tube in-plane bending moment measured at different strain gauge locations

Because the average axial forces on the outer tube did not reach more than 10kN (less than 10% of the maximal load exerted on the core bar =128.9 kN) as shown in Fig. 2.22, it can be said that friction forces between the outer tube and the spacers are likely to have small values.

Visual inspection of the inner tube and outer tube was performed. As expected, these elements did not suffer apparent deformation because their safety factor was larger than unity for both cases (Section 3.1). This was also confirmed by the data recorded by the strain gauges on the outer tube surface, as presented in Figs. 2.22 and 2.23.

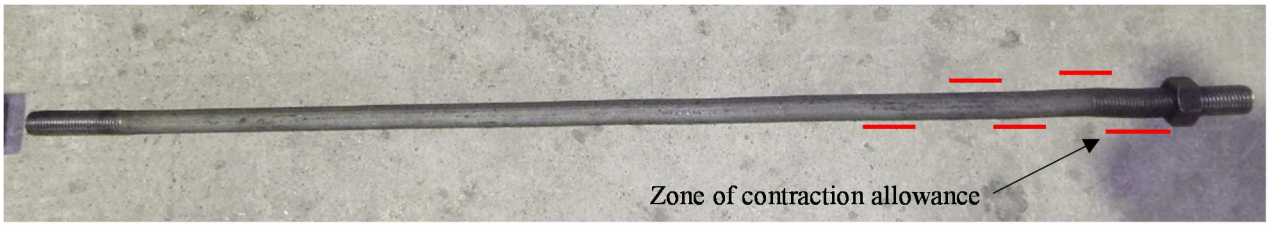

Figure 2.24 Lower core bar deformation after loading test (T-1)

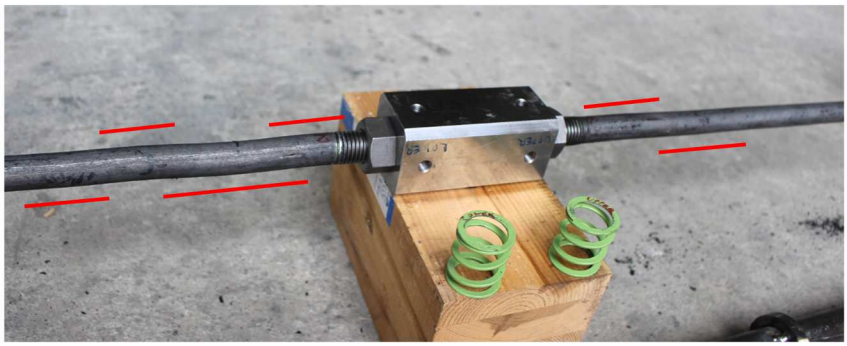

Figure 2.25 Core bar deformation at central contraction allowance zones (T-2)

2.7. Theoretical design method

A design guideline for the proposed BRB was developed because of its complexity of components. It has a scope of use for low to mid-rise buildings.

2.7.1 Design procedure for the proposed BRB

Fig. 2.26 portrays the proposed design flowchart, which highlights the recommended order of design of the respective parameters along with details of each step. Considering the proposed order

and procedure, effective design, in terms of calculation iterations to find the appropriate BRB elements and in terms of lowest weight of materials for the BRB components, will be achieved for the proposed BRB, which has equal material strength for all components. However, it is also possible to assign different material strengths for some components when necessary. Particular details for each step are described in Appendix A.

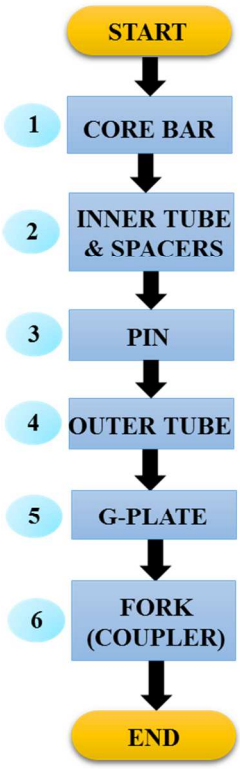

Steps:

Step 1- Design of the core bar

Step 2- Design of the inner tube and number of spacers. It is based on Eqs. (2) to (4). Three to five spacers per inner tube shall be considered for the design.

Step 3- Design of pin

Step 4- Design of outer tube: It is based on Eqs. (5) to (7).

Step 5- Design of the gusset plate

Step 6- Design of the end coupler's fork area

*Note: Details of each step are explained in Appendix A

Figure 2.26 Design flowchart

2.7.2 Comments on development of design guideline

Scope

To determine the proposed design procedure, 9 design possibilities or "Design trial conditions" are considered, as shown in Table 3. Each "Design trial condition" is a combination of one length value and one expected brace (core bar) strength value, from among the following: lengths of 3 m, 6 m, and 9 m, and expected brace (core bar) strengths of 100 kN, 300 kN, and 500 kN. With the aim of finding the most optimal sections for each design trial condition, the main objective is to determine the lightest brace section configuration.

Table 3

Tag names of design trial conditions

Conditions		BRB strength		
		100 kN	300 kN	500 kN
Brace length	3 m	1A	1B	1C
	6 m	2A	2B	2C
	9 m	3A	3B	3C

Considerations and analysis procedure

There are seven main parameters of design, namely: core bar, inner tube, number of spacers, outer tube, couplers, pin, and gusset plate. The main variables are: firstly, a yield stress σ_y of 300 N/mm^2, as example for all the steel components; secondly, a constant safety factor of 1.0, as example for all design trial conditions; and thirdly, a general design based on Eqs. (2.2) to (2.7). Other considerations are: the weight per meter of length of brace and the estimation of longitudinal components (core bar, inner tube, and outer tube) of the different design trial conditions as percentages of the total length of the brace pin-to-pin L (core bar is 0.80L, inner tube is 0.75L, and outer tube is 0.95L). The pin diameter d_p and gusset plate thickness t_p are both estimated as proportions of the coupler's width s, i.e., 0.6s and 0.25s, respectively. These proportions were selected as a result of the iterations in design of a wide range of sections for the design trial conditions.

As for the analysis procedure which was performed by using a calculation sheet, a wide range of section dimensions or "trial cases" were considered for the inner tube and the outer tube in order to find the optimal section for each design trial condition.

Background and notes on design procedure for the outer tube and inner tube

The proposed theoretical design method procedure was determined based on a series of iterative calculations for the "Design trial conditions" of Section 4.2.1. For each design trial condition, a wide range of brace sections or "trial cases" of the inner tube and outer tube was numerically and graphically analyzed.

Firstly, the number of spacers per inner tube and the required inner tube thickness $_{it}$ were compared graphically in Fig. 2.27. As the number of spacers decreases, the spacers' separation $_{s}d_1$ in Eq. (2.2) increases, and thus, the required inner tube thickness increases to satisfy Eq. (2.4). Overall, it can be

seen that for almost all BRB lengths it is impractical to use more than 6 to 7 spacers, because a larger number of these would have an insignificant effect on improving the inner tube-spacers' optimal performance and would increase the number of pieces to be welded. Therefore, it was concluded that the ideal number of spacers is between 3 to 5. This low range number is economically advantageous because the welding work time and cost are highly proportional to the number of units to be welded.

From the design flowchart shown in Fig. 2.26, it can be seen that the pin design precedes the outer tube, the gusset plate, and the coupler's fork designs. Based on the considerations written in Section 4.2.2, it was found that the optimal coupler's and outer tube's sections can be determined efficiently, provided that the pin design is performed in advance. This will be discussed further in the following paragraphs.

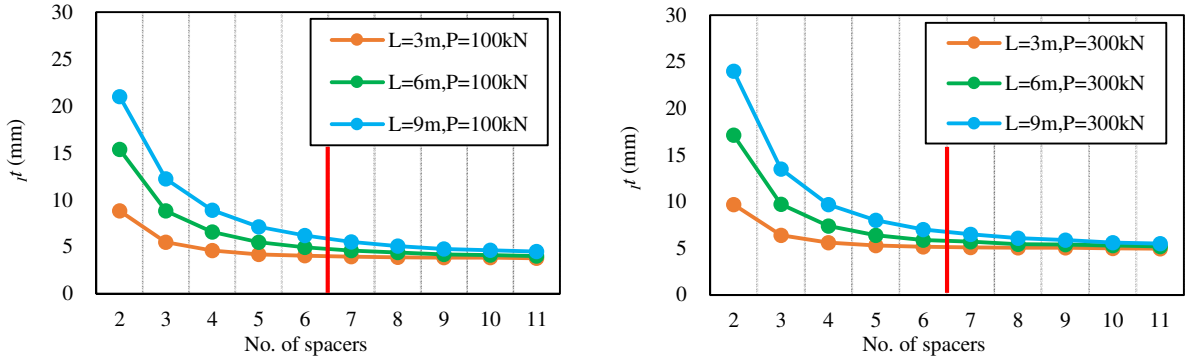

(a) 1A, 2A, and 3A (b) 1B, 2B, and 3B

Figure 2.27 Variation of the inner tube thickness vs. number of spacers

Calculation of the trial cases for each design trial condition was performed to graphically compare, via Fig. 2.28, the outer tube weight ow, the coupler weight w_c, and their combination $ow + w_c$. The lateral axis indicates the dimensions of the outer tube section $B \times ot$, where the sections are ordered in increasing values of the width B. It can be seen that as B gradually increases, ot decreases. This is because each trial-case section must preserve the same safety factor ($oSF = 1.0$). w_c was estimated by considering cross sections that fit their corresponding outer tube trial-case section and by assuming their total length along the brace to be $11s$ (based on dimensioning of test specimens). Overall, ow tends to decrease as its section becomes transversally larger. By contrast, as B becomes larger, w_c becomes considerably larger as well. However, their combined weight $ow + w_c$ shows a different perspective, revealing that the lightest section combination tends to be in the mid-range of the trial-case sections of the design trial conditions.

Designs of the pin, gusset plate, and coupler were compared for the wide range of trial cases. Considering same material properties, e.g., σ_y = 300 N/mm^2, and based on dimensioning proportions suggested in Section 4.2.2, it was revealed that the gusset plate and the coupler strength would be satisfactory provided that the pin satisfies the strength requirement $\sigma_{py} > \sigma_{pb}$, where σ_{py} is the pin yield strength and σ_{pb} is the pin's bending stress under the expected axial load. Based on the previous statements, trial-case sections that satisfy pin strength requirements ("Allowable sections-1" in Fig. 2.28) were highlighted to the right side of the red segmented line. Through the graphical comparison of the allowable sections and the general trend of all design trial conditions, the sections which slightly satisfy the pin strength requirement ($\sigma_{py} > \sigma_{pb}$) are revealed to very likely be the optimal section weight combination ("Optimal section-1" in Fig. 2.28). Therefore, through the designing of the pin prior to the outer tube and through the pre-dimensioning of the coupler based on suggested proportions, the ideal $_{O}w + w_c$ can likely be effectively estimated without carrying out a repetitive iteration process as is used in common design.

Furthermore, it is possible to modify or increase σ_{py} when necessary in order to re-dimension or reduce the pin diameter d_p. For example, large loads on braces tend to demand larger and heavier brace cross sections and, consequently, larger pin sizes (as in design trial condition 1C). Because the pin size influences the BRB design, it is possible to increase its σ_{py} to reduce its diameter and the weight and size of the combined coupler and outer tube sections. This is exemplified in Fig. 28 by considering a pin with σ_{py} = 500N/mm^2. Trial-case sections that satisfy pin strength requirements ("Allowable sections-2") were highlighted to the right side of the blue segmented line. Although, in this case, a pin design with a higher σ_{py} than that of the brace components does not provide an optimal weight $_{O}w + w_c$ for most sections (see arrow of "Optimal section-2" in Figs. 2.28(a), 2.28(b), and 2.28(c)), it can significantly decrease the BRB cross section by reducing B by about 10-15%. By contrast, strengthening the pin does not have a substantial effect on reducing $_{O}w + w_c$ (0-1% for cases 1A and 2B, and 7% for 3C), except for case 1C (Fig. 2.28(d)). For 1C, which has the shortest brace length and the largest load condition, the proposed design method with σ_{py} = 300N/mm^2 results in a wide and heavy section (150 × 2.6). However, by increasing σ_{py} to 500 N/mm^2, it is possible to find a notably narrower section (127.5 × 4.2) and to decrease $_{O}w + w_c$ considerably (by more than 40%).

Finally, the trial-case allowable sections are also narrowed down by verifying the local buckling of the outer tube with the width-to-thickness ratio $B/_{O}t$. For the allowable sections, this ratio will be smaller than $735/\sqrt{\sigma_y}$. This is 42.4 in Figs. 2.28(a) and 2.28(b), assuming σ_y = 300 N/mm^2 for the outer tube.

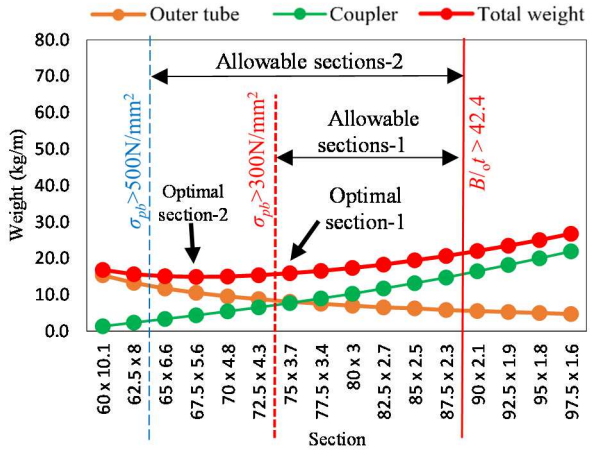

(a) 1A (L = 3 m, P = 100 kN)

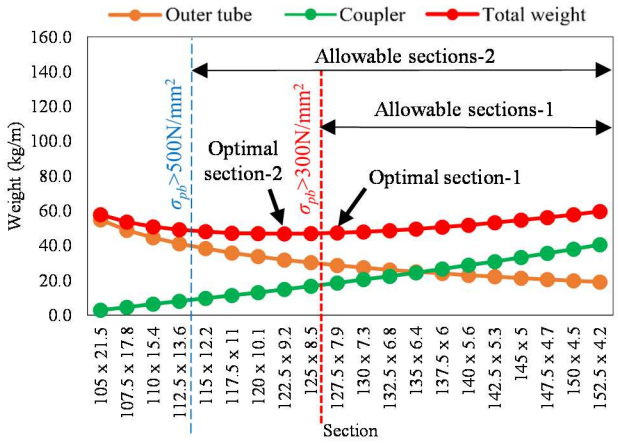

(b) 2B (L = 6m, P = 300kN)

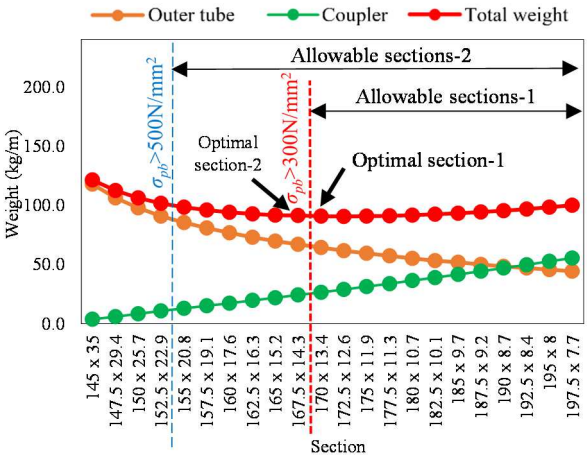

(c) 3C (L = 9 m, P = 500 kN)

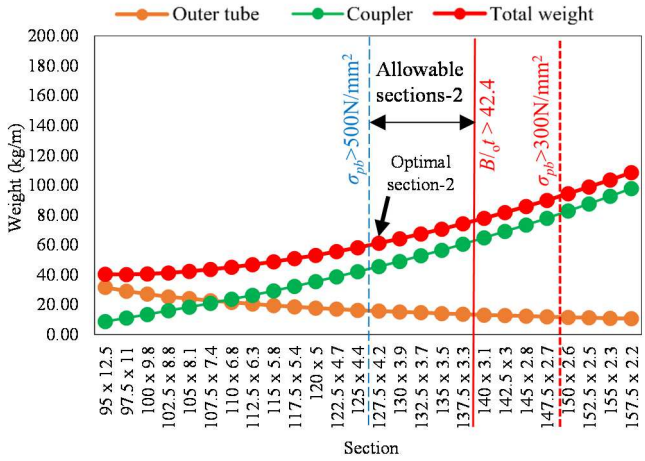

(d) 1C (L = 3 m, P = 500 kN)

Figure 2.28 Optimal combination of outer tube and coupler sections for the different design trial conditions

2.8. Conclusions

In this chapter, a buckling-restrained brace which is composed of round steel bar cores restrained by inner round steel tubes and an outer square steel tube was presented as a preliminary research.

Loading tests were conducted on two specimens of the proposed BRB; in these tests, both specimens presented good energy dissipation performance. It was revealed that when the number of

contraction allowance zones is increased, the efficacy and performance of the brace becomes more satisfactory. As for the restrainers, neither the outer tube nor the inner tubes demonstrated notable signs of deformation because sufficient safety factors were provided for both designs. Noticeable buckling was observed at the respective contraction allowance zones of the core bars. In contrast to what was expected, the buckling of the core bars was not symmetric. Whereas a larger yielding of the core bar was observed at the upper part of the brace under tensile forces, a larger shrinkage of the core bar was seen at the lower part under compressive forces. This result indicates that the inserted length of the end couplers into the outer tube should be sufficiently long. The proposed BRB of the present version has been enhanced by simplifying the coupler connection and by considering a different outer restrainer section to increase the moment of inertia of the buckling restrainer.

The second main part of this study was the proposal of a simplified theoretical design method. When similar strength material properties for all BRB components were considered, it was revealed that the outer tube and couplers represented the largest weight percentage of the brace, and that their combined weight can be optimal for coupler and outer tube sections that slightly satisfy pin strength requirements. Regarding the inner tube, designing it with the optimal and minimal sections that satisfy strength requirements was found to be possible through the use of three to five spacers for almost any given length. From the proposed design guidelines, it can be highlighted that pin design should be performed prior to the outer tube design, and that its diameter should be determined in proportion to the outer tube and the coupler's size. It can also be highlighted that the gusset plate and the fork area of the coupler should be pre-dimensioned as proportions of the outer tube and coupler section dimensions.

References

[2.1] Fujii S, Tagawa H. Experimental study on buckling-restrained braces using round steel bar cores and double steel tubes. J Struct Constr Eng Trans AIJ 2010;75(650):879-85 (in Japanese).

[2.2] Fujii S. Tagawa H. Cyclic loading tests on buckling-restrained braces using round steel bar cores and double steel tubes. Joint Conf. Proc. 7th International Conference on Urban Earthquake Engineering (7CUEE) & 5th International Conference on Earthquake Engineering (5ICEE), Tokyo, Japan 2010:1133-6.

[2.3] Takeuchi T, Ozaki H, Matsui R, Sutcu F. Out-of-plane stability of buckling-restrained braces including moment transfer capacity. Earthq Eng Struct Dyn 2014;43:851-69.

[2.4] Takeuchi T, Wada A. Buckling restrained braces and applications. Tokyo: The Japan Society of Seismic Isolation; 2017.

[2.5] Fujimoto M. Wada A. Saeki E. Watanabe A. Hitomi Y. A study on the unbonded brace encased in buckling-restraining concrete and steel tube. J Struct Engineering AIJ 1988;34B:249-58 (in Japanese).

[2.6] Architectural Institute of Japan: Recommendations for stability design of steel structures, Sec. 3.5 Buckling restrained braces, 2009 (in Japanese).

[2.7] ANSI / AISC 341-16, Seismic Provisions for Structural Steel Buildings 2016.

[2.8] Building Center of Japan. Specifications for BRB certification, 2016 (in Japanese).

[2.9] GD Corte, M D'Aniello, R Landolfo. Field testing of all-steel buckling-restrained braces applied to a damaged reinforced concrete building. J Struct Eng ASCE 2014;141:D4014004 1-11.

Nomenclature

A_b cross-section area of the steel core bar
b inner width of the outer tube
B width of the square tube
c_1 clearance No. 1, space between the core bar screw and the inner tube's inner width
c_2 clearance No. 2, space between the core bar and the inner tube's inner width
c_3 clearance No. 3, space between the spacer and the outer tube's inner width
c_4 clearance No. 4, space between the coupler and the outer tube's inner width
d inner diameter of the inner tube
D diameter of the inner tube
d_{sb} core bar screw diameter
Ns number of spacers
E steel young modulus
$_I$ refers to the inner tube
$_II$ inner tube moment of inertia

$_IM_y$ inner tube flexural strength

$_IN_E$ buckling strength of the inner tube

$_ISF$ inner tube safety factor

$_It$ inner tube thickness

L_{in} length of insertion of the end coupler into the outer tube

l_k total length of the brace (pin to pin)

N brace axial force

N_y core bar / brace yield strength

o refers to the outer tube

oI outer tube moment of inertia

$_OM_y$ outer tube flexural strength

$_ON_E$ outer tube buckling strength

$_OSF$ outer tube safety factor

$_ot$ outer tube thickness

$_Ow$ outer tube weight

P horizontal load on the frame when carrying the experiment

R story rotation angle

s coupler's width

$_sd_1$ spacers separation

t_p gusset plate thickness

u axial deformation of the brace

w_c coupler weight

β compression to tension ratio

δ lateral displacement of the brace due to load P

θ angle of the brace with respect to the horizontal

σ_y yield stress of the steel material

σ_{pb} pin's bending stress

ξ amplification factor, which considers overstrength and strain hardening of the core bar. ξ = 1.5 is adopted in this study.

3. PROPOSED BAR DAMPER FOR SPINE FRAME SYSTEM

3.1. Introduction

Spine frames are innovative systems to reduce the seismic risk of a structure by preventing weak story collapse. In Chapter 1, background on spine frames research and their implementation was introduced. As stated in Section 1.2, this study proposes the use of "buckling-restrained-steel-bar dampers", based on the concept of the BRB in Chapter 2 (as explained in Section 3.2) and similar to the BRBs in previous research by Tagawa et al. [3.1–3.5], as energy dissipation devices for the spine frame system investigated by Takeuchi et al. [3.6] (Fig. 1.15). The proposed buckling-restrained-steel-bar dampers" are composed of round steel bar cores restrained by round steel tubes Fig. 3.2 (b)). Instead of using BRCs, the spine side columns are extended to the base (Fig. 3.1 (a) enabling the proposed dampers to be attached to these columns using thin-plate elements called "supporters" which partially restrain the round tubes. One benefit of the proposed damper, in comparison to similar core bar dampers such as in Section 1.1.2 [1.12-1.14], is that its buckling length can be reduced by using supporters attached to the column web, thereby also reducing the section of the buckling restrainer. In this paper, the proposed damper design considering its particular characteristics is presented. Cyclic loading tests are conducted on 10 scaled specimens that differ with regard to the location and use of supporters, number of contraction allowance zones of the core bar, fixation method of the lower damper connection (pinned or fixed), and length of the core bar. One of the specific features of the proposed damper is its usage of the steel core bar with roll-threaded screws and non-reduced shank section as described in Section 3.1.2. Thus, the deformation characteristics at the screw portion are discussed based on the test results in Section 3.5.1.

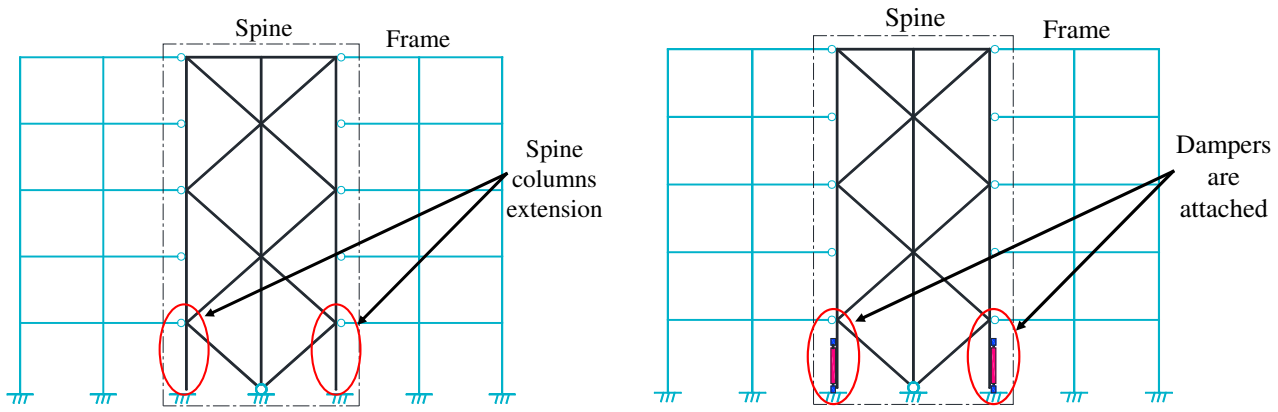

(a) Spine frame before attachment of dampers (b) Attachment of dampers

Figure 3.1. Proposed “buckling-restrained steel bar dampers” for spine frame

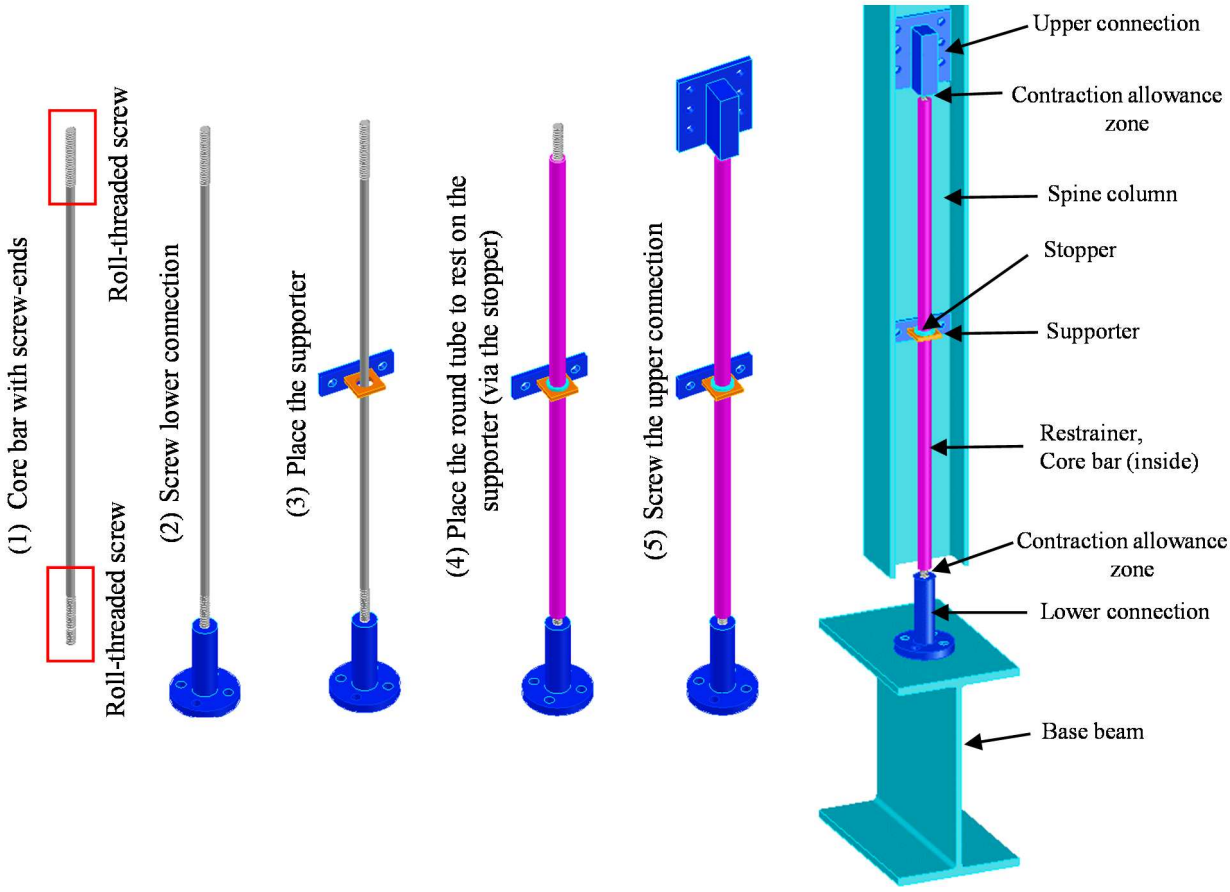

(a) Build-up process (b) Final view at spine and details

Figure 3.2. Build-up and details of the proposed damper

3.2. Outline of the proposed damper

Fig. 3.1(b) shows the position of the proposed damper on the spine frame which is composed of welded steel H-section members. The spine frame is pin-supported at the central column base and has dampers attached to the lower part of the spine columns.

The details and build-up process of the damper are illustrated in Fig. 3.2. The core of the damper is a round steel bar with roll-threaded ends, buckling restrained by a round steel tube. Through allowing the threads to be inserted into the round tube, the non-threaded part of the core bar can be ensured to be completely buckling restrained. The core bar is isolated from the round tube by clearances, as shown later in Fig. 3.9(a). Unrestrained parts of the core bar called "contraction allowance zones" are left at the ends of the damper to prevent compressive forces from acting directly on the restrainer. Thin-plate elements called "supporters" are fixed to the spine frame using bolts. The supporter function is to partially restrain lateral displacement of the round steel tube so as to reduce the buckling length. Furthermore, the supporters are used to maintain the lower contraction allowance through the use of a "stopper" which is a steel ring welded to the round tube that allows the tube to be held resting on the supporter. The core bar is screwed to the upper and lower connections. The upper connection is fixed via bolting to the spine frame, and the lower connection is bolted to the base through a pin or a fixed connection.

The design and assembly concept of the proposed buckling-restrained steel bar damper is based on the BRB proposed in Chapter 2. The main difference between them is the type of second restrainer implemented, i.e., the column web for the proposed damper and the outer square tube for the BRB of Chapter 2.

3.3. Design method for the proposed damper

3.3.1. Steel core bar

Considering the dimensions, constraint, and load on the spine frame, as shown in Fig. 3.3, the axial force demand (i.e., core bar yield strength N_y) at the damper can be calculated as

$$N_y = \frac{P_y H}{2w}, \tag{3.1}$$

where H is the total frame height measured from the pin support, w is the horizontal distance between the pin support and the damper, and P_y is the horizontal strength of the spine. Assuming the same stiffness for the screw part and the non-threaded part of the core bar, the core bar length L can be determined as

$$L = \frac{\Delta_y E}{\sigma_y}, \tag{3.2}$$

where E is Young's modulus of the steel material, σ_y is the yield stress of the core bar, and Δ_y is the expected core bar yield deformation. Further, Δ_y can be determined as

$$\Delta_y = R_y w, \tag{3.3}$$

where R_y is the expected story drift angle of design at which the damper yields.

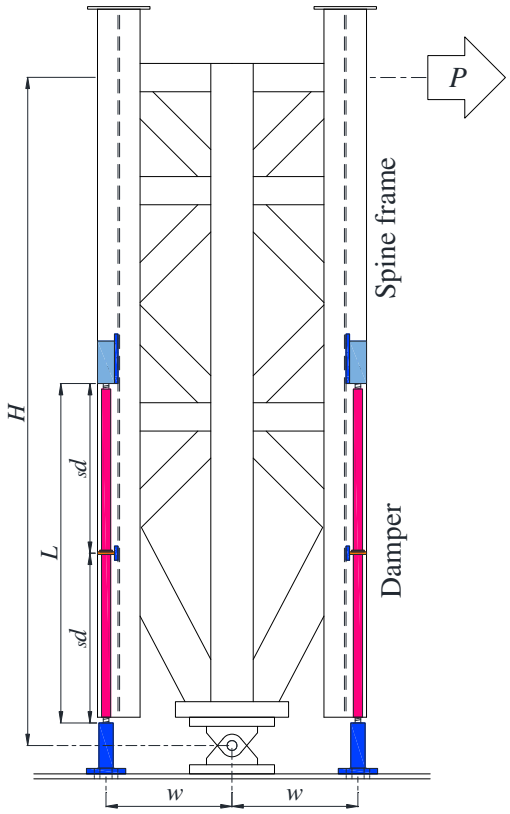

Figure 3.3. General dimensions of spine frame and damper length

3.3.2. Round tube length

The round tube length can be calculated by subtracting the total contraction allowance zone length from the core bar length L. Assuming that the damper has two zones of contraction allowance (one at each end), the length of one contraction allowance zone can be calculated as $0.5wR_{max}$, where R_{max} is

the maximal expected story drift angle of design. Thus, the round tube length can be calculated as $L - wR_{max}$.

3.3.3. Buckling restrainer

The round tube is able to restrain the core bar buckling when the bar undergoes compressive forces. Its elastic buckling strength N_E can be determined based on

$$N_E = \frac{\pi^2 EI}{{}_s d^2}, \tag{3.4}$$

where I is the moment of inertia of the round tube and ${}_s d$ is the largest separation between the supporters including the top and bottom fixed points, i.e., the buckling length.

Based on BRB design theory [3.7–3.9], the round tube shall restrain the buckling of the core bar based on

$$M_y > \frac{\xi N_y c_5}{1-\left(\xi N_y / N_E\right)}, \tag{3.5}$$

where M_y is the round tube flexural strength, N_y is the core bar yield strength, c_5 is the clearance between the round tube inner surface and the non-threaded part of the core bar, and ξ is an amplification factor that considers the overstrength and strain hardening of the core bar. $\xi = 1.5$ is adopted in this paper [3.8, 3.9]. To satisfy Eq. (3.5), the safety factor SF is considered, which is defined as

$$SF = \frac{M_y}{\left(\dfrac{\xi N_y c_5}{1-\left(\xi N_y / N_E\right)}\right)} \geq 1.0. \tag{3.6}$$

3.3.4. Supporter

Rotation of the spine frame induces axial loads on the core bar. As the core bar buckles, normal forces to the core bar axis are exerted on the supporters. These forces can result in damage to the spine column's web. Uplifting of the columns' web, as shown in Fig. 3.4(c), may be caused by the damper normal forces on the supporter. Therefore, it is a design requirement that the yielding load at the columns' web caused via uplifting P_{yw} should be larger than the damper normal forces on the supporter F_n:

$$P_{yw} \geq F_n. \tag{3.7}$$

Considering Winter's approach [3.10], F_n can be calculated as

$$F_n = \frac{2N_{\max}}{{}_s d}(\Delta_0 + \Delta) = \frac{2N_{\max}}{{}_s d}(\Delta_T), \tag{3.8}$$

where $N_{\max} = 0.95N_E$ is the maximal expected axial load on the core bar. The round-tube buckling strength N_E is used to ensure a conservative design. The total damper deflection $\Delta_T = \Delta_0 + \Delta$ considers the damper's out-of-straightness $\Delta_0 = {}_s d/500$ and the total lateral deflection owing to clearances $\Delta = c_5 + c_6$, where c_6 is the clearance between the round tube's outer surface and the supporter (Fig. 3.7(b)).

Using collapse mechanism analysis [3.11,3.12], the principle of virtual work, and considering the yield line shown in Fig. 3.4(b), the yielding load at the web P_{yw} can be calculated as

$$P_{yw} = \sigma_{yw} t_w^{\,2} \left(l/n + \pi \right), \tag{3.9}$$

where σ_{yw} is the yield stress of the column's web, t_w is the web thickness, l is the separation between bolts, and n is the radius around the bolts in which yield is expected to take effect.

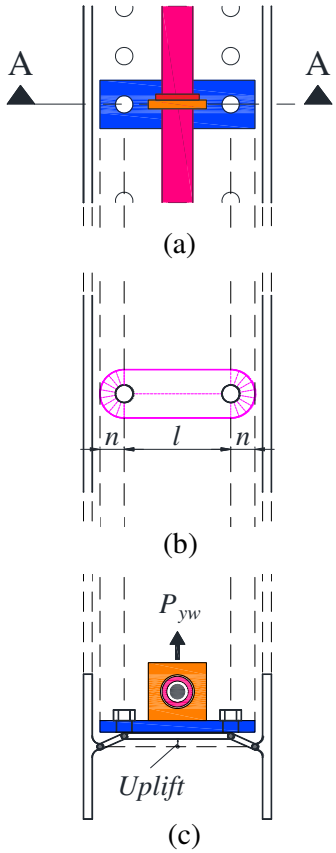

Figure 3.4 Collapse mechanism of column's web: (a) supporter, (b) yielding line, and (c) web uplift (A-A)

3.4. Loading tests

3.4.1. Test specimens

Spine frame

Fig. 3.5 portrays the general setups of the different spine frame specimens (explained later in detail), and Fig. 3.6 shows photographs with side and front views of the spine frame. The spine frame height measured from the pin support is 2363 mm, and the frame width is 800 mm. Steel section H 194 × 150 × 6 × 9 (H depth × flange width × web thickness × flange thickness) was used for the columns and the lowest two diagonal members of the spine frames. For the beams and other diagonal members, section H 200 × 100 × 5.5 × 8 was used. To allow swaying under lateral loads, the spine was pin-connected to its base using one pin joint.

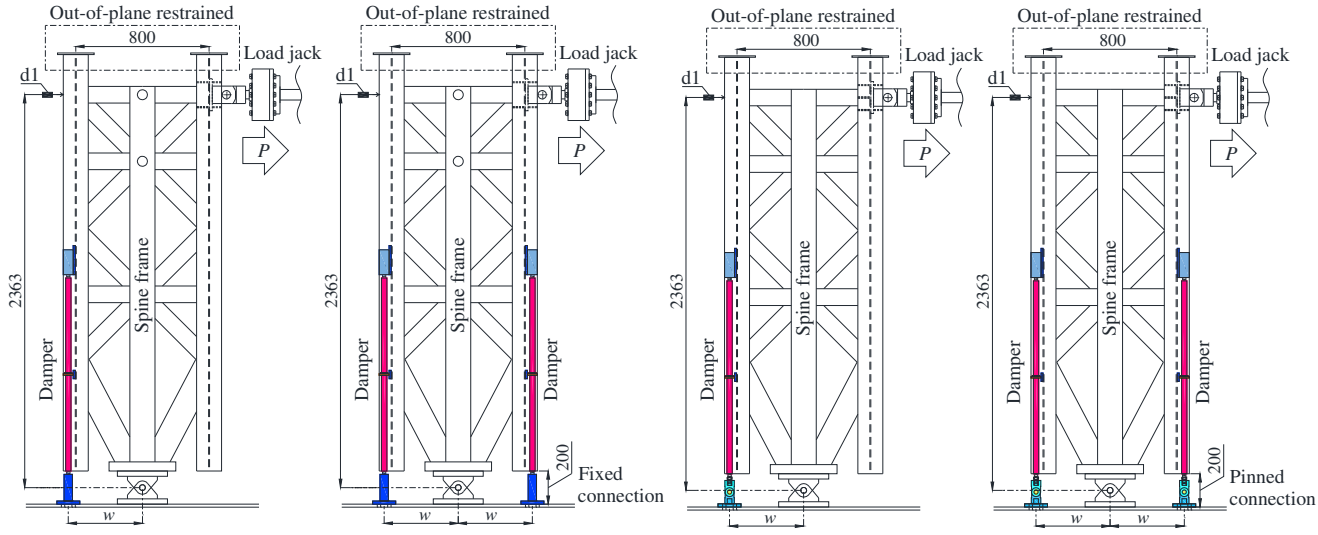

Figure 3.5 Setup of different spine configurations: (a) single fixed damper (FS1-FS6, FS1C), (b) double fixed damper (FD), (c) single pinned damper (PS), and (d) double pinned damper (PD)

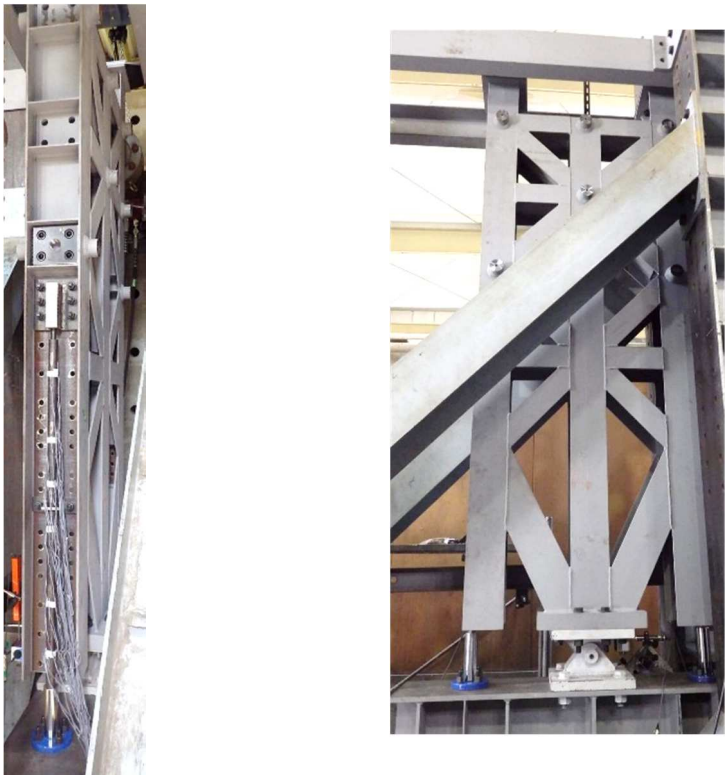

(a) Side view (FS2) (b) Front view (FD)

Figure 3.6 Photographs of test specimens

Core bar with roll-threaded screws

Considering a conventional design specification-based yield stress of 235 N/mm^2, ABR400 round steel bars were adopted for the core bars. ABR400 is originally stipulated for the ductile anchor bolts that has the roll-threaded screws at the bar ends. Satisfactory performance of this material as core bars have been revealed in Ref. [3.1,3.2,3.5]. Based on Eq. (3.1), the bars with M20 roll-threaded screws at both ends and the non-threaded part 18.2 mm in diameter were selected for the test specimens. The previous studies using steel bar cores [3.13-3.16] often apply the core bar with reduced cross-section at its middle portion as expected for plastic deformation. For that case, the cutting screws can be made at the bar-ends. Because the steel bar cores used in this study were rather long, the cost of milling down of the bar shank became notably high. Thus, this study adopted the steel bar with roll-threaded screws that were strengthened under the rolling process. An additional advantage of using the core bars with roll-threaded screws is that a small clearance between the bar shank and the round tube inner surface (c_5) can be attained. Thus, grouting such as in [3.13] is not necessary and effective buckling-restrain of the core bar can be attained according to Eq. (3.5). Because the difference in diameter between the threaded portion and the bar shank is rather small, the yield could occur in the threaded part. Nevertheless, the concentration of the plastic deformation

into the threaded portion can be avoided by proper designing of the contraction allowance zones as demonstrated in Section 3.5.1 where the performance of the threaded portions will be examined.

Buckling restrainer

An STKM 13A S round steel tube with dimensions of 31.8 × 5 (diameter × thickness) was selected based on Sections 3.3.2 and 3.3.3 as the buckling restrainer for all specimens. Clearances between the core bar and the round tube (Fig. 3.7(a)) were c_5 = 3.6 mm and c_7 = 1.8 mm, where c_5 is the clearance between the round tube inner surface and the non-threaded part of the core bar and c_7 is the clearance between the round tube inner surface and the roll-threaded part of the core bar. The clearance between the round tube outer surface and supporter c_6 (Fig. 3.7(b)) was 3.2 mm. M16 bolts were used for all connections.

The threaded part of the core bar was inserted 60 mm into the round tube, as shown in Figs. 3.9(a) and 3.9(c), to ensure that the non-threaded part of the core bar is completely buckling-restrained during the test even when the maximal elongation occurs.

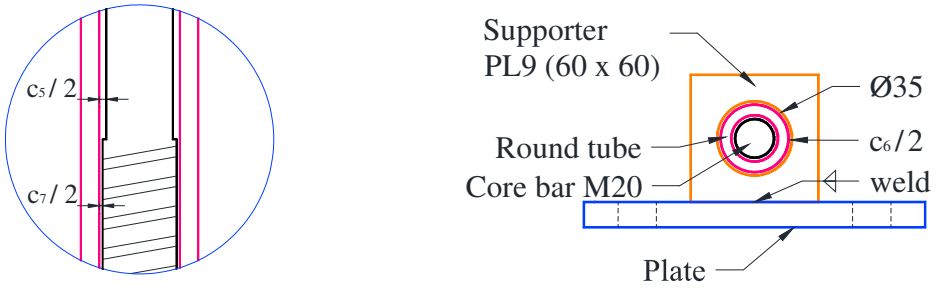

(a) Between core bar and round tube (b) Between supporter and tube

Figure 3.7 Clearance details

Detailed description of specimens

Loading tests were conducted on 10 specimens. The specimens differed in their buckling length (controlled through the number of supporters used), the type of connection to the spine frame base (fixed or pinned), the number and location of contraction allowances zones, and the total length of the damper *L*. Spine specimens (Fig. 3.5) have either a single or double damper configuration. Single damper configurations were used for most specimens because damper characteristics such as compression-to-tension ratio cannot be examined using the double damper configuration, as dampers on both sides of double damper specimens affect each other's performance. Fig. 3.8 shows the configuration scheme of the dampers, and Table 1 summarizes their main characteristics. The

specimens were identified based on their type of connection to the base (F for fixed and P for pinned) and the number of dampers used (S for single and D for double). Overall, there were six fixed single-damper configurations (FS1 to FS6), one pinned single configuration (PS), two double-damper configurations (FD and PD), and one specimen with the same configuration as FS1 but with a constant amplitude loading protocol (FS1C). All dampers except FS2 and FS3 had contraction allowance zones of 20 mm at each end. FS2 and FS3 had only one 40-mm contraction allowance zone, located at the upper and lower ends, respectively. The length of the core bar L between connections was 1200 mm for all dampers except for FS6 which was the only short damper specimen with L = 550 mm. R_y = 0.0043 rad was obtained using Eqs. (3.2) and (3.3) for L = 1200 mm, considering the steel bar yield stress as shown in Table 2. As a reference, connection and supporter details of FS1 are displayed in Fig. 3.9.

Table 1

Nomenclature and characteristics of specimens

Specimen	No. of dampers	Damper base	Core bar length	No. of supporters per damper	No. of contraction allowance zones	Supporter's separation, $_sd$ (mm)	Loading amplitude
FS1	1	fixed	long [a]	1	2	600	increasing
FS1C	1	fixed	long	1	2	600	constant
FS2	1	fixed	long	1	1 [c]	600	increasing
FS3	1	fixed	long	1	1 [d]	600	increasing
FS4	1	fixed	long	1 [c]	2	1150	increasing
FS5	1	fixed	long	2	2	400	increasing
FS6	1	fixed	short [b]	1	2	300	increasing
FD	2	fixed	long	1	2	600	increasing
PS	1	pin	long	1	2	600	increasing
PD	2	pin	long	3	2	550	increasing

a: L = 1200 mm, b: L = 550 mm, c: at upper end, d: at lower end

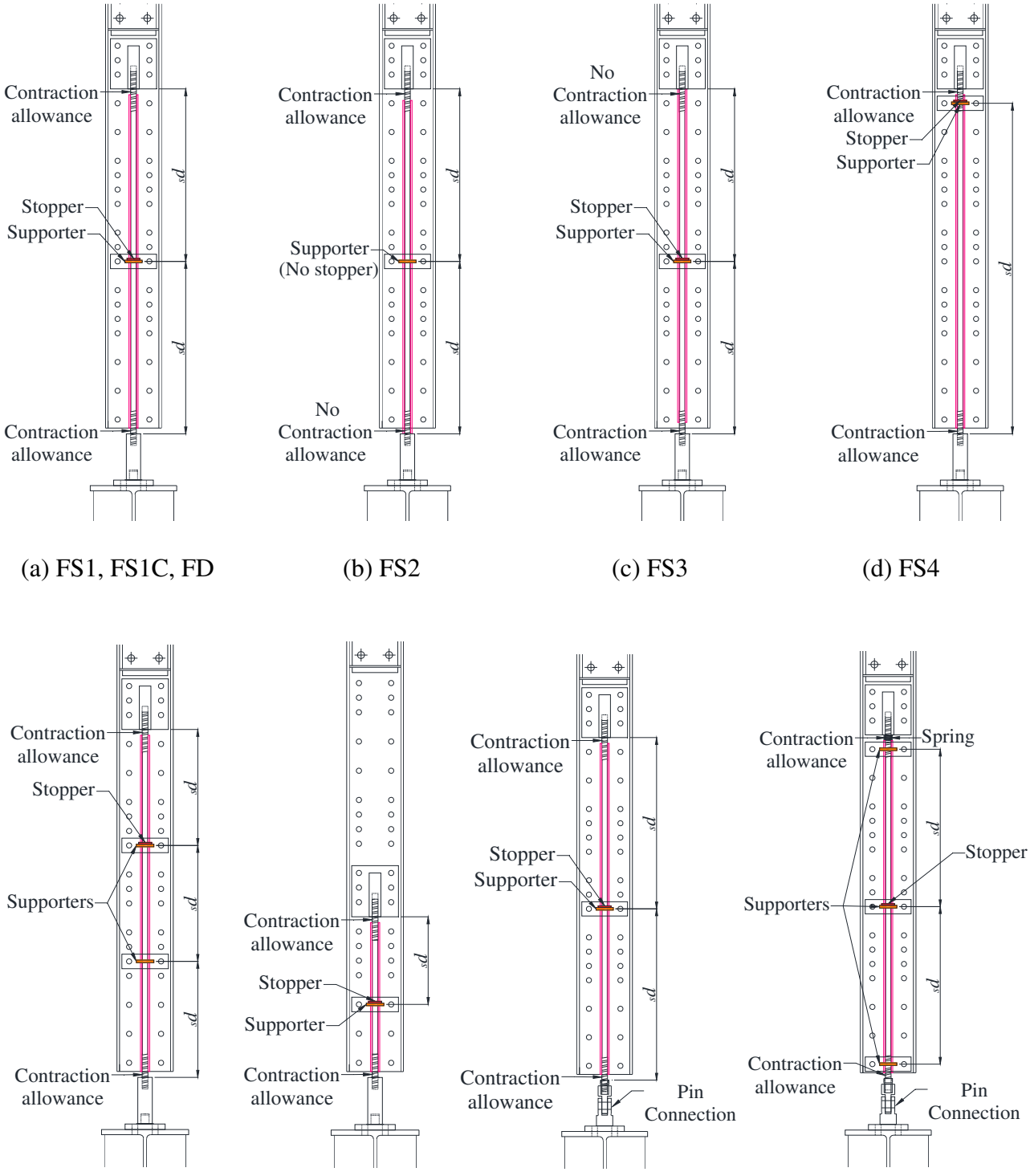

Figure 3.8 Test specimens with different damper configurations

Material properties based on coupon tests of the main damper components are displayed in Table 2. Based on these data, the core bar yield strength N_y (used to assess experimental results) and the round tube flexural strength M_y (used for damper design) were obtained as 87.6 kN and 831.4 kN mm, respectively. The round tube buckling strength N_E and safety factor SF of the specimens are listed in Table 3 (See Appendix B). Values of N_E for each specimen directly reflect the influence of the buckling length ${}_sd$ not only on the round tube buckling strength N_E (Eq. 3.4) but also on the buckling restraining capacity of the damper, represented by SF (Eq. 3.6). The table shows that a shorter ${}_sd$ results in higher N_E and SF values, such as in FS5 and FS6, while a longer ${}_sd$ results in lower N_E and SF values, or an insufficient SF value, such as in FS4. The upper and lower connections were made of high-strength steel to ensure their elastic behavior during the loading test.

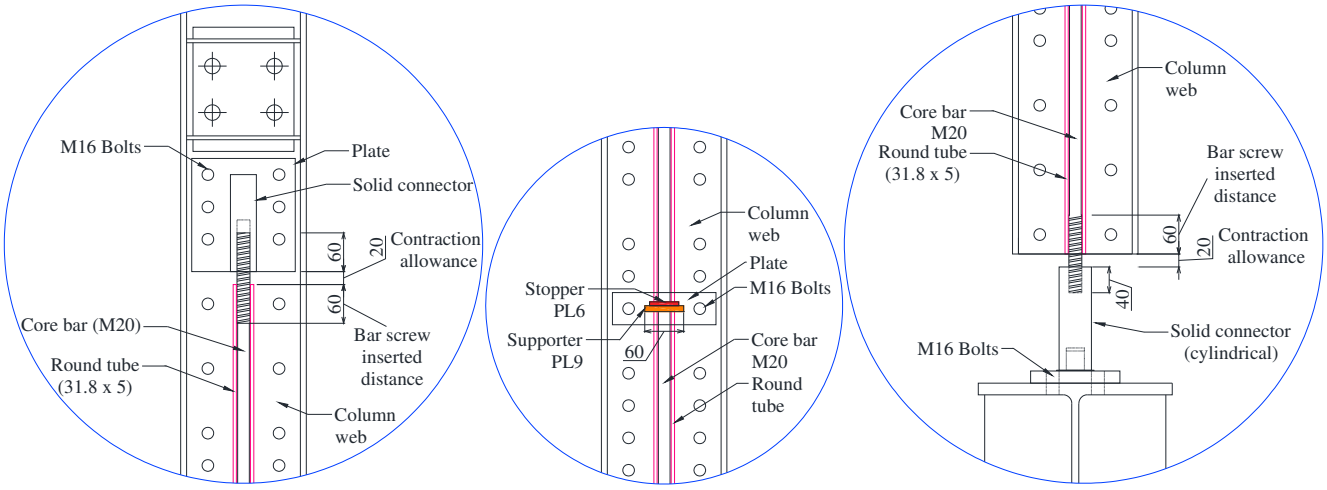

(a) Upper end (b) Center (c) Lower end

Figure 3.9. Details of connection (FS1)

Table 2

Material properties of dampers' main components

Item	Material and Geometry	Yield stress (N/mm^2)	Ultimate strength (N/mm^2)	Elongation (%)
Steel bar	ABR400 (M20, D = 18.2)	326	463	26
Steel bar (FS6 only)	ABR400 (M20, D = 18.2)	315	465	30
Round steel tube	STKM 13 A S (D = 31.8, t = 5)	338	459	59

Table 3

Loading capacity characteristics of round tubes

Item	FS1, FS1C, FD	FS2	FS3	FS4	FS5	FS6	PS	PD
$_sd$ (mm)	600	600	600	1150	400	300	600	550
N_E (kN)	220	220	220	60	494	879	220	262
SF	1.4	1.4	1.4	-	2.0	1.9	1.4	1.6

3.4.2. Loading conditions and measurements

The spine frame was pin-connected to the base beam of the loading testing frame, as shown in Fig. 3.5. Depending on the specimen characteristics, the dampers may have pin or fixed lower connections to the base beam. At the top part, the spine frame was restrained against out-of-plane displacement. One displacement sensor, denoted by d1 in Fig. 3.5, was installed at the spine top to measure top horizontal displacement u_h. Considering a rigid body motion of the spine frame, story drift angle R was obtained as u_h/H. Based on this, the expected elongation of the core bar for the largest amplitude during the test, R = 0.03 rad, was calculated as 13.4 mm.

To record strain data, strain gauges were strategically located on the round tube surface of the specimens, as shown in Fig. 3.10. While positions A and C of the round tube transversal section as shown in Fig. 3.10(b) indicate gauges that measured in-plane bending moments, positions B and D indicate gauges that measured out-of-plane bending moments. Lateral cyclic loads P was applied through a load jack located at the top-right part of the spine frame. For spine frame specimens with single damper configuration, positive direction of P and R correspond to tension forces exerted on the damper.

Finally, the loading program for all specimens except FS1C is shown in Fig. 3.11. The figure compares the number of loading cycles vs. R. The specimens were subjected to a total of 12 cycles with two cycles at each amplitude. R was gradually increased from 0.5% to 3.0% [3.9,3.17,3.18]. FS1C was subjected to 100 constant amplitude cycles with R = 0.01 rad to test the damper's fatigue capacity.

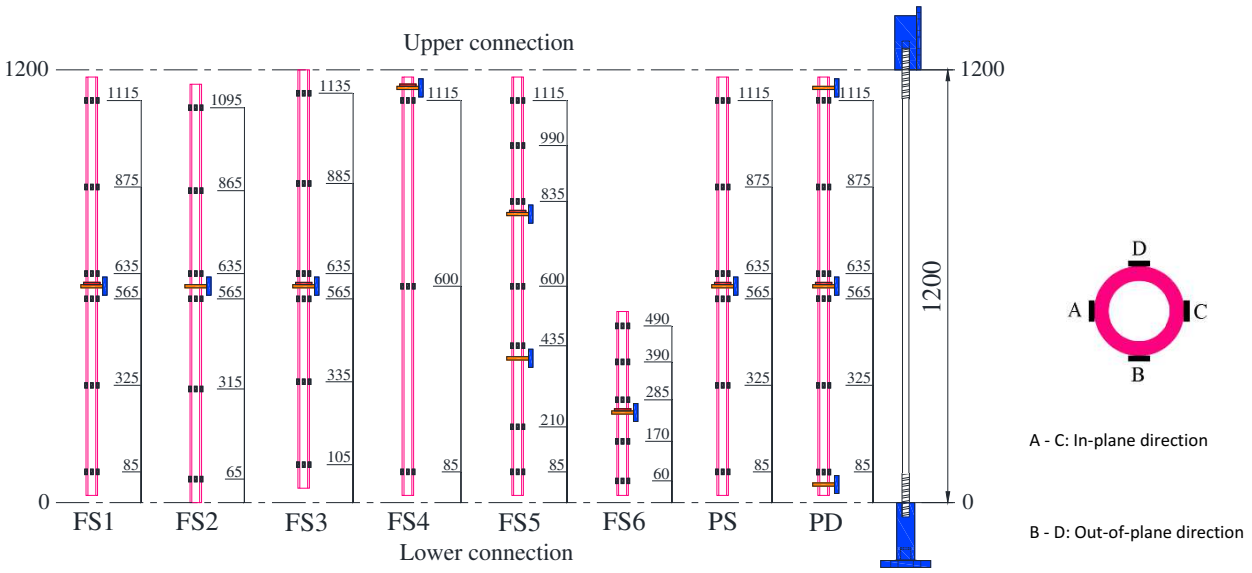

(a) In height (b) Transversal location

Figure 3.10 Strain gauge locations

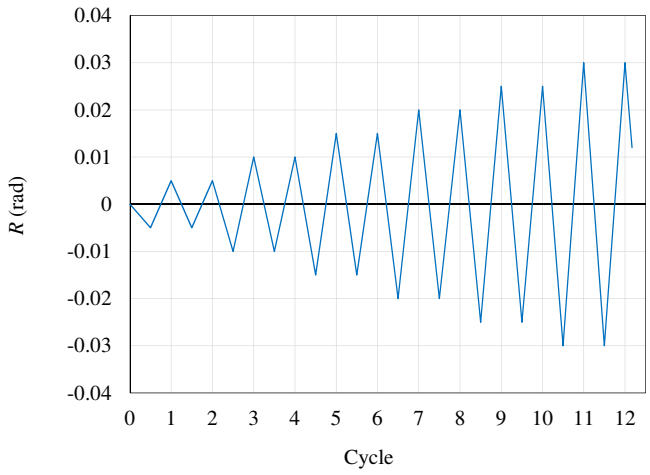

Figure 3.11 Loading program for all specimens except FS1C

3.5. Test results

3.5.1. Load deformation hysteresis and failure behavior

The results of the cyclic loading test of the specimens are presented in this section. The discussion of the test results includes hysteretic behavior (Figs. 3.12 to 3.14), initiation of local buckling, and the failure mode of the proposed damper. Loading started from the negative direction. The cyclic behavior of the test specimens was quantitatively evaluated and compared. Table 4 summarizes the

test results of all specimens. Figs. 3.15 and 3.16 show the failed and satisfactory specimens after the test, respectively.

Hysteretic behaviors for spine specimens with single damper configurations (FS1 to FS6 and PS) are presented in Fig. 3.12. The charts compare the story drift angle R and P/P_y which is the lateral load P normalized by the predicted lateral yield load P_y. The predicted lateral yield load P_y was calculated based on the measured steel strength obtained from the coupon test results. The figure shows that specimens FS3, FS4, and PS presented earlier failure behavior. Specimen FS3, which had one contraction allowance at the lower end, presented local buckling failure at the lower end during the first compression cycle for R = 0.025 rad (Fig. 3.15(b)), followed by fracturing of the screw part of the core (Fig. 3.15(c)) during the first tension cycle for R = 0.03 rad. Because the lower contraction allowance zone of FS3 is noticeably long (40 mm) in comparison to the core bar's diameter, the spine frame rotation increased the bending moment there. The hysteretic performance of FS3 shows that the specimen presented an accumulation of forces in compression, reaching a peak of $|P/P_y|$ = 1.46 in comparison to the tensile forces which reached only P/P_y = 1.16. Specimen FS4 presented global buckling (Fig. 3.15(d)) during the compression cycle for R = 0.01 rad. This result was expected because of the specimen's long buckling length. Specimen PS presented instability failure (Fig. 3.15(g)) during the compression cycle for R = 0.02 rad. This was caused by the rotation of the lower pin support (Fig. 3.15(f)). This result demonstrated that one supporter is insufficient to provide rotation stability to the pin-supported damper.

By contrast, specimens FS1, FS2, FS5, and FS6 presented full hysteresis loops until the final amplitude of R = 0.03 rad. Among these, specimen FS2 (which had one 40-mm-long contraction allowance at the upper part) presented a similar behavior to FS3, as FS2 also had a large accumulation of forces in compression, reaching $|P/P_y|$ = 1.54, in comparison to forces in tension which reached P/P_y = 1.29. In contrast to FS3, specimen FS2 did not fail because the effect of the spine frame rotation was much smaller on the upper contraction allowance zone, since the upper connection is directly attached to the spine column. However, the specimen presented initial signs of local buckling at the upper end (Fig 15(a)) during the second compression cycle for R = 0.03 rad. Test results of FS2 and FS3 (Figs. 3.16(a) and 3.16(b)) revealed that the screw part was likely to fail if damper configurations were not well designed, which indicates a possible disadvantage of using core bars with roll-threaded screws and non-reduced shanks. The short damper specimen FS6 underwent large forces, reaching $|P/P_y|$ = 1.69 in compression and P/P_y = 1.51 in tension compared to the other specimens, whose compressive and tensile forces ranged between 1.2 and 1.3. Specimens FS1 and FS5 had the most satisfactory performance (Figs. 3.16(a) and 3.16(b)), displaying stable behavior during the cycles and similar magnitudes in both compressive and tensile forces.

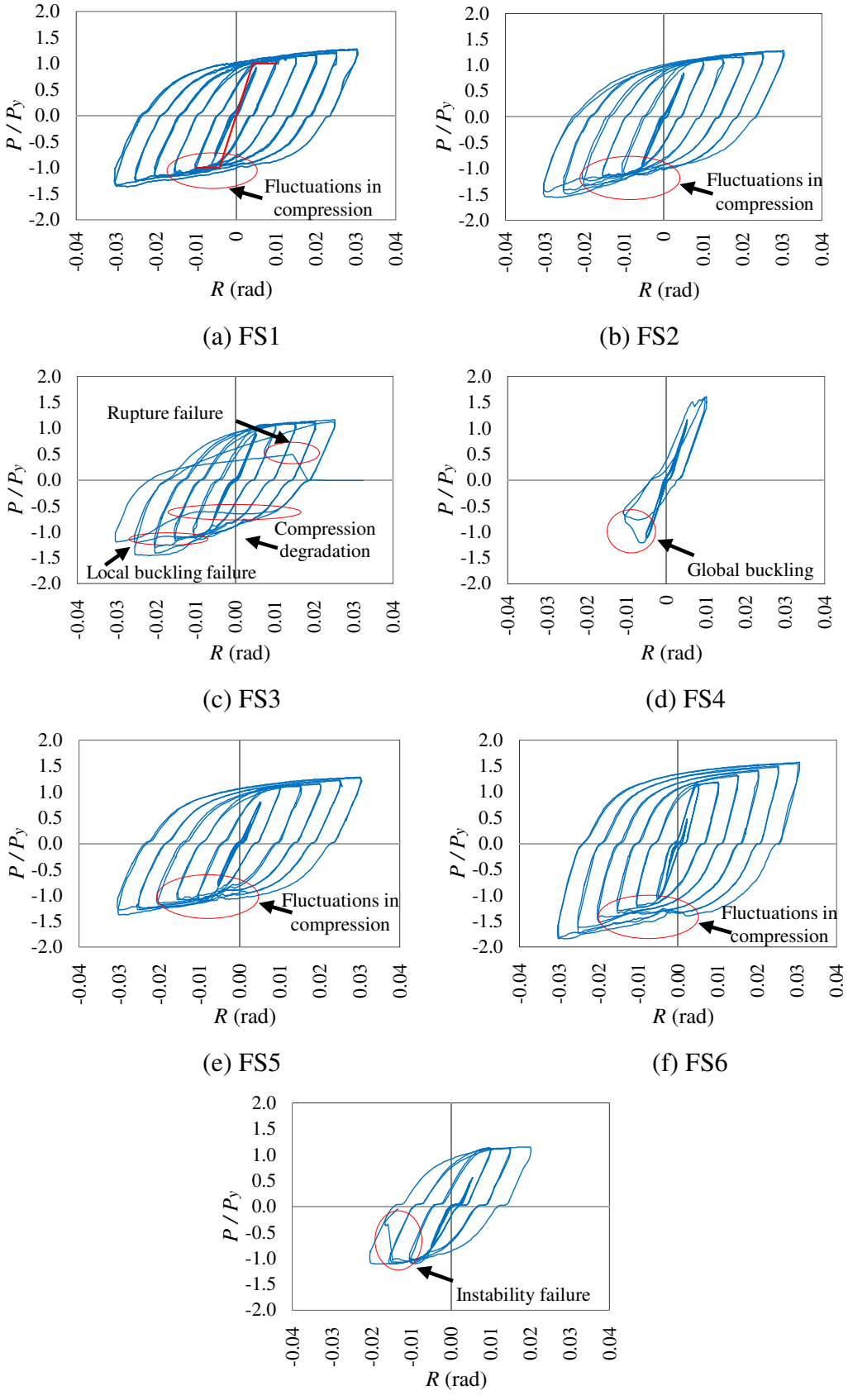

(a) FS1 (b) FS2

(c) FS3 (d) FS4

(e) FS5 (f) FS6

(g) PS

Figure 3.12 Lateral load and story drift angle relations for single-damper configuration specimens

Finally, specimens FS1, FS2, FS5, and FS6 presented fluctuations during compression cycles. These were probably caused by the buckling of the core bar within the restrainer. In addition, the fluctuations could have been caused by the interaction between the screw and the round tube, in which the round tube probably displaced gradually through stepping on each screw thread. Figs. 3.16(a), 3.16(b) and 3.15(e) show screw abrasion caused by this interaction in FS1, FS5 and FS6, respectively. In summary, specimen FS1 was regarded as the most suitable among the specimens because it is simpler in terms of build-up and because it requires only one supporter in comparison to FS5. The red line in Fig. 3.12(a) indicates the predicted stiffness and strength of specimen FS1, which was calculated using Eqs. (3.1), (3.2) and (3.3). The predicted stiffness is slightly larger than that of the test results because the calculation did not consider deformation of the bolted connections. The predicted strength is approximately in agreement with that of the test results.

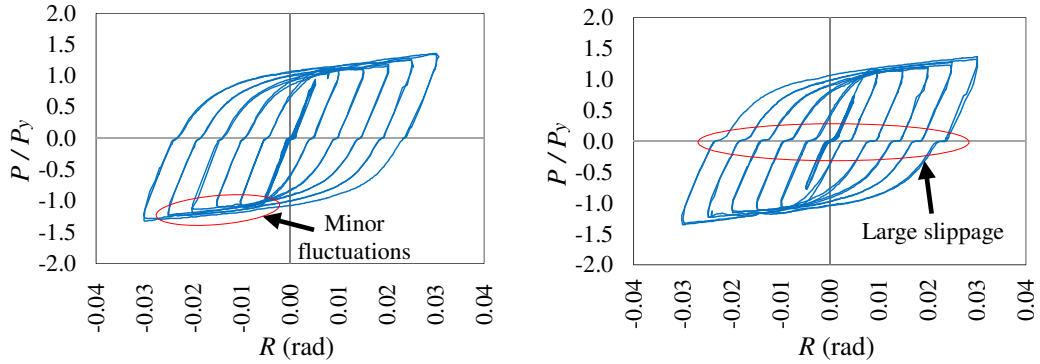

(a) FD (b) PD

Figure 3.13 Lateral load and story drift angle relations for double-damper configuration specimens

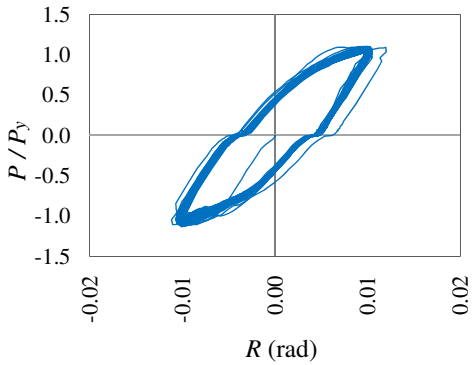

Figure 3.14 Lateral load and story drift angle relations for specimen FS1C

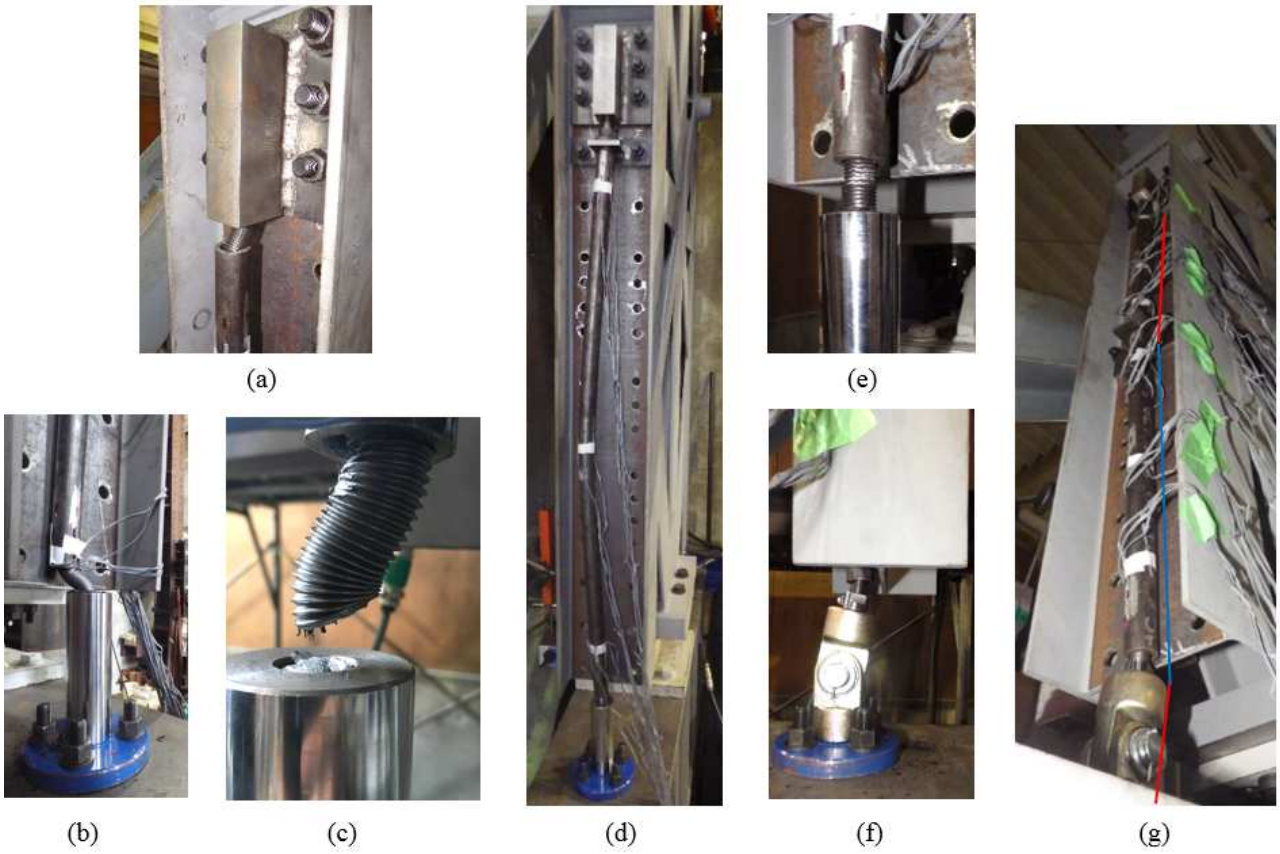

Figure 3.15 Post-test failure characteristics of specimens: (a) FS2: initiation of local buckling, (b) FS3: local buckling failure, (c) FS3: fracture, (d) FS4: global buckling, (e) FS6: effect of interaction screw-round tube, (f) PS: pin rotation caused by instability, and (g) PS: instability failure

Specimens with double damper configurations FD and PD also had a satisfactory performance. Their hysteretic behavior is presented in Fig. 3.13. Specimen FD is the two-damper version of optimal specimen FS1. In contrast to FS1, the hysteretic performance of FD seems to show a lower degree of fluctuations during the loading cycles. This is probably because FD has two dampers, in which the buckling of the core bar (caused by cyclic loads, as mentioned in the previous paragraph) of one damper is attenuated by the damper at the opposite side of the spine frame. As a result, the hysteretic diagram of FD displays an average tension and compression load that result from both side dampers undergoing opposite forces. PD is a specimen that uses three supporters to prevent instability caused by rotation of the lower pin connection, such as in PS. Specimen PD was tested to reduce the interaction between the bar screw and the round tube by allowing rotation of the lower damper support through a pin connection. No abrasion at the screw was observed, as shown in Fig. 3.16(d). Furthermore, the hysteretic loops of PD were notably similar to those of FD, but those of PD were clearer and smoother, as observed in Figs. 3.13(a) and 3.13(b). These results reflects the effect of

reduced contact between the tube and the bar screw. Nevertheless, the slippage of PD is notably larger than that of FD (Fig. 3.13), attributed to the gap at the pin connections and deformation of the base bolted connections.

Finally, a constant amplitude test was performed on specimen FS1C to examine FS1 fatigue capacity performance. The results in Fig. 3.14 indicate that after 100 cycles, the specimen did not present any fatigue failure and therefore displayed satisfactory fatigue capacity performance.

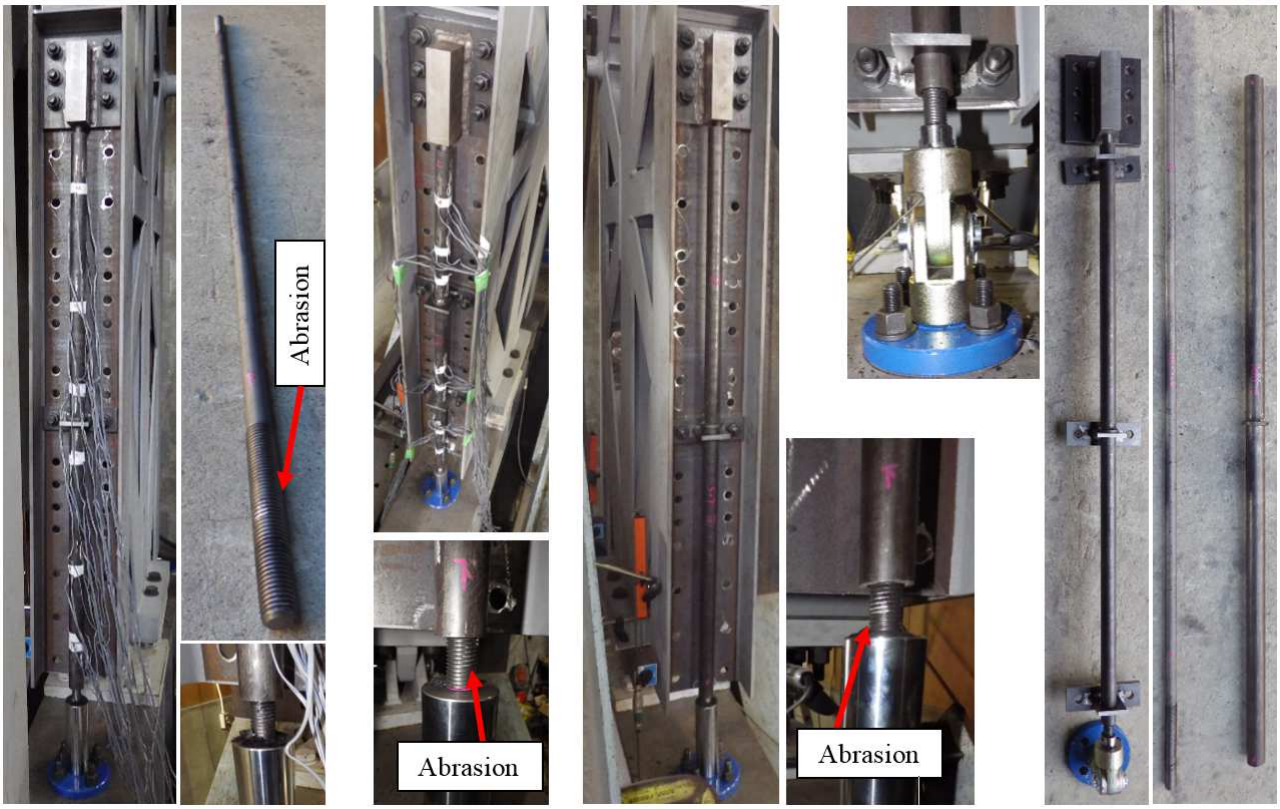

(a) (b) (c) (d)

Figure 3.16. Final state of satisfactory specimens: (a) FS1, (b) FS5, (c) FD, (d) PD

Table 4

Test results

Specimen	Max β	ω	Performance	Test result observation
FS1	1.06	1.28	Satisfactory	Optimal performance among specimens
FS1C	-	-	Satisfactory	No fatigue failure after 100 cycles
FS2	1.22	1.29	Not satisfactory	At upper contraction allowance: Initiation of local buckling at R = 0.03 rad (1C)
FS3	1.26	1.12	Not good	At lower contraction allowance: Local buckling failure at R = 0.025 rad (1C), fracture at R = 0.03 rad (1T)
FS4	-	-	Not good	Global buckling failure at R = 0.01 rad (1C)
FS5	1.07	1.28	Satisfactory	Slightly better performance than FS1, but FS5 requires more supporters
FS6	1.18	1.51	Not satisfactory	Large forces with respect to N_y because of insufficient length for energy dissipation. Highest strain hardening factor
FD	-	-	Satisfactory	Better performance than FS1. FD displayed reduced effect of bar screw and tube interaction
PS	-	-	Not good	Instability failure at R = 0.02 rad (2C)
PD	-	-	Satisfactory	Performance was slightly better than FD, but using three pins caused large slippage (0.9 mm)

(1C): first compressive cycle, (1T): first tensile cycle, (2C): second compressive cycle
- : No evaluation

3.5.2. Peak strain hardening and compression-to-tension ratio

Table 4 also shows the peak strain hardening adjustment factor ω [3.19,3.20] for each specimen, which provides an indication of the magnitude of material strain hardening. It is calculated based on the following expression:

$$\omega = T_{\max} / N_y , \tag{3.10}$$

where T_{max} is the maximal tension load for the peak cycle. Normal values of ω for the specimens that completed full loading cycles ranged from 1.28 to 1.29 except for FS6 which had a considerably larger strain hardening factor at 1.51 as a result of its short length.

Fig. 3.17 presents the variation of the compression-to-tension ratio β [3.9,3.20], defined as the ratio between the maximal compressive force and the maximal tensile force for each cycle. A β value near unity indicates equality of both compression and tension loads. In Japan, the BCJ specification permits a ratio $\beta \leq 1.2$ [3.9]. It can be observed that β is within 1.1 during all cycles for specimens FS1 and FS5, thus exhibiting satisfactory performance. Specimen FS6 is also within the acceptance criterion, reaching peak values of 1.16-1.18 for the final cycles between R = 0.025-2 to R = 0.03-2.

Specimens FS2 and FS3 only satisfy the criteria for amplitudes within R = 0.025-1 and R = 0.02-1, respectively. The peak values of β (Max β) for each specimen are also listed in Table 4.

Note that Max β and ω values of some specimens were not evaluated because the specimens either did not complete the full test, as in FS4 and PS, or were not required to estimate the values, as in FS1C. Furthermore, it was not necessary to estimate the Max β and ω ratios on specimens FD and PD which had dampers on both sides of the spine, because their respective pair of dampers underwent opposite forces, thus affecting the measurement of each damper's pure compression and tension.

First, it can be concluded from the chart that using two contraction allowance zones allows for more efficient energy dissipation performance, as displayed by specimens FS1, FS5, and FS6. By setting two contraction allowance zones, the core bar apparently yielded more uniformly along its length. Second, it can be stated that a short damper length leads to large strain demands, as reflected by ω of FS6, which increases the risk of fracture failure. A short damper length also leads to large compressive forces in comparison to tensile forces, as reflected by Max β of FS6, which may result in the buckling of weaker zones such as the contraction allowance zones.

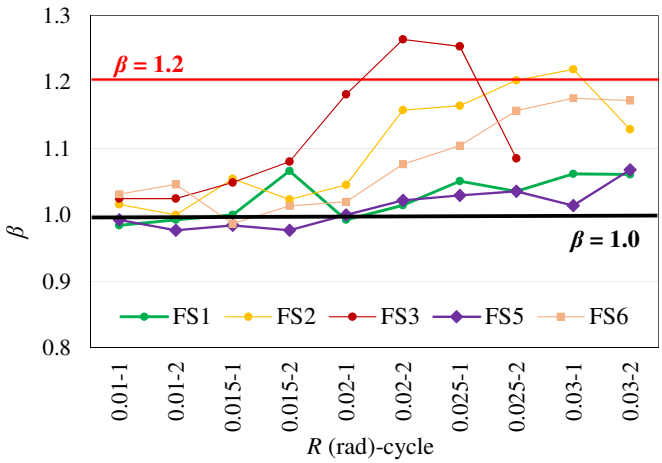

Figure 3.17 Compression-to-tension ratio

3.5.3. Round tube axial force and bending moment distribution

Using data from the strain gauges, the axial force and bending moments of the round tubes were calculated for compressive axial loads of specimens FS1, FS2, FS3, and FS6 (For other specimens, the results are not presented because earlier failure occurred (FS4 and PS), the strain was not measured (FS1C and FD), or the results were similar to those of FS1 (FS5 and PD)). Note that what all these specimens have in common is the use of only one supporter at the center. Strain was

measured in reference to the gauge positions shown in Fig. 3.10(a). Zero represents the height level at the lower end of the damper, where the core bar starts, and 1200 is the height level at the upper end of the core bar for all specimens except FS6.

First, the axial force distribution shown in Fig. 3.18 is discussed. The round tube yield strength was calculated as N_{ty} = 142 kN. Fig. 3.18 shows that the round tube axial force N_t is concentrated in the lower half of FS2, probably attributed to the specimen having only one upper contraction allowance zone (instead of two). In contrast, N_t is distributed all along the tube for FS3, attributed to a combined effect of its long contraction allowance zone, and increased friction in its contraction allowance caused by large rotations of the spine frame ($R \geq 0.025$). Note that the round tube axial force N_t for R = 0.03 rad was not displayed for FS2 and FS3, because only the elastic range force can be obtained from the strain gauge values. Specimen FS6 showed a satisfactory force distribution up to R = 0.025 rad, in which N_t was concentrated at the center of the damper (at the supporter location). However, FS6 started to exhibit larger forces in the lower half during the final cycle for R = 0.03 rad, probably resulting from the short length of this specimen. Finally, FS1 displayed a satisfactory force distribution over all cycles, with N_t concentrated mainly at the center of the damper for ranges under 20 kN.

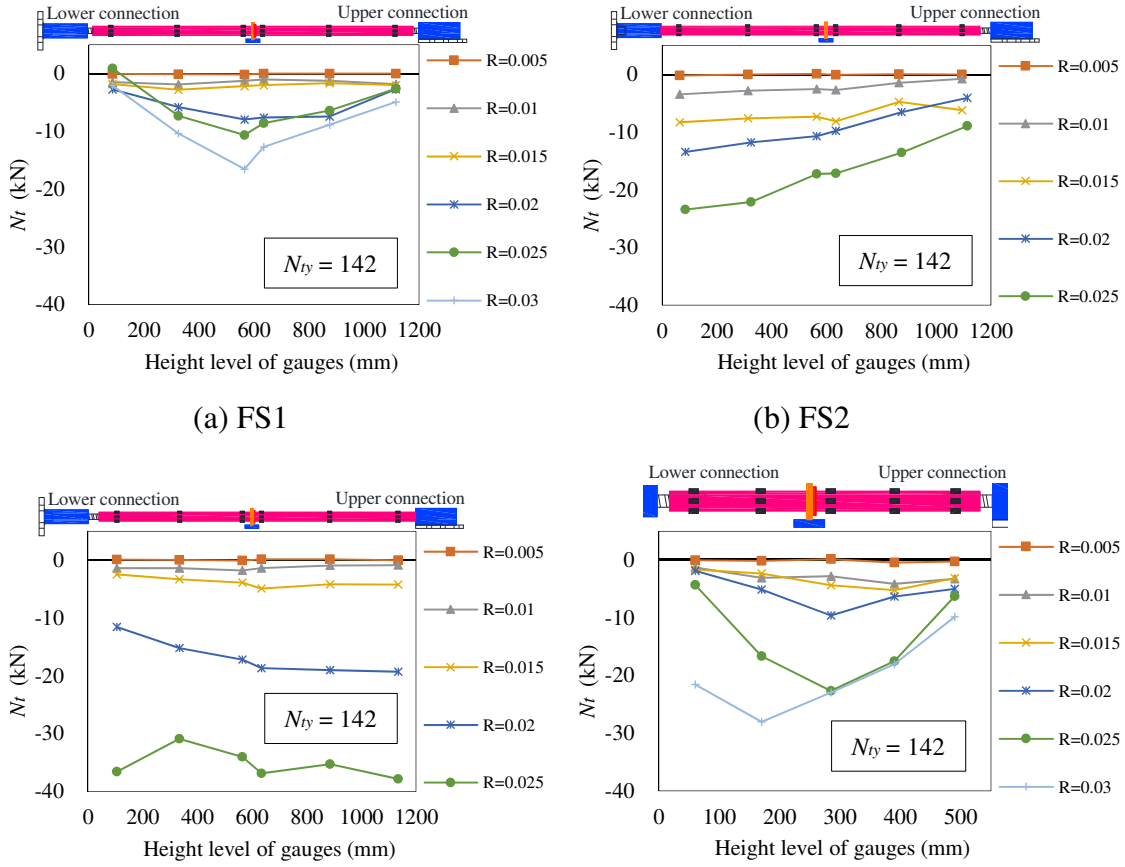

(a) FS1 (b) FS2

(c) FS3 (d) FS6

Figure 3.18 Axial force distribution in round tube

Second, the distribution of the in-plane moment $M_{A\text{-}C}$ and out-of-plane moment $M_{B\text{-}D}$ along the tube was calculated. $M_{A\text{-}C}$ distribution for specimens FS1, FS2, FS3, and FS6 is shown in Fig. 3.19. The flexural yield strength of the round tube was calculated as $M_y = 0.83$ kN m. Overall, the negative in-plane moments were concentrated in the lower half of the damper, and the positive in-plane moments were concentrated in the upper half. $M_{A\text{-}C}$ reached the plastic range during the final cycles for FS2 and FS3 at the lower and upper ends and at the supporter zone for FS6. In contrast, $M_{A\text{-}C}$ values of FS1 ranged between −0.15 and 0.2 kN m, remaining in the elastic range and displaying satisfactory performance. The out-of-plane moment was small for all specimens, and thus the graphical results are omitted in this paper. Overall, $M_{B\text{-}D}$ ranged between −0.15 and 0.1 kN m, displaying irregular distribution patterns. These patterns were probably caused because the out-of-plane direction is secondary to the main plane of forces, and because buckling of the core within the tube could take any direction as a buckling pattern [3.3].

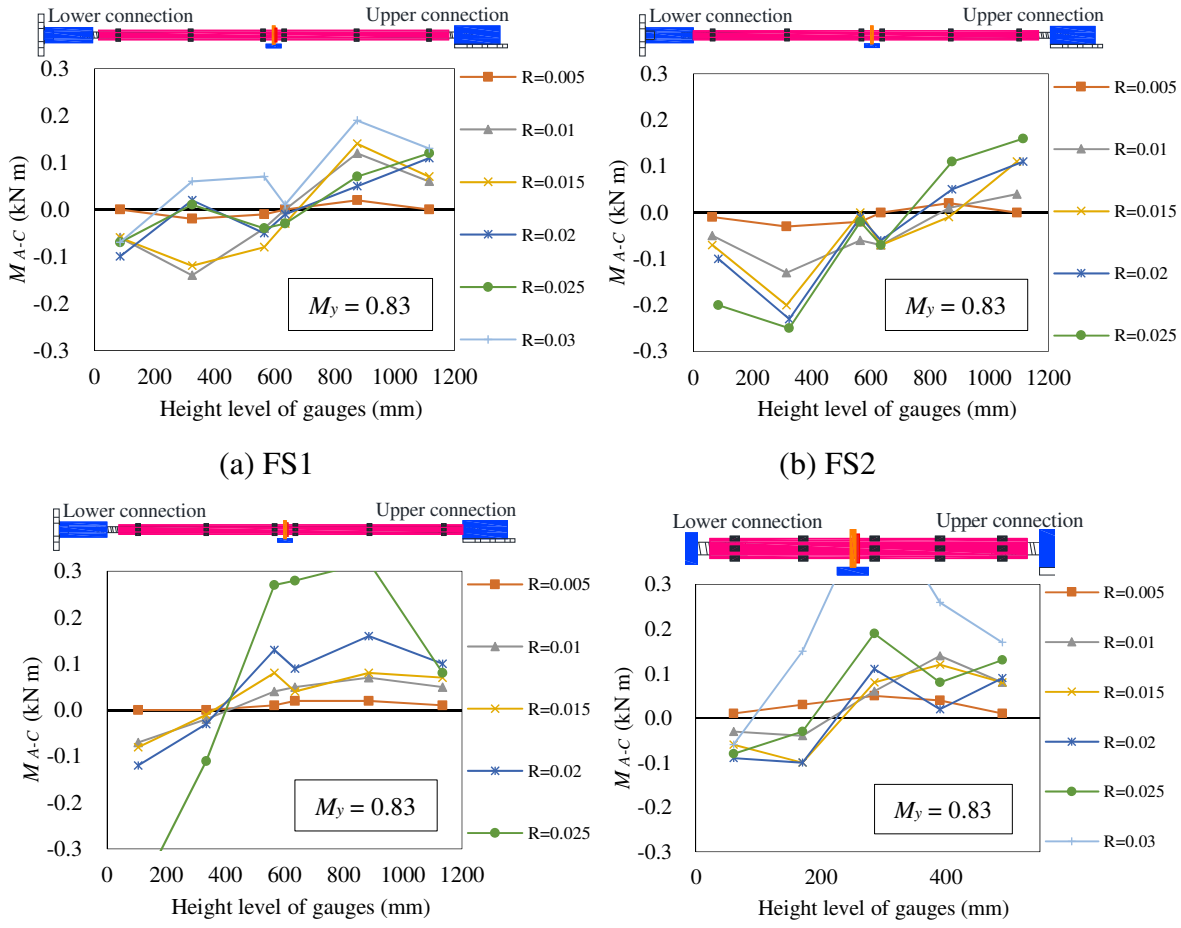

(a) FS1 (b) FS2

(c) FS3 (d) FS6

Figure 3.19 In-plane bending moment distribution of round tube

3.5.4. Performance of damper connections and supporters

Because the effect of spine rotation is considerably small at the spine base (where the dampers are located), dampers with fixed connections to the base did not present apparent damage through the loading cycles for all fixed connected specimens. Pin connections in dampers with only one supporter displayed instability, such as in PS. In contrast, pin connections in dampers with the proper number and location of supporters, as in PD, seemed to be satisfactory. At least two supporters are required if the dampers are pin-connected at the lower end: one at the lower end near the pin to prevent pin connection instability, and another one at the center to ensure proper buckling strength of the damper. Because spine frame rotation does not significantly affect the performance of dampers with fixed connections, and pin-connected dampers require more supporters and have noticeable slippage, it can be concluded that dampers that use fixed connections are preferred over pin-connected dampers.

Supporter design based on the theory in Section 3.3.4 revealed that the influence of the damper axial load on the supporter is rather small, transferring forces with ranges under 4% of the damper axial load. These results were reflected during the experiments. The supporters did not present any sign of deterioration for all specimens and thus showed satisfactory performance.

3.6. Conclusions

In this chapter, a buckling-restrained steel bar damper as an alternative energy dissipation device for a spine frame system was proposed. The damper design was presented considering its specific characteristics. Loading experiments were conducted on 10 specimens which mainly differed with regard to the number of contraction allowance zones of the core bar, number of supporters of the buckling restrainer, damper length, type of connection to the base, and number of dampers per spine. The results revealed that dampers with two contraction allowance zones and fixed connections at their base exhibit the most satisfactory performance. For that case, at least one supporter is needed at the center. The damper length should be sufficient to avoid overstress and overstrain, as these can lead to concentration of forces on contraction allowance zones (or connections) and to fracture failures.

Despite observed interaction between the core bar screw and round tube at the lower ends of fixed damper base, it was revealed that spine frame rotation does not significantly affect the lower contraction allowance zones of these dampers. Overall, the functionality and mechanical behavior of

the connections were satisfactory for all specimens. This was confirmed visually after loading experiments. The experiments also revealed that despite the slippage, pin connections can be used at the damper lower end only if the damper has at least two supporters located strategically near the pin connection to avoid instability and at the center to provide the necessary buckling strength.

An optimal spine frame specimen with two dampers was also tested using the damper configuration that exhibited the best performance among the single-damper test specimens. Lateral loads were exerted on both dampers of the proposed configuration (which underwent compression and tension at each side at the same time), resulting in average forces that react to the imposed cyclic lateral loads. Test results of the optimal specimen with two dampers confirmed the efficacy of the proposed system.

References

[3.1] Fujii S, Tagawa H. Experimental study on buckling-restrained braces using round steel bar cores and double steel tubes. J Struct Constr Eng Trans AIJ 2010;75(650):879-885 (in Japanese).

[3.2] Fujii S, Tagawa H. Behavior characteristics of buckling-restrained braces using round steel bar cores and double steel tubes. J Struct Constr Eng Trans AIJ 2011;76(659):167-174 (in Japanese).

[3.3] Fujii S, Tagawa H. Finite element analysis of buckling-restrained braces using round steel bar cores and double steel tubes. Proceedings of Constructional Steel. Japan Society of Steel Construction, Tokyo, Japan 2010;18:377-382 (in Japanese).

[3.4] Mateus J, Tagawa H, Chen X. Application of round steel bar cores and simplified end-couplers to buckling-restrained braces. The 7th Asia Conference on Earthquake Engineering (7ACEE), Bangkok, Thailand 2018.

[3.5] Mateus JAS, Tagawa H, Chen X. Buckling-restrained brace using round steel bar cores restrained by inner round steel tubes and outer square steel tube. Eng Struct 2019;197.

[3.6] Takeuchi T, Chen X, Matsui R. Seismic performance of controlled spine frames with energy-dissipating members. Journal of Constructional Steel Research 2015;114:51-65.

[3.7] Fujimoto M. Wada A. Saeki E. Watanabe A. Hitomi Y. A study on the unbonded brace encased in buckling-restraining concrete and steel tube. J Struct Engineering AIJ 1988;34B:249-258 (in Japanese).

[3.8] Architectural Institute of Japan: Recommendations for stability design of steel structures, Sec. 3.5 Buckling restrained braces, 2009 (in Japanese).

[3.9] Takeuchi T, Wada A. Buckling restrained braces and applications. Tokyo: The Japan Society of Seismic Isolation; 2017.

[3.10] Yura JA. Winter's bracing approach revisited. Eng Struct 1996;18(10):821-825.

[3.11] Tagawa H, Liu Y. Stiffening of bolted end-plate connections with steel member assemblies. J Constr Steel Res 2014;103:190-199.

[3.12] Mansfield EH. Studies in collapse analysis of rigid-plastic plates with a square yield

diagram. Proc R Soc Lond A 1957;241:311–338.

[3.13] Sarti F, Palermo A, Pampanin S. Fuse-Type External Replaceable Dissipaters: Experimental Program and Numerical Modeling. J Struct Eng (United States) 2016;142(12):Article 04016134.

[3.14] Wang CL, Liu Y, Zhou L. Experimental and numerical studies on hysteretic behavior of all-steel bamboo-shaped energy dissipaters. Eng Struct 2018;165(November 2017):38-49.

[3.15] Liu Y, Wang CL, Wu J. Development of a new partially restrained energy dissipater: Experimental and numerical analyses. J Constr Steel Res 2018;147:367-379.

[3.16] Yang S, Guan D, Jia LJ, Guo Z, Ge H. Local bulging analysis of a restraint tube in a new buckling-restrained brace. J Constr Steel Res 2019;161:98-113.

[3.17] ANSI / AISC 341-16, Seismic Provisions for Structural Steel Buildings 2016.

[3.18] Building Center of Japan. Specifications for BRB certification, 2016 (in Japanese).

[3.19] AISC 341-10 - American Institute of Steel Construction. Seismic Provisions for Structural Steel Buildings. Seism Provisions Struct Steel Build 2010;(1):402.

[3.20] Maurya A, Eatherton MR, Matsui R, Florig SH. Experimental investigation of miniature buckling restrained braces for use as structural fuses. J Const Steel Res 2016;127:54-65.

Nomenclature

c_5 clearance No. 5, space between the core bar and the round tube's inner width

c_6 clearance No. 6, space between the round tube's outer surface and the supporter

c_7 clearance No. 7, space between the round tube inner surface and the roll-threaded part of the core bar

$_sd$ largest separation between the supporters, including top and bottom fixed points (i.e., "the buckling length")

E steel Young's modulus

F_{br} bracing force at the supporter

H frame total height measured from the pin support

I round tube moment of inertia

l separation between bolts

L core bar length

$M_{A\text{-}C}$ in-plane moment on the round tube

$M_{B\text{-}D}$ out-of-plane moment on the round tube

M_y round tube flexural strength

n radius around the bolts in which yield is expected to take effect

N_E elastic buckling strength of the round tube

$N_{\max}$ maximal expected axial load on the damper

N_t round tube axial force

N_{ty} round tube yield strength

N_y core bar/brace yield strength

P horizontal load on the spine frame

P_y predicted lateral yield strength

P_{yw} yielding load at the web

R story drift angle

R_{max} maximal expected story drift angle of design

R_y yield story drift angle of design

SF damper's buckling-restraining capacity

T_{max} maximal tension load of the damper's peak cycle

t_w web thickness

u_h spine's top horizontal displacement

w horizontal distance between the pin support and the damper

β compression-to-tension ratio

ξ amplification factor, which considers overstrength and strain hardening of the core bar. ξ = 1.5 is adopted in this study

Δ total lateral deflection owing to clearances

Δ_0 damper's out-of-straightness

Δ_T total damper deflection

Δ_y expected core bar yield deformation

σ_y yield stress of the steel material

σ_{yw} yield stress of the column's web

ω peak strain hardening adjustment factor

4. APPLICATION OF THE PROPOSED DAMPER TO A SPINE FRAME SYSTEM FOR A REAL SCALE BUILDING

4.1. Introduction

This chapter presents an application of the proposed "buckling-restrained steel bar damper" to a real scale building prototype. The main purpose is to design the damper based on a real size building model, in order to evaluate its practicality of application and to discuss the method of installation of the proposed bar damper. The prototype building used is part of a currently ongoing research "Seismic response of steel structures with super elastic system using parallel spine frames" which is based on reference [4.1].

Firstly, background on the structural system of the prototype building is described in Section 4.2. Afterwards, the characteristics and dimensions of the prototype building are presented in Section 4.3. Details and dimensions of the spine frame are shown in Section 4.4. Design of the proposed bar damper and its attachment to the building prototype are presented in Section 4.5. Finally, the applicability of the proposed damper to the building prototype is discussed in Section 4.6.

4.2. Background on the structural system used for the prototype building

In this chapter, the earthquake energy dissipation system used for the prototype building is explained. In building structures, high magnitude earthquakes are likely to cause large residual deformations on buildings which, in consequence, may lead to forced demolition of the buildings and considerable economic losses, particularly for ductile moment-resisting frame buildings which rely on plastic behavior to dissipate earthquake energy [4.2].

There are several approaches to reduce the residual deformation in building structures. One of the approaches is using self-centering lateral-resisting systems such as rocking frames. Structural spines typically use their self-weight combined with posttensioned members to generate self-centering lateral force (Fig. 4.1). An alternative approach to reduce the residual deformation is to increase the postyield lateral stiffness. This can be achieve by, for instance, using controlled spine

frame systems [4.3–4.5] with envelope moment-resisting frames designed to remain elastic and consequently provide self-centering force during major earthquakes (Fig. 4.2 (a)). However, the high post-elastic stiffness expected from moment frames of this system could be difficult to achieve for story drift angles larger than a specific level (for instance, 0.01 rad for steel moment-resisting frames). Therefore, an elastic system composed of two parallel spine frames linked to the moment frames (which is the structural system of the prototype building used in this design example) as shown in Fig. 4.2 (b) can be a recommendable alternative.

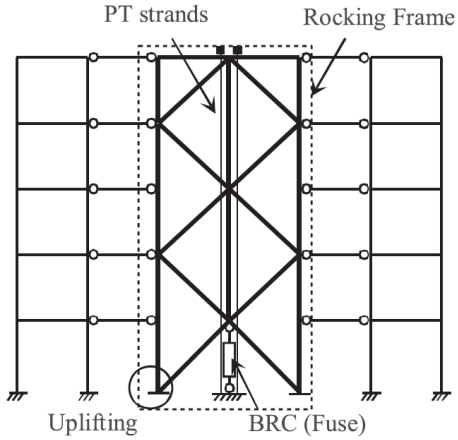

Figure 4.1 Structural rocking frame with posttension (PT) member [4.5]

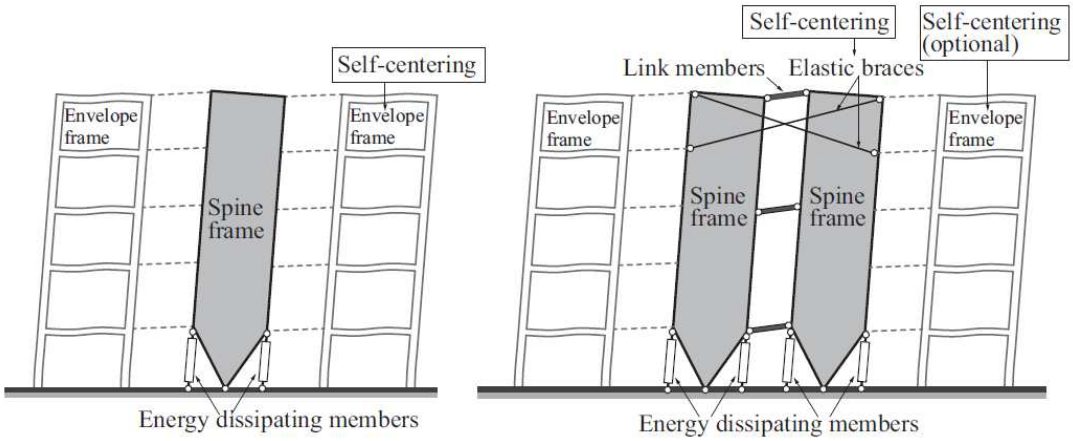

(a) with envelope moment resistant frames (b) with parallel spines

Figure 4.2 Types of spine frames [4.1] which can reduce residual deformation by increasing of the postyield lateral stiffness.

4.3. Prototype structure

A scheme of a 5-story building prototype as shown in Fig. 4.3 is used to implement the proposed damper system**.** The building adopts combined moment frames and spine frames. The building has a

total height of 20.6 m, where the first story has a height of 4.6 m and the other stories have heights of 4 m each. Plan dimensions of each floor are 32 m × 32 m, with bays of 6.4 m in each direction. The coupled spine frames are located symmetrically at the second and forth bays of the front and rear frames. The spines are pin-supported at their bases, and pin-connected to the moment frames to avoid concentration of forces at connections. The dampers will be place at the bottom side columns of the spine frames. Pin-end link members are used to connect the spine frames at each floor. Additionally, elastic braces are adopted at the top floors of the spine. SN490B (nominal yield strength F = 325 MPa) steel is adopted for members in moment frame and spine frames.

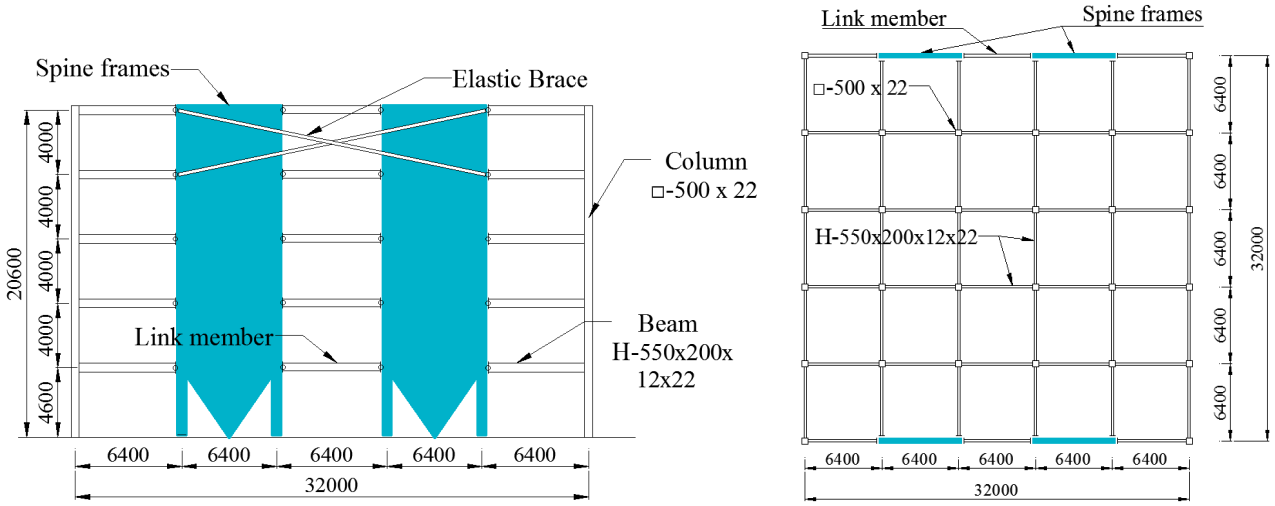

(a) Front View (b) Plan view

Figure 4.3 Prototype building

4.4. Spine frames

Fig. 4.4 shows the dimensions and components of the spine frames. The section of vertical and diagonal members is H-498×432×45×70 (Height × width × web thickness × flange thickness) and the section of horizontal members is H-550×200×12×22. The web of the spine components is in-plane with the expected load direction. The spine frame is divided in large assembled parts. Fig. 4.4 shows the division of this parts, which corresponds to the lines of welding at the construction site. Details on the pin support connection and the connection of the spine to the beam are explained in the following subsections.

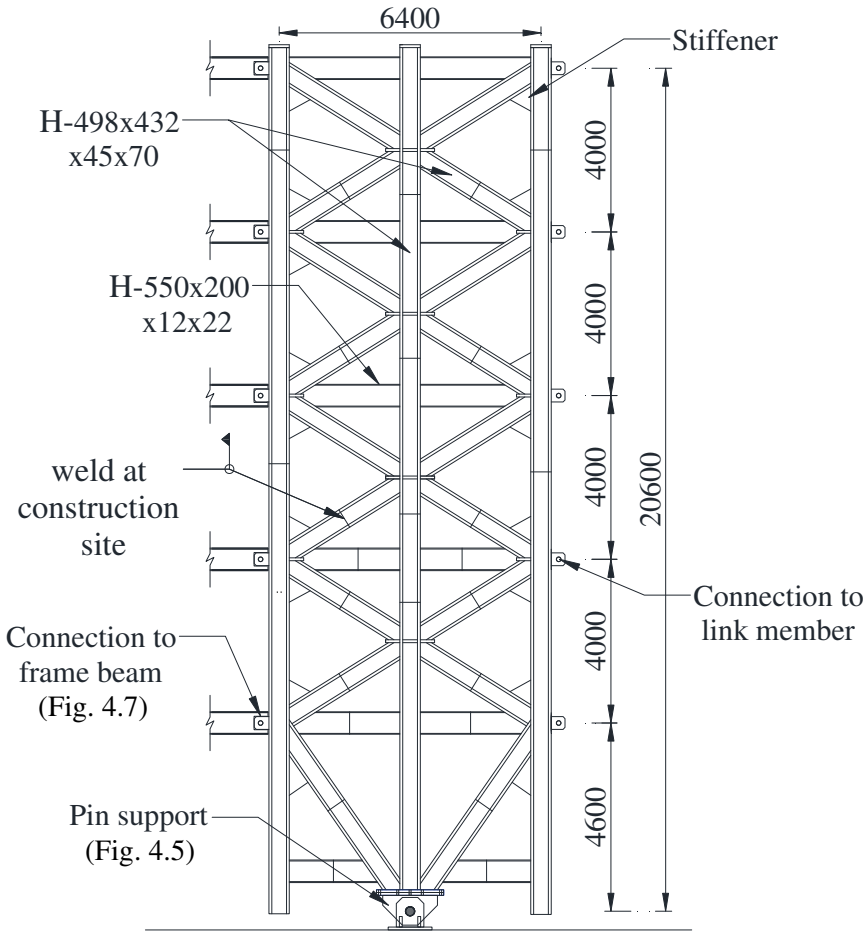

Figure 4.4 Spine frame dimensions

4.4.1. Pin support of the spine frame

The pin support enables the spine to pivot when the structure is subjected to horizontal displacement. Fig. 4.5 shows 3D views and dimension details of the designed pin support. Multiple forks distributed as shown in the figures were used to reduce the load effect on the pin cylinder. The pin was designed considering the maximal shear force 8069 kN amplified by a safety factor of 2, and thus, the design force on the pin at the support is V = 16139 kN. This force is transmitted through the forks to the pin cylinder as represented in Fig. 4.6 (a). The distribution of this force on the pin was simplified as shown in Fig. 4.6(b) to calculate a conservative bending moment on the pin M_{pin} by using Eq. (4.1), where L_p is the pin's length.

$$M_{pin} = \frac{(V/3)(L_p/3)}{4} = \frac{VL_p}{36} . \tag{4.1}$$

Flexural strength of the pin

To provide sufficient flexural strength, the pin's bending stress σ_{pb} shall be smaller than the pin's yield stress σ_y , i.e., $\sigma_{pb} < \sigma_y$, where:

$$\sigma_b = M_{pin} / Z_{pin} \quad , \quad Z_{pin} = \frac{\pi d_p^{\,3}}{32}, \tag{4.2, 4.3}$$

Z_{pin} is the section modulus of the pin cross section and d_p is the pin's diameter. For L_p = 450 mm and d_p = 235 mm, the condition ($\sigma_{pb} < \sigma_y$) = (206 N / mm^2 < 325N / mm^2) is satisfied.

Shear strength of the pin

To provide sufficient shear strength, the shear stress per shear plane of the pin V_{pl} shall be smaller than the pin's shear strength τ, i.e., $V_{pl} < \tau$, where:

$$V_{pl} = \frac{V}{N^o_{planes} A_{pin}} \quad , \quad \tau = \sigma_y / \sqrt{3}\,, \tag{4.4, 4.5}$$

$N^o{}_{planes}$ is the number of shear planes and A_{pin} is the cross-section area of the pin. For $N^o{}_{planes}$ = 6 and d_p = 215 mm^2, the condition ($V_{pl} < \tau$) = (74 N / mm^2 < 188 N / mm^2) is satisfied.

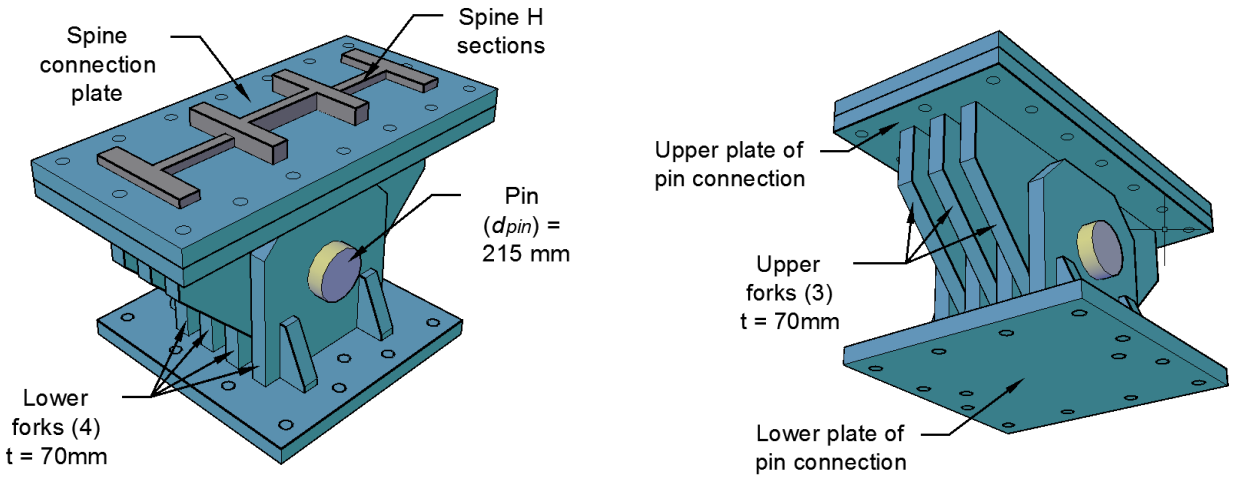

(a) 3D-view (b) 3D-view

Figure 4.5 Spine pin-support

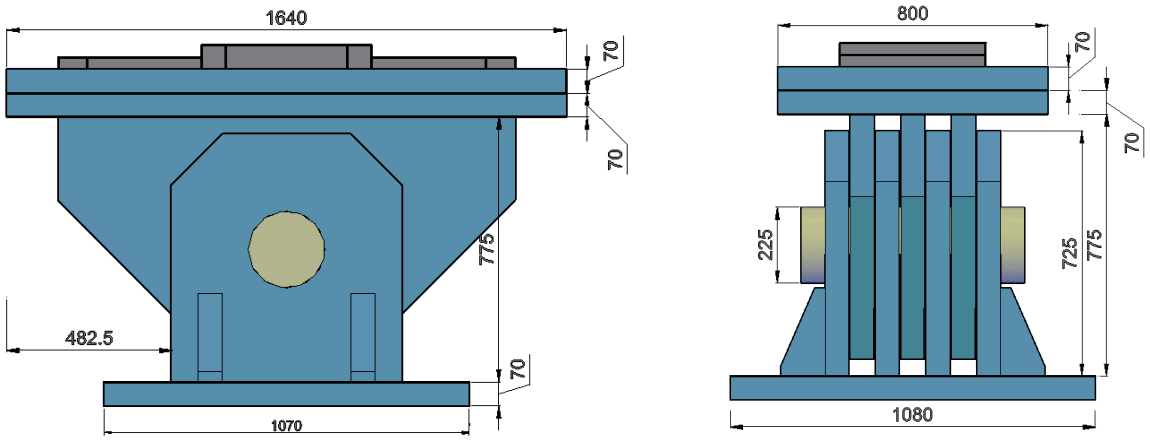

(c) Front view (d) Side view

Figure 4.5 Spine pin-support (cont.)

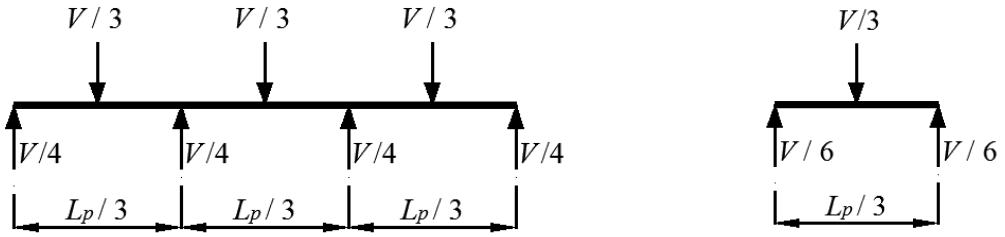

(a) Fork loads distribution on pin (b) Simplified load distribution

Figure 4.6. Load distribution on the spine frame support's pin

Design of forks of the pin connection

The yield strength, tensile and shear rupture at the forks of the spine base pin were calculated based on AISC D2.215.

The pin support of the spine frame has been designed in one direction (the main direction of the spine frame). Adjustments should be implemented to consider out-of-plane effects on the pin support, such as allowing uplifting of the pin base at the out-of-plane direction, or implementing shear keys under the pin base plate.

4.4.2. Pin-connection of beams to the spine frame

Pin-connections were used to attach the frame beams to the spine frame in order to avoid concentration of forces at the connection due to rotation of the spine frames. Fig. 4.7 shows the details of the designed pin-connection. The pin was designed considering a maximal shear force

264.4 kN amplified by a safety factor equal to 1.5. The design force on the pin of the beam connection is V_b = 396.6 kN.

Flexural strength of the pin

To provide sufficient flexural strength, the beam pin's bending stress σ_{bb} shall be smaller than the pin's yield stress σ_y , i.e., $\sigma_{bb} < \sigma_y$, where:

$$\sigma_{bb} = M_{bpin} \Big/ Z_{bpin} \quad , \quad Z_{bpin} = \frac{\pi d_{bp}^{\,3}}{32}, \tag{4.6, 4.7}$$

Z_{bpin} is the section modulus of the pin cross-section and d_{bp} is the pin's diameter. For L_{bp} = 61 mm and d_{bp} = 110 mm, the condition ($\sigma_{bb} < \sigma_y$) = (46 N / mm^2 < 325N / mm^2) is satisfied.

Shear strength of the pin

To provide sufficient shear strength, the shear stress per shear plane of the pin at the beam connection V_{bpl} shall be smaller than the pin's shear strength τ, i.e., $V_{bpl} < \tau$, where:

$$V_{bpl} = \frac{V_b}{N^o_{bplanes} A_{bpin}} \quad , \quad \tau = \sigma_y \Big/ \sqrt{3}\,, \tag{4.8, 4.9}$$

$N^o_{\ bplanes}$ is the number of shear planes at the beam's pin and A_{bpin} is the cross-section area of the beam's pin. For $N^o_{\ planes}$ = 2 and d_p = 9503 mm^2, the condition ($V_{bpl} < \tau$) = (21 N / mm^2 < 188 N / mm^2) is satisfied.

Clearance between the beam and the spine frame column

During rotation of the spine frame, enough clearance between the beams and the spine column is necessary to avoid interaction between both the spine column and the beam edge. Fig. 4.8 shows the relation between the story drift ratio R and the beam end rotation at each floor of the building. It can be seen that for R_{max} = 0.03, a beam rotation α = 0.025 is expected. Thus, the total beam rotation is calculated as $R_{max} + \alpha$ = 0.055. The necessary clearance between the beam and the spine frame column c_{bc} is determined through Eq. (4.10). Thus, for H_{beam} = 550, c_{bc} shall be at least 15 mm.

$$c_{bc} \geq (\alpha + \beta) H_{beam} \Big/ 2\,. \tag{4.10}$$

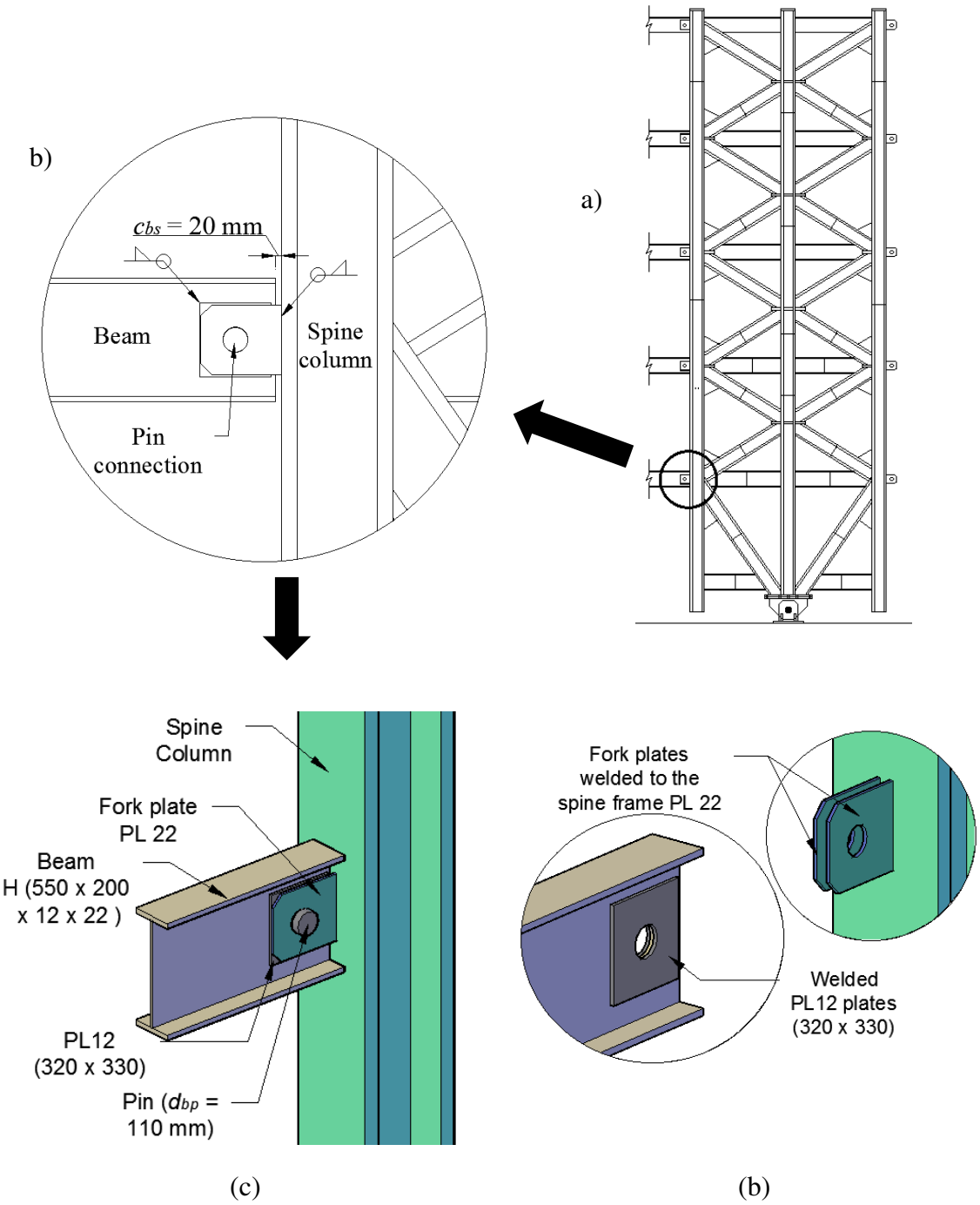

Figure 4.7. Pin connection of the beam: c) 3D view of connection, (d) Reinforcement plates welded to the H beam (left) and pin fork plates welded to the spine column (right)

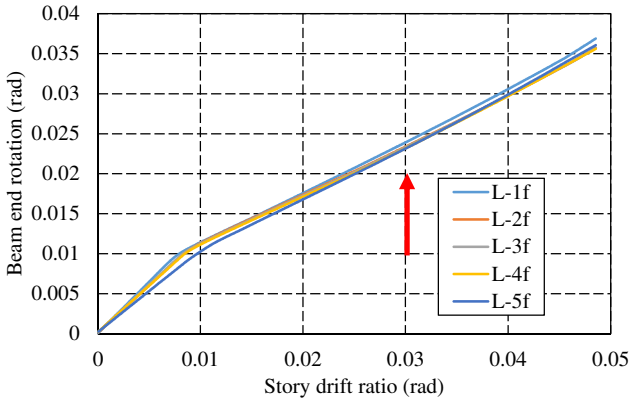

Figure 4.8 Story drift ratio vs. Beam end rotation.

Design of the pin forks was performed based on AISC D2. Sufficient welding was provided to the forks and the welded plates.

4.5. Implementation of the damper into the spine frame

This section describes the configuration of the proposed damper implemented to one of the spine frames as shown in Fig. 4.9. The configuration is based on the model and design considerations of Chapter 3 for a strength demand N_y of 4000 kN per spine column, a maximal expected story drift R_{max} of 0.03 and yield story drift R_y of 0.005.

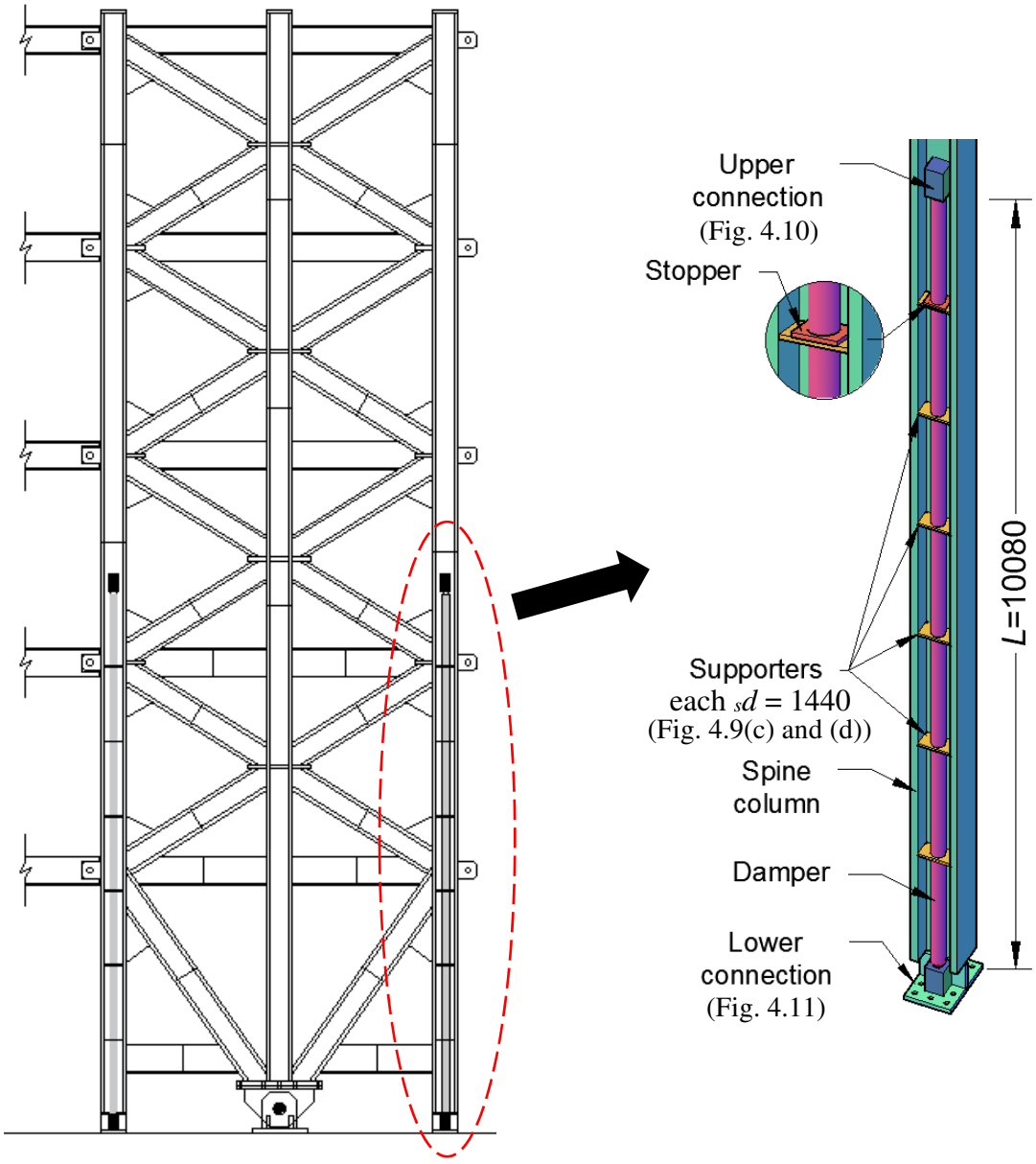

(a) Location at the spine frame

(b) 3D view and components

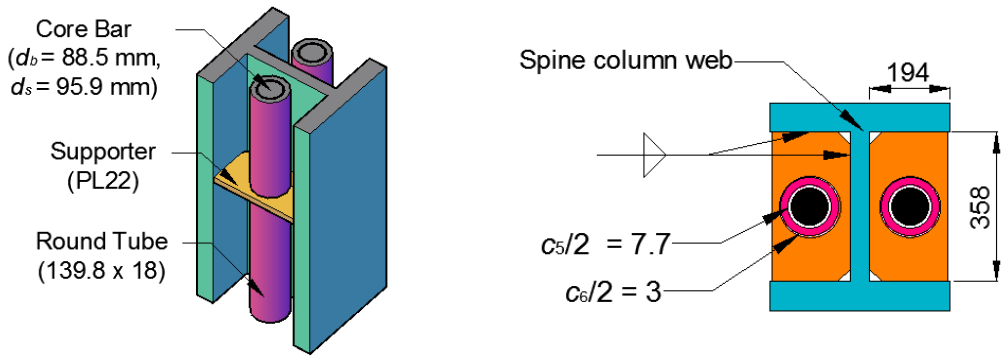

(c) 3D view at supporter zone

(d) Cross section at supporter

Figure 4.9 Implementation of the damper into the spine frame system

4.5.1. Details of configuration

To satisfy the required strength demand (Section 4.5.2), a set of two dampers were attached to each spine column as shown in Fig. 4.9 (c). To satisfy the required plastic deformation capacity (Section 4.5.2), a length of 10080 mm is adopted for the damper's core bar. For each damper, a core bar with a diameter of 88.5 mm and a screw diameter of 95.9 mm was adopted. A round tube with dimensions of 139.8 × 18 (diameter × thickness) was used as buckling restrainer. Six supporters per damper were used to reduce the buckling length by setting them every 1440 mm. Because the spine web have the dampers at each side of the column web, the supporters were attached by welding (instead of bolting). The stopper is a PL22 plate welded to the round tube (Fig. 4.9 (b)). By resting the stopper on the top supporter, it is possible to enable the 50 mm contraction allowance zones at both damper ends (Figs. 4.10 (a) and 4.10 (a)).

Clearances, as shown in Figs. 4.9 (d), 4.10 (b) and 4.11 (b), are c_5 = 15.3 mm, c_6 = 6 mm and c_7 = 8 mm, where c_5 is the clearance between the round tube inner surface and the non-threaded part of the core bar, c_6 is the clearance between the round tube outer surface and the supporter, and c_7 is the clearance between the round tube inner surface and the roll-threaded part of the core bar. The screw parts are inserted 200 mm into the round tube at both ends (Figs. 4.10(b) and 4.11(b)). The core bars ends are screwed at both ends to the upper and lower connections. The upper connections are fixed via welding to the spine frame as shown in Fig. 4.10 (a). The lower connection are composed of a welded plate assembly, which is anchor-bolted to the base beam (Fig. 4.11 (a) and (c)). All the components of the damper use steel material with a yield strength of 325 N/mm^2.

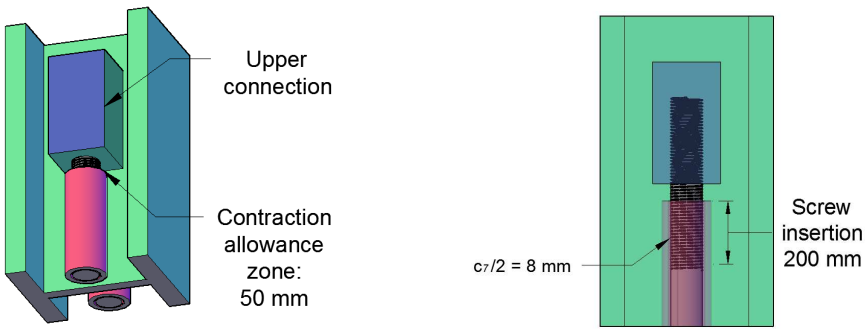

(a) 3D view (b) Clearance and screw insertion

Figure 4.10 Upper connection details

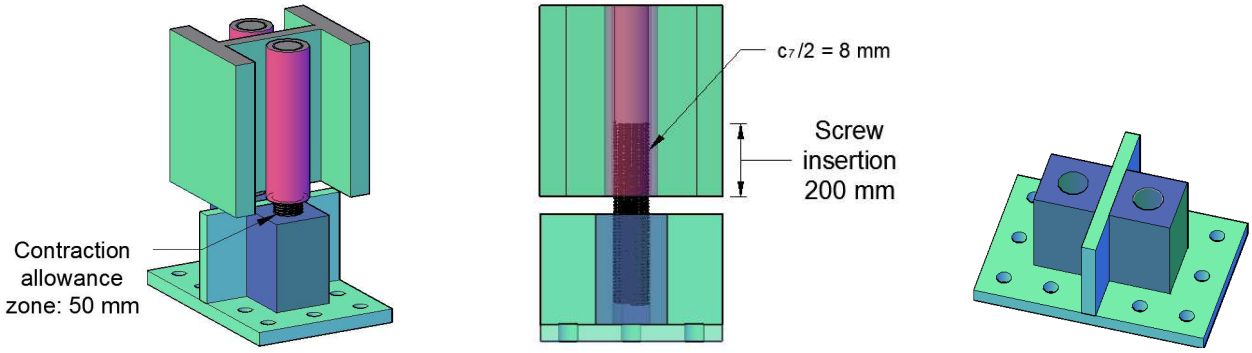

(a) 3D view (b) Clearance and screw insertion (c) Connection assembly

Figure 4.11 Lower connection details

4.5.2. Details of design

As previously mentioned in section 4.5, the building is expected to remain elastic for $R_y = 0.005$. Additionally, the expected load on each spine column is $N_y = 4000$ kN. In this section, the design of the damper is performed considering the previously mentioned and within the limits of the spine column web and flanges. Details of design are shown in Appendix C.

Steel core bar

Because the damper force demand has been specified in advanced, the necessary cross-sectional area for the core bar A_b can be obtained by Eq. (4.11) as 12307 mm^2, where σ_y is the nominal yield strength of the core bar (325 N / mm^2). For this core bar cross-sectional area, two round steel core bars with a diameter of 88.5 mm as shown in Fig. 4.9 (c) and (d) can be used within the dimension limits of the column web and flanges.

$$A_b = \frac{N_y}{\sigma_y}. \tag{4.11}$$

Sufficient length of the core bar is necessary to ensure sufficient plastic deformation capacity of the damper. The expected core bar yield deformation Δ_y was determined using Eq. (4.12), where w is half of the spine width. Thus, for $w = 3200$ mm, $\Delta_y = 16$ mm.

$$\Delta_y = R_y w \tag{4.12}$$

By assuming the same stiffness for the screw part and the non-threaded part of the core bar, the core bar length L was determined using Eq. (4.13) as 10080 mm, where E is the Young's modulus of the steel material (205000 N / mm^2). The determined damper length L is considerably long in comparison to the building height. As observed in Eq. (4.13), this length depends not only on the required R_y to preserve elastic behavior of the damper, but also on the spine frame width w. Because the spine frame requires a large w to have high stiffness, a large damper length is also necessary as reflected in the Equation.

$$L = \frac{R_y w E A_b}{N_y} \tag{4.13}$$

Buckling-restrainer

Considering a round tube with dimensions of 139.8 × 18 (diameter × thickness) and a buckling length ${}_sd$ of 1440 mm, the buckling strength N_E was determined using Eq. (4.14) as 12734 kN, where I is the moment of inertia of the round tube (13051431 mm^4).

$$N_E = \frac{\pi^2 E I}{{}_s d^2} \tag{4.14}$$

For the clearance $c_5 = d - d_{cb}$ = 15.3mm, (where d is the inner diameter of the round tube and d_{cb} is the diameter of the non-threaded part of the steel core bar), the round tube restrains the buckling of the core based on the Eq. (4.15), where M_y (= $\sigma_y z$ = 60682618 N mm) is the round tube flexural strength, $0.5N_y$ = 2000 kN is the core bar yield strength per damper, and ξ = 1.5 is an amplification factor that considers the overstrength and strain hardening of the core bar.

$$SF = \frac{M_y}{\left(\dfrac{\xi\left(0.5N_y\right) c_1}{1-\left(\xi\left(0.5N_y\right)/N_E\right)} \right)} \geq 1.0 \ \left(=1.01 \geq 1.0\right) \tag{4.15}$$

Contraction allowance zones and round tube length

Assuming two zones of contraction allowance zones (one at each end of the damper), the length of one contraction allowance zone is calculated as $(wR_{max})/2 = 48 \approx 50$ mm. The round tube length was estimated as $L - (wR_{max}/2) = 9980$ mm.

Supporter

One of the key features of the proposed damper is the use of supporters, which by reducing the buckling length of the damper, enables a considerable reduction of the buckling-restrainer cross-section. As per Sections 3.3.4 and 3.5.4, normal forces from the core bar axis exerted on the supporters are expected to be under 4% of N_y (very small), that is 80 kN. This force is resisted by the six supporters, which were distributed along the damper length and placed every 1440 mm. A plate thickness of 22 mm was used for the supporters.

4.6. Discussion

The buckling-restrained steel bar damper proposed in Chapter 3 was implemented into a real scale building example. The characteristics that mainly influenced the implementation of the damper are discussed in the following paragraphs.

Firstly, the required damper length, necessary to satisfy the expected strain demand, was considerably long, reaching up to half of the building height. Thus, up to 6 supporters were necessary to partially restrain the damper. Secondly, using of two dampers is desirable to satisfy the necessary strength demand.

For implementation of the damper with the previous characteristics, the spine components were configured so that the spine H-section's webs are in the same plane of the spine pivoting direction. This way, it was possible to configure two dampers per spine column at both sides of each column web (as using only one damper would result in a cross section out of the limits of the spine column flanges and the web). Additionally, the web direction of the spine column also allowed the damper to reach its required length (which surpassed the first two levels of the building) without affecting the connections at the first and second floor levels.

Because the dampers were attached at both sides of the spine column webs, welding was used for the supporters, instead of bolting, to avoid difficulty of installation and obstacle of bolts at the opposite side of the web.

Another characteristic which influenced the implementation of the damper to the real scale model was the use of screwed solid connections at both ends. To attach the upper connections to the spine, welding was used instead of bolting (similarly to the supporters) to avoid difficulty of installation and obstacle of bolts. To attach the lower connections to the base (after screwing of the core bars), the couple of solid sections per spine column are welded together through a plate assembly which can be bolted to the base beam.

As a consequence of the previous characteristics of configuration, it is necessary that the proposed damper be set up and attached to the spine column at the assembly factory, where welding of the supporters and connections shall be performed. Because the spine frame is divided into different large assembled parts, the damper can be attached to the spine column at the assembly factory to the respective column. The spine frame single components can be welded at the assembly factory and the large assemble parts of the spine frame can be welded at the construction field.

Bolting of the damper connections and supporters to the spine frame column is possible when only one damper is used. When two dampers are required per column, it is recommendable that connections and supporters be welded at the assembly factory. Overall, the main advantage of the proposed damper is not only its compactness, as it only requires the hollow spaces within the spine column, but also its small cross-section compared to the necessary one for a single buckling-restrained column.

Regarding the damper contribution to the seismic performance of the building, the dampers are able to reduce the story drift ratio R by 23-47% and the first vibration period by 12-19%, based on the ongoing seismic response analysis.

4.7. Conclusion

The implementation of the damper was notably influenced by the required damper length to satisfy the expected strain demand and by the required number of dampers to satisfy the strength demand. In contrast to the damper connections used for the test, welding was necessary for the supporters, instead of bolting.

References

[4.1] Chen X, Tagawa H. Super elastic system using parallel spine frames with steel braces. Earthq Eng Struct Dyn 2020;1-21.

[4.2] Ramirez CM, Miranda E. Significance of residual drifts in building earthquake loss estimation. Earthq Eng Struct Dyn 2012;41(11):1477-1493.

[4.3] Takeuchi T, Chen X, Matsui R. Seismic performance of controlled spine frames with energy-dissipating members. Journal of Constructional Steel Research 2015;114:51-65.

[4.4] Chen X, Takeuchi T, Matsui R. Simplified design procedure for controlled spine frames with energy-dissipating members. J Constr Steel Res. 2017;135:242-252.

[4.5] Chen X, Takeuchi T, Matsui R. Seismic performance and evaluation of controlled spine frames applied in high-rise buildings. Earthq Spectra. 2018;34(3):1431-1458.

5. CONCLUSION

This study investigated the use of “buckling-restrained steel bar dampers” as energy dissipation devices for spine frame systems. Below are stated a summary of the conclusions on each chapter.

In Chapter 2, a preliminary study on the application of round steel bars as buckling-restrained brace was executed, aiming to reveal its applicability. The core bar was restrained by double tubes, and solid end-connections to which the core bar can be screwed were implement to simplify the assembly. Loading tests were conducted on two specimens which differed on the number of contraction allowance zones. The tests revealed satisfactory performance for both specimens, but particularly for the specimen with higher number of contraction allowance zones. End-connections also displayed satisfactory performance, thus, revealing the applicability of the proposed BRB in the preliminary study.

In Chapter 3, which is the main part of this study, a buckling-restrained steel bar damper (whose design concept is based on the preliminary research) was implement into a spine frame system. The damper is composed of round steel bar cores restrained by a round steel tube. The main feature of the damper is that its buckling length can be notably reduced by implementing thin-plate elements called supporters. The supporters, which are attached to the spine frame extended columns, partially restrain the round tube thus notably reducing the cross-section area of the damper. Loading experiments were conducted on 10 specimens which mainly differed with regard to the number of contraction allowance zones of the core bar, number of supporters of the buckling restrainer, damper length, type of connection to the base, and number of dampers per spine. The results revealed that dampers with two contraction allowance zones, at least one supporter at the center, and fixed connections at their base exhibit the most satisfactory performance. Overall, functionality of the spine, the supporters and end-connections were satisfactory as visually confirmed after the test.

In Chapter 4, the proposed buckling-restrained steel bar damper was implemented into a real scale building example to assess the practicality of its application. The implementation of the damper was notably influenced by the required damper length to satisfy the expected strain demand, which was considerably long (in relation to the building’s height), and by the required number of dampers to

satisfy the strength demand. The orientation of the spine frame was adapted to implement the proposed damper, whose length surpassed half of the building height (two stories). Up to six supporters were necessary to partially restrain the damper. In contrast to the damper connections used for the test, welding was necessary for the supporters, instead of bolting, to avoid difficulty of installation and obstacle at the spine column web caused by connection. Welding was also necessary for the end connections. Thus, for a building with dimensions and strength demand as in the design example, it is necessary that the proposed damper be set up and attached to the spine column at the assembly factory, where welding of the supporters and connections shall be performed.

In Chapter 5, conclusions of the research are stated. Overall, it can be concluded that the damper can be implemented as an energy dissipation system for spine frame systems. Depending on the damper length and its strength requirements, the damper can be attached to the spine column by bolting at the construction field, or by welding at the assembly factory.

APPENDIX A

A: Design procedure and recommendations

Details of each design step of the flowchart shown in Fig. 26 are described as follows:

Start

Step 1- Design of the core bar: Find A_b that satisfies the desired strength N_y in Eq. (A.1), where A_b is the cross-section area of the steel core bar.

$$N_y = \sigma_y A_b \tag{A.1}$$

Step 2- Design of the inner tube and the number of spacers:

- Select a clearance c_1, which should be as small as possible (c_1 = 2 mm recommended).
- Determine the inner diameter $d = d_{sb} + c_1$ for the inner tube, where d_{sb} is the core bar screw diameter.
- Use 3 to 5 spacers per inner tube as design criteria.
- Based on the previous conditions, select an inner tube thickness t that matches SF = 1.0 (Eqs. (2.2) to (2.4)).
- Calculate the inner tube diameter $D = d + 2t$ (Fig. A.1)

Step 3- Design of pin: Calculate the pin diameter as 60% of the coupler's width s, i.e., $d_p = 0.6s$. It should satisfy $\sigma_{py} > \sigma_{pb}$, where:

$$s \geq \frac{20}{9}\sqrt{5\xi N_y / \pi\sigma_y}\,. \tag{A.2}$$

Once the pin strength is designed based on its size (diameter), proportional with respect to the coupler's width, it is possible to estimate the optimal outer tube-coupler section combination.

As a note, Eq. (A.2) is the result of finding the optimal s for $\sigma_{py} > \sigma_{pb}$, where:

$$\sigma_{pb} = M_{pin} / Z_{pin},\ M_{pin} = \frac{(\xi N_y) L_{pin}}{4},\ L_{pin} = \frac{2}{3}s,\ Z_{pin} = \frac{\pi d_p^{\,3}}{32}, \tag{A.3-A.6}$$

in which:

M_{pin}: Moment at pin generated by the coupler's fork, Eq. (A.4).

L_{pin}: Distance between the reaction forces of the fork, as defined in Eq. (A.5) and as seen in Fig. A. 2(b). The reference points are the segmented black lines of Fig. A.2(a), which show mid-lines of the fork component.

Z_{pin}: Section modulus of the pin cross section, Eq. (A.6).

Step 4- Design of outer tube:

- Determine the inner width b as $b = s + c_4$ ($c_4 = c_3 = 3$ mm recommended)
- Find $_o t$ that satisfies $_o SF = 1.0$ (Eqs. (2.5) to (2.7)).
- Determine the width B as $B = b + 2_o t$ (Fig. A.3).
- Confirm that the width-to-thickness ratio satisfies: $B/_o t \leq 735/\sqrt{\sigma_y}$

Step 5- Design of the gusset plate: Its thickness can be assumed to be $t_p = 0.25s$ and should satisfy Eq. (A.7), where f_t is the bearing strength of the gusset plate.

$$1.2\left(\xi N_y\right) < d_p t_p f_t \tag{A.7}$$

Step 6- Design of the coupler's fork area: Use Eq. (A.8) to verify that the coupler's fork area A_f is enough to satisfy $N_{yF} > \xi N_y$, where N_{yF} is the strength capacity of the coupler's fork area, and A_f is the area of the coupler's fork, as defined in Fig. A.4.

$$N_{yF} = \sigma_y A_f \tag{A.8}$$

End

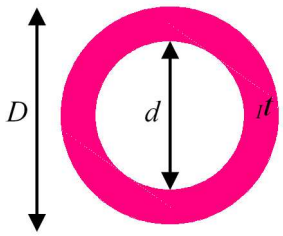

Figure A.1 Definition of D, d and t

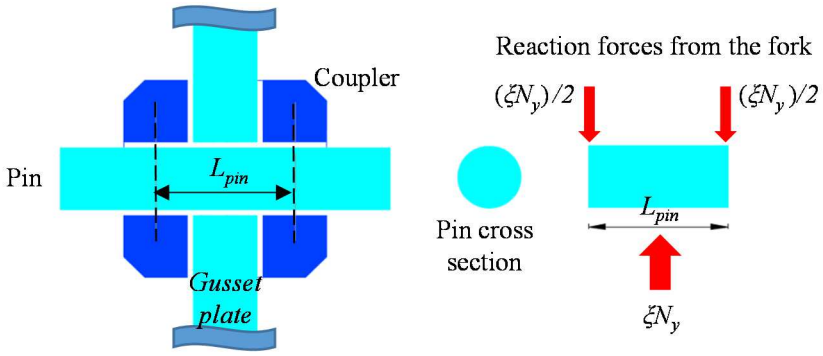

(a) Cross-section view (b) Top view and pin cross section

Figure A.2 Cross section of the coupler at pin zone and load effect on the pin

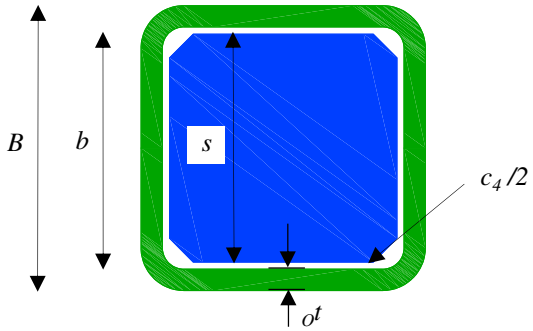

Figure A.3 Definition of *B*, *b*, and *ot*

(a) Perspective view of end coupler (b) Section view of end-coupler smallest area

Figure A.4 Fork area

Nomenclature

A_b cross-section area of the steel core bar

A_f area of the coupler's fork

b inner width of the outer tube

B width of the square tube

c_1 clearance No. 1, space between the core bar screw and the inner tube's inner width

c_3 clearance No. 3, space between the spacer and the outer tube's inner width

c_4 clearance No. 4, space between the coupler and the outer tube's inner width

d inner diameter of the inner tube

D diameter of the inner tube

d_p pin diameter

d_{sb} core bar screw diameter

f_t bearing strength of the gusset plate

$_It$ inner tube thickness

L_{pin} distance between the reactions forces of the fork (Fig. A.2 (b))

M_{pin} moment at pin generated by the coupler's fork

N_y core bar / brace yield strength

N_{yF} strength capacity of the coupler's fork area

$_ot$ outer tube thickness

$_oSF$ outer tube safety factor

s coupler's width

t_p gusset plate thickness

Z_{pin} section modulus of the pin cross section

σ_y yield stress of the steel material

σ_{pb} pin's bending stress

σ_{py} pi's yield strength

ξ amplification factor, which considers overstrength and strain hardening of the core bar. ξ = 1.5 is adopted in this study

APPENDIX B

B: Details of design buckling-restraining mechanism of test specimens

The following tables show the details of design of the buckling restraining mechanism for the specimens of Chapter 3.

Round Tube 31.8 x 5

D	31.80
d	21.80
I (mm4)	39,110.6
Z (mm3)	2,459.8
A (mm2)	421.0

SPECIMEN FS1, FSC,FD

STEEL

σy (N/mm2)	235.0
E (N/mm2)	205,000.0

Core Bar M20 yield strength	
d_screw	20.0
A1-e	314.2
dp	18.2
A2-p	268.8
Ny1-e	73,827.6
Ny2-p	63,168.0

Clearances (mm)	
ec	1.80
pc	3.60

Round Tube Design	
$_s d$ (mm)	600.0
σy (N/mm2)	338.0
NE	219,810.2
My	831,408.3
Right side	599,551.5
FS	1.39

SPECIMENS FS2 AND FS3

STEEL

σy (N/mm2)	235.0
E (N/mm2)	205,000.0

Core Bar M20 yield strength	
d_screw	20.0
A1-e	314.2
dp	18.2
A2-p	268.8
Ny1-e	73,827.6
Ny2-p	63,168.0

Clearances (mm)	
ec	1.80
pc	3.60

Round Tube Design	
$_s d$ (mm)	600.0
σy (N/mm2)	338.0
NE	219,810.2
My	831,408.3
Right side	599,551.5
FS	1.39

SPECIMEN FS4

STEEL

σy (N/mm2)	235.0
E (N/mm2)	205,000.0

Core Bar M20 yield strength	
d_screw	20.0
A1-e	314.2
dp	18.2
A2-p	268.8
Ny1-e	73,827.6
Ny2-p	63,168.0
Clearances (mm)	
eC	1.80
pC	3.60

Round Tube Design		
s d (mm)		1,150.0
σy (N/mm2)		338.0
NE		59,834.9
My		831,408.3
Right side	-	584,531.2
FS	-	1.42

SPECIMEN FS5

STEEL

σy (N/mm2)	235.0
E (N/mm2)	205,000.0

Core Bar M20 yield strength	
d_screw	20.0
A1-e	314.2
dp	18.2
A2-p	268.8
Ny1-e	73,827.6
Ny2-p	63,168.0

Clearances (mm)	
eC	1.80
pC	3.60

Round Tube Design	
s d (mm)	400.0
σy (N/mm2)	338.0
NE	494,573.0
My	831,408.3
Right side	421,944.8
FS	1.97

SPECIMEN FS6

STEEL

σy (N/mm2)	235.0
E (N/mm2)	205,000.0

Core Bar M20 yield strength	
d_screw	20.0
A1-e	314.2
dp	18.2
A2-p	268.8
Ny1-e	73,827.6
Ny2-p	63,168.0

Clearances (mm)	
eC	1.80
pC	3.60

Round Tube Design	
s d (mm)	300.0
σy (N/mm2)	315.0
NE	879,240.9
My	774,833.2
Right side	401,497.8
FS	1.93

SPECIMEN PS

STEEL

σy (N/mm2)	235.0
E (N/mm2)	205,000.0

Core Bar M20 yield strength	
d_screw	20.0
A1-e	314.2
dp	18.2
A2-p	268.8
Ny1-e	73,827.6
Ny2-p	63,168.0

Clearances (mm)	
eC	1.80
pC	3.60

Round Tube Design	
s d (mm)	600.0
σy (N/mm2)	338.0
NE	219,810.2
My	831,408.3
Right side	599,551.5
FS	1.39

SPECIMEN PD

STEEL

σy (N/mm2)	235.0
E (N/mm2)	205,000.0

Core Bar M20 yield strength	
d_screw	20.0
A1-e	314.2
dp	18.2
A2-p	268.8
Ny1-e	73,827.6
Ny2-p	63,168.0

Clearances (mm)	
$_{e}C$	1.80
$_{p}C$	3.60

Round Tube Design	
$_{s}d$ (mm)	550.0
σy (N/mm2)	338.0
NE	261,592.3
My	831,408.3
Right side	534,828.9
FS	1.55

APPENDIX C

C: Details of design of the damper for the building prototype

Steel Material

σy (N/mm2)	325.0
E (N/mm2)	205,000.0

Damper Length	
R_y =	0.005
w (mm)	3,200
$v=Ry*w$	16.0
L_{pl} (mm)	10,092

Ny (kN)-REQUIRED	4,000.0

For 4000kN x 2 Dampers

A (mm2)	6,153.8
$dbar$ (mm)	88.5
$dscrew$ (mm) / 8.3%	95.9

Expected axial deformation	
$Rmax$	0.030
$0.5w$ (mm)	3,200
$v=Rmax*0.5w$	96.0
Contraction allowance Zone	
CAZ	50.0
Screw Length	250.0

Round Tube	
D	139.8
d	103.8
t	18.0
I (mm4)	13,051,431
Z (mm3)	186,716
A (mm2)	6,888
Clearances	
c_e	7.94
c_p	15.28

Round Tube Design	
$_s d$ (mm)	1,440
σy (N/mm2)	325
NE	12,734,702
My	60,682,618
Right side	59,977,609
FS	1.01

No. of segments	7.0
No of Supportes	6.0

Related Publications:

1. Buckling-restrained steel bar damper for spine frame system, Mateus JAS, Tagawa H, Chen X. *Engineering Structures*, Vol. 229, No. 111593, **2020.11.**

2. Cyclic loading tests on spine frame with buckling-restrained steel bar dampers, Mateus J, Tagawa H, Chen X. *Proceedings of the 12th Pacific Structural Steel Conference (PSSC2019)*, paper ID 1-5-1, 9-11, Tokyo, **2019.11.**

3. Buckling-restrained brace using round steel bar cores restrained by inner round steel tubes and outer square steel tube, Mateus JAS, Tagawa H, Chen X. *Engineering Structures*, Vol. 197, No.109379, **2019.7.**

4. Application of round steel bar cores and simplified end-couplers to buckling-restrained braces, Mateus J, Tagawa H, Chen X. *Proceedings of the 7th Asia Conference on Earthquake Engineering (7ACEE)*, paper ID: ACEE0053, Bangkok, Thailand, **2018.9.**

5. Cyclic loading tests on Buckling-Restrained Braces using round steel bar cores restrained by inner round steel tubes and an outer square steel tube, Mateus J, Tagawa H. *Proceedings of the AIJ annual meeting, AIJ*, pp.1177-78, **2017.8.**